Nanocellulose production from low-cost agricultural residues: process development, economic assessment, and process robustness

Danielle Uchimura Pascoli

A dissertation

submitted in partial fulfillment of the

requirements for the degree of

Doctor of Philosophy

University of Washington

2022

Reading Committee:

Renata Bura, Chair

Anthony Dichiara

Rick Gustafson

Program Authorized to Offer Degree:

School of Environmental and Forest Sciences

University of Washington

Abstract

Nanocellulose production from low-cost agricultural residues: process development, economic assessment, and process robustness

Danielle Uchimura Pascoli

Chair of the Supervisory Committee:
Renata Bura
Bioresource Science and Engineering

The 21st century has been marked by the transition from a petroleum-based economy to a more renewable and sustainable era. Nanocellulose is a plant-based material and an excellent alternative for petroleum-based materials and chemicals in various applications due to its abundance, sustainability, and exceptional properties. Yet, major barriers such as high production costs hinder nanocellulose from achieving its full application potential. Thus, this research project presented a unique interdisciplinary approach that combined efforts in process engineering, computational modeling, and materials science to develop a sustainable and scalable process to produce nanocellulose from low-cost, unconventional waste feedstocks. First, the conversion process developed in this work effectively produced lignocellulosic nanomaterials from a wide range of low-cost feedstocks (wheat straw, corn stover, reed canary grass, and industrial hemp), as demonstrated through laboratory experimentation. All feedstocks generated

two product fractions comprising lignocellulosic nanofibrils (LCNF) and microfibrils (LCMF). LCNFs had similar morphology and behavior in aqueous media as nanofibrils produced via conventional TEMPO oxidation (~2 nm wide and ~1 μm long - characteristic of elementary fibrils) while undergoing a milder and more environmentally friendly process. LCMFs, on the other hand, comprised extremely long fibrils ~16 nm wide that formed a web-like network. Second, a large-scale facility using 100-tonne wheat straw feedstock per day was modeled with process simulation software with an 18,400 tonnes/year of lignocellulosic nanomaterials production capacity. The economic analysis revealed an outstanding minimum product selling price (MPSP) of US$4.60/kg at a 15% discount rate as a result of low-cost feedstock and conversion process simplicity. Finally, the nanomaterials were applied as reinforcing agents in polyvinyl alcohol (PVA) plastic composite films, with a remarkable case of simultaneous strengthening and toughening of the polymer nanocomposite with high specific tensile strength (up to 59.5 MPa g^{-1} cm^3), elastic modulus (up to 2.6 GPa g^{-1} cm^3), and fracture strain (up to 138%), while maintaining excellent optical transmittance in the visible region (up to 92%). The excellent improvements in the composites' mechanical properties demonstrate the application potential of these nanomaterials in plastics and packaging. This research project has shown the effectiveness and robustness of a novel conversion process to produce lignocellulosic nanomaterials using various low-cost feedstocks. The process comprises mild reaction conditions and employs green chemistry principles, resulting in lower cost and environmental impact than conventional nanocellulose production methods. This commercially viable process could produce nanomaterials at a large scale with commodity product economics, enabling their use as petroleum-based materials substitute in high-volume applications.

TABLE OF CONTENTS

LIST OF FIGURES

LIST OF TABLES

ACKNOWLEDGMENTS

This work would not have been possible without the many people who supported and helped me throughout this journey. First, I want to express my sincere gratitude to my advisor, Prof. Renata Bura, for guiding me and supporting me like no other mentor could have. She helped me step out of my comfort zone and try out new things (maybe too many things), and she promised me a Ph.D. project in a completely different area with lots of new experiences – and well, how she delivered! It feels great looking back and seeing how much I have learned and matured, both as a professional and an individual, while working with her during the past 5 years. She understood me like very few do and was always there for me, for all the good and bad data. Thank you for being a role model of a successful, confident woman in STEM that knows she can change the world.

I want to express my gratitude to the other members of my reading committee, Prof. Rick Gustafson and Prof. Anthony Dichiara, for their help and advice with the research and dissertation writing. Prof. Gustafson's vast knowledge of process design and scale-up, economic analysis, and industry practices was a very alluring diversion from my laboratory experiments, and I appreciate the many times he gave a reality check on my research findings. Prof. Dichiara's expertise in material science and sustainable materials was crucial for this project's success, and I truly enjoyed the opportunity to work with him and learn so much about this field. I also want to thank the other members of my committee, Prof. Eleftheria Roumeli and Prof. Heidi Gough, for the insightful discussions during meetings and exams, collaboration on different research projects, and assistance with paper writing. Having such a wonderful multidisciplinary committee during my Ph.D. taught me the importance of learning other disciplines and how they can be applied to my specific area of study. Thank you for sharing your knowledge with me.

Appreciation is extended to the different sources of funding that made this research project possible, especially the Washington State Legislature, the Lewis County .09 Rural Economic Development Fund, and the Centralia Coal Transition Grants. Additional support was provided by the McIntire-Stennis Cooperative Forestry Research Program (No. 1020630) from the USDA-NIFA, and by the University of Washington Denman Professorship Fund.

I also wish to thank some of my colleagues from the BSE department, Dr. Sheila Goodman, Dr. Heather Wise, Dr. Kurt Haunreiter, and Dylan Edmundson, for their time and patience in sharing their knowledge on several laboratory procedures with me and for being always available whenever I had questions. I want to thank the undergraduate students Linghong Schoch, Jackie Chou, and Brooke Lillie for helping me with the experiments for this project and to Dr. Andrew Jimenez, Ian Campbell, and Paul Grandgeorge from Prof. Roumeli's group for helping me collect data for my research from their facilities.

I am grateful for my parents, family, and friends from Brazil. Their constant love and support made a real difference. There were always those days when being so far from home hit a little harder, but knowing that they were always by my side, cheering for me and my successes, made those days a bit more manageable. Finally, I want to thank Dr. Gabriel Seufitelli, who was always my biggest supporter, both as my husband and colleague. Whenever I had a terrible day at work, I knew he would always be at home later to cheer me up, make me laugh, and help me solve my many scientific problems. He always believed in me, even during my worst times when I doubted myself and thought I could not make it. Only he knows all my ups and downs during this journey, and I am extremely grateful for having him as my partner in life. I would not be reaching this milestone without him. Ps: Thank you for double-checking all my dilution calculations during these years!

DEDICATION

This dissertation is dedicated to my parents, Elizabeth and Pedro Pascoli, who always taught me the value of education and encouraged me to pursue my dreams – even if that meant living more than 10,000 kilometers away from home. And to my husband, Gabriel, who never stopped believing in me and was my rock throughout this journey.

Chapter 1. Introduction

1.1 NANOCELLULOSE NOMENCLATURE AND DEFINITIONS

Cellulose is a polysaccharide found in plant cell walls and the most abundant biopolymer existing in nature. Cellulose fibrils (bound with hemicellulose and lignin) comprise long chains hierarchically organized that can be broken down into microfibrils and nanofibrils (Figure 1.1). Thus, the term 'nanocellulose' is broadly defined as any cellulose product originating from nanofibrils less than 100 nm wide. The two main types of nanocellulose products are cellulose nanofibers (CNF) and cellulose nanocrystals (CNC), and the main difference between the two is the presence or absence of amorphous cellulose regions (Figure 1.1). CNFs are long fibrils comprising both crystalline and amorphous regions, while CNCs consist of short fibrils comprising only crystalline regions (1). This research project is focused exclusively on the production of CNFs.

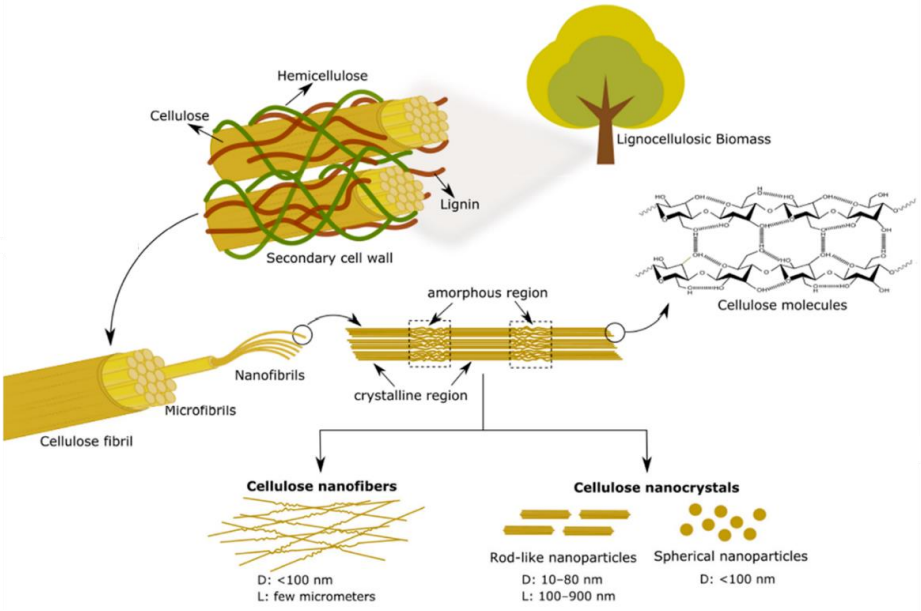

Figure 1.1. Hierarchical structure of plant biomass leading to the production of nanocellulose products (nanofibers and nanocrystals). Reproduced from (2) with modifications.

The terminology ‘CNF’ has been used interchangeably in the literature to refer to any cellulose-derived fibril product with widths up to 100 nm, with synonyms including nanofibrillated cellulose (NFC), cellulose microfibrils (CMF), microfibrillated cellulose (MFC), among other variations (1,3), which may cause confusion to the readership. Thus, this dissertation adopted more specific terminologies for clarity purposes. In this study, the term ‘nanofibrils’ refers to individual elementary fibrils up to 5 nm in width (4), while the term ‘microfibrils’ describes all other individual fibrils and bundles with widths between 10-100 nm (5,6). In addition, the terms ‘CNF’ and ‘nano-microfibrils’ are used interchangeably throughout this dissertation to represent both nanofibrils and microfibrils in a more general sense. Finally, the term ‘nanocellulose’ is used therein to refer to all cellulose-based nanoproducts, including both CNFs and CNCs products.

1.2 NANOCELLULOSE PROPERTIES AND POTENTIAL APPLICATIONS

Due to its hierarchical structure, nanocellulose contains unique properties that make it of interest for many applications. It is renewable, non-toxic, biocompatible, and biodegradable, providing end-of-life with low environmental impacts. Also, because of its high surface area, nanocellulose offers excellent mechanical properties while being extremely lightweight (7). Thus, nanocellulose’s abundance, sustainability, and unique properties make it a suitable alternative to replace petroleum-based chemicals and materials in several applications, promoting the reduction in CO_2 emissions associated with the production and end-of-life of such synthetic materials. In addition, utilizing plant-based nanomaterials instead of petroleum-based ones contributes to a lower carbon economy, given that the CO_2 absorbed by the plants during their growth is captured in the form of a long-lasting biomaterial. The potential applications for nanocellulose include paper products (8,9), food packaging (10–12), water treatment (13,14), cement composites (15), electronics and sensors (16), automotive parts (17), drug delivery (18), among others. These

applications can be divided into high-volume/low-cost applications (e.g., packaging, paper products, construction) and low-volume/high-cost applications (e.g., electronics, drug delivery).

1.3 CELLULOSE NANOFIBRILS PRODUCTION METHODS

The process of generating CNFs can be simplified into four main stages, as illustrated in Figure 1.2. The first stage consists of selecting the feedstock, which is the raw material utilized to produce the CNFs. Historically, nanocellulose products (including CNFs and CNCs) were primarily obtained from high-quality fiber materials such as bleached wood pulp containing virtually pure cellulose. However, this raw material presents economic and environmental issues, as its production involves several reaction steps at high temperatures and pressure that, most often, utilize harmful chemicals (19). For this reason, there has been increased interest in producing nanocellulose from other types of feedstocks, including agricultural residues (e.g., wheat straw, rice husk, corn stover, sugarcane bagasse), forest residues (sawdust, logging residues, fiberboard), natural plant fibers (jute, flax, hemp), industrial by-products (fruits and tuber waste, waste paper, waste pulp), and others (20,21). These feedstocks are currently used in low-value markets (e.g., animal bedding, cattle feed, ropes, electricity generation, etc.) or are disposed of. Thus, by using them to produce high-value CNF products, not only the process becomes more sustainable, but it also gives these feedstocks an increased market value.

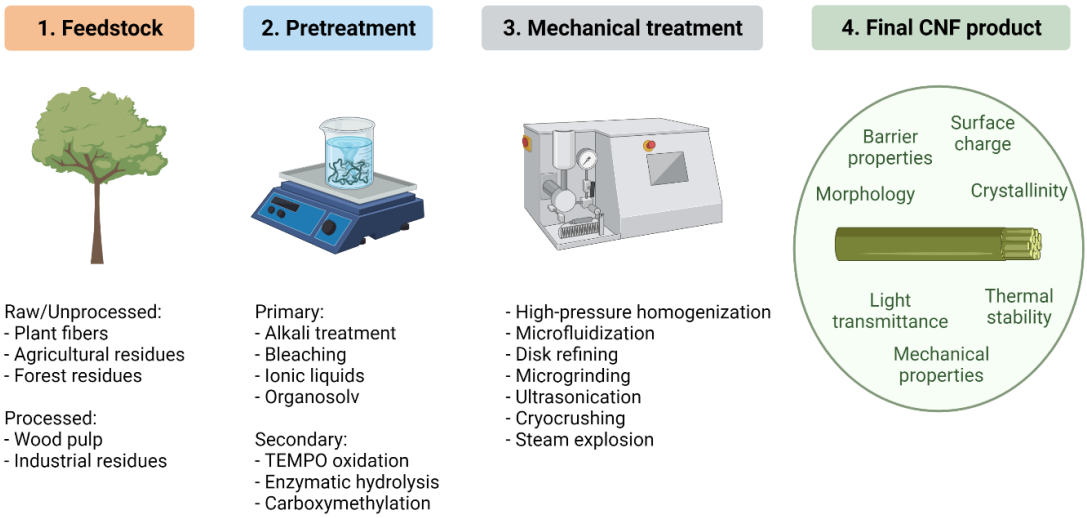

Figure 1.2. Scheme showing different types of processing steps that can be utilized in CNF production.

The second stage in CNF production is called pretreatment, and it is optional. Pretreatment usually refers to chemical or enzymatic treatments that can change the chemistry of the feedstock to either facilitate the mechanical fibrillation (third stage) and/or promote specific chemical changes to the fibers (1,3). Figure 1.2 includes examples of pretreatments currently used in the production of CNFs. When using a raw/unprocessed feedstock such as agricultural and forest residues, primary chemical pretreatments can be applied to remove specific biomass components (e.g., lignin and hemicellulose). These chemical pretreatments include alkali treatments, bleaching, ionic liquids, and organosolv (1,3). Furthermore, pretreatments such as TEMPO oxidation, enzymatic hydrolysis, and carboxymethylation are often considered as secondary pretreatments because they are usually performed on processed feedstocks like bleached pulp (3). Generally, secondary pretreatments promote chemical and physical changes to the cellulose fibers, facilitating the mechanical fibrillation step and/or adding specific surface functionalization to the fibers.

After the optional pretreatment stage, there is the mechanical fibrillation stage. This stage is crucial for decreasing the fiber size and isolating the nano-size fibrils, which requires intensive mechanical treatments (22). Several types of mechanical approaches to reducing the fiber size to the nano-level have been reported (Figure 1.2), such as high-pressure homogenization, microfluidization, refining, and ultrasonication (22). Some methods for CNF production are considered 'purely mechanical' as they do not include a pretreatment stage. An example of a purely mechanical process is that of the University of Maine. UMaine's process to produce CNF utilizes wood pulp as starting material that undergoes several passes in a refiner (23,24). Furthermore, the literature commonly refers to this purely mechanical process as a very energy-intensive and expensive process that is not economically feasible. As a common solution to this problem, the various pretreatment methods described above can be utilized to facilitate fibrillation during mechanical treatments, reducing its energy requirements. However, it is essential to realize that some pretreatments also come with drawbacks that should be considered, such as difficult scale-up, expensive chemicals or enzymes, toxic chemicals, and excessive depolymerization, among other issues (25).

As can be seen in Figure 1.2, the number of possibilities to produce CNF is vast due to the different choices of feedstock, pretreatment, and mechanical fibrillation techniques that can be used (26). Thus, depending on the process conditions, the resulting CNF products will present very different characteristics that can be suitable for different applications. In addition, CNFs can undergo post-production surface modification reactions to incorporate specific chemical functionalization into the material (1). For example, acetylation modifications can make CNFs more hydrophobic so they can be dispersed in nonpolar polymeric matrices (27), and the addition

of specific chemical groups in the fibrils can make them able to absorb certain pollutants in water treatment applications (14).

1.4 LIGNOCELLULOSIC NANOFIBRILS

The combined utilization of raw/unprocessed feedstocks with mild pretreatment reactions results in a unique type of CNF product containing not just cellulose, but also hemicellulose and residual lignin, which is referred to as lignocellulosic nanofibrils (LCNFs) or lignin-containing cellulose nanofibrils in some cases (19,28). In LCNF production, the different components from biomass' native state are preserved, resulting in higher yields. Process-wise, eliminating the several process steps involved in making the high-purity pulp (i.e., intensive pulping and bleaching) significantly reduces production costs. In addition, using low-cost waste feedstocks to produce nanomaterials is much more sustainable than using the conventional bleached pulp. Therefore, LCNFs comprise a new way to make nanomaterials with significant economic and environmental benefits compared to the conventional types (19).

LCNFs also present unique properties that pure cellulose CNFs do not have due to the presence of hemicellulose and lignin components (Figure 1.3). Hemicellulose is a low molecular weight, highly-branched heteropolysaccharide containing uronic acid groups (depending on the feedstock type) that promote easier fibrillation colloidal stability of the nanocellulose product (29,30). Lignin, on the other hand, is a highly-crosslinked aromatic molecule that can promote hydrophobicity, UV absorption, improved barrier properties, and thermal stability (31,32). These two components, along with cellulose fibers that confer strength and rigidity, form a nanomaterial with excellent properties. Therefore, LCNFs have been considered for applications such as thin barrier films in packaging and reinforcing agent in polymer composites and paper products (19).

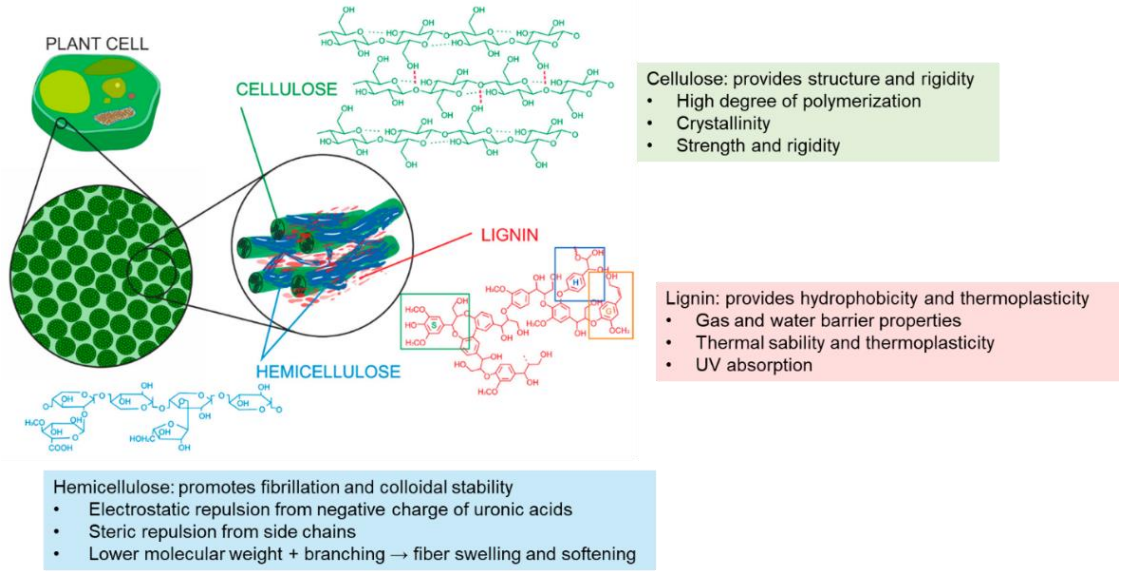

Figure 1.3. Scheme showing specific properties derived from different plant cell wall components (i.e., cellulose, hemicellulose, and lignin).

1.5 LABORATORY TO INDUSTRY: MARKET PERSPECTIVES

Because of the enormous application potential of nanocellulose, its desirable properties, and its sustainability benefits compared to petroleum-based chemicals and materials, the market for this biomaterial is expected to grow rapidly. Nanocellulose market is projected to grow 30% annually, reaching a volume around 250,000 tonnes of nanomaterials in 2025 (33). The CNFs product segment contributes to the largest market share of nanocellulose products (more than 50%), followed by CNCs, bacterial nanocellulose (BNC), and others - and this difference is expected to keep growing in the following years (34). In addition, the composites and packaging applications represent the major market driver for nanocellulose (34,35). As can be seen, there is a lot of potential for utilizing nanocellulose in the current market, especially for CNFs applied in composites and packaging. Yet, the worldwide production of nanocellulose products is far from reaching this high demand. According to TAPPI Nano 2018 Cellulose Nanomaterials Production

Summary, less than 13,000 tonnes/year of nanocellulose products were reported to be produced worldwide, with CNFs representing only 10% of this capacity (36).

Currently, the leading global producer of nanocellulose products is FiberLean Technologies (UK), with the capacity to produce 8,800 dry tonnes/year of microfibrils (~100 nm in width) via co-grinding mineral with pulp fibers (36,37). Other key producers include Borregaard (Norway), with a capacity of 1,100 dry tonnes/year of microfibrils (widths ranging between 20 - 300 nm) (36,38); Nippon Paper Industries Co. (Japan), with 560 dry tonnes/year of nanofibrils (3 - 4 nm in width) (36,39), thus producing the smallest nanofibrils from all companies due to the utilization of TEMPO oxidation method; and University of Maine (US) with a production capacity of 260 dry tonnes/year of CNF (widths ranging between 5 – 200 nm) through purely mechanical treatments (i.e., pulp refining) (36,40). Altogether, as of 2018, the total reported production capacity of CNFs was less than 12,000 dry tonnes/year globally (36), which is not enough to reach the current market potential for these products.

One of the main reasons for the low CNF production capacity worldwide is the high production costs. Nanocellulose production is very capital-intensive, therefore requiring high initial investments. The high production costs make scale-up more challenging, which in turn increases the price of nanocellulose products and limits their applications. As a result, most CNF produced nowadays is used mainly in lab-scale research efforts or low-volume applications. An exception to this rule is the case of paper product application since CNFs can be made in-house at pulp and paper mills and utilized in their own products, therefore significantly reducing their costs (33,36,41). In order to have CNF manufactured at large-scale and enable its utilization in various applications, the barrier of production costs must be addressed. Only by achieving cost-effective

and scalable production practices the transition of CNF from the laboratory to industry will be possible.

1.6 RESEARCH OBJECTIVES

The research presented in this dissertation aimed to develop a sustainable and scalable process to produce nanocellulose from low-cost, unconventional waste feedstocks with the ultimate goal of making this biomaterial more affordable and accessible to its many applications. To achieve this goal, this project employed a unique research approach at the intersection of process engineering, computational modeling, and material science. This interdisciplinary approach enabled the a) development of a comprehensive and robust conversion process in the laboratory and collection of key conversion yields and characterization data; b) determination of economic feasibility of a large-scale operation based on the process developed therein; and c) application of the nanomaterials as polymeric reinforcing agents in plastic composites.

The specific objectives of this research included:

1. Developing a new conversion process to obtain lignocellulosic nanomaterials from wheat straw feedstock. An environmentally-friendly pretreatment was evaluated as an alternative to conventional TEMPO oxidation pretreatment, and the produced nanomaterials were characterized and compared. Finally, the application of these nanomaterials as polymeric reinforcing agents in plastic composites was investigated.
2. Performing techno-economic analysis (TEA) of the proposed process in Objective 1 through modeling and simulation techniques to determine the production costs of a large-scale operation and the minimum product selling price (MPSP) of the nanomaterials generated. The impact of facility size and co-location on final MPSP was also evaluated.

3. Assessing the robustness of the process developed in Objective 1 by utilizing different types of waste feedstocks, including corn stover, industrial hemp stalks, and reed canary grass, to produce lignocellulosic nanomaterials. The impacts of feedstock chemical and physical characteristics on the production yields and the final nanomaterials' properties were elucidated.

1.7 DISSERTATION OVERVIEW

This dissertation comprises three original research papers that will be individually submitted to peer-review journals for publication. For this reason, Chapters 2, 3, and 4 of this dissertation include their own summary, introduction, methods, results and discussion, and conclusions. Chapter 2 comprises the first research paper about the development of a conversion process to produce lignocellulosic nanomaterials from wheat straw and their application in plastic composites. Chapter 3 consists of the second research paper about the economic feasibility of a large-scale facility based on the process developed in Chapter 2. Then, Chapter 4 presents the third research paper about testing the robustness of the process developed in Chapters 2 and 3 using different heterogeneous feedstocks. Finally, Chapter 5 summarizes the key conclusions from all three studies from a broader impact perspective and provides direction for future work.

Chapter 2. Lignocellulosic nanomaterials production from wheat straw via peracetic acid pretreatment and their application in plastic composites

2.1 SUMMARY

Cellulose nanofibrils are typically prepared from high-purity bleached pulp through harsh chemical treatments (e.g., TEMPO oxidation), resulting in high costs and environmental impact. In this work, we utilize inexpensive wheat straw feedstock and alkaline peroxide pulping followed by mild peracetic acid (PAA) pretreatment to produce lignocellulosic nanomaterials (nano and microfibrils) with potential bioplastics applications. PAA was chosen due to its biodegradability, non-toxicity, and high reaction selectivity. As-synthesized lignocellulosic nanomaterials were thoroughly characterized and compared to nanofibrils produced via TEMPO oxidation pretreatment and then applied as reinforcing agents in plastic composites. A remarkable case of simultaneous strengthening and toughening of the polymer nanocomposite was achieved with high specific tensile strength (up to 59.5 MPa g^{-1} cm^3), elastic modulus (up to 2.6 GPa g^{-1} cm^3), and fracture strain (up to 138%). This work is a comprehensive investigation of all process steps involved in lignocellulosic nanomaterials production, from original residue feedstock to final product application.

Pascoli DU, Dichiara AB, Roumeli E, Gustafson R, Bura R.

Manuscript published in Carbohydrate Polymers journal (2022)

2.2 INTRODUCTION

Cellulose nanofibrils (CNFs) have unique properties (e.g., large surface area, biocompatibility, outstanding mechanical properties, low thermal expansion, low density, and biodegradability) that make them a great candidate for application in packaging, construction, cosmetics, biomedical, automotive, papermaking, and more (1). For example, CNF is a biomaterial that can be used in polymer composites to reduce the amount of fossil-based plastics used in packaging, thereby reducing the environmental issues associated with plastics production and disposal. If 5% of the 367 million tonnes of plastic produced globally in 2020 were replaced by CNF, it would generate a market of about 18 million tonnes of CNF per year (42,43). Still, the full potential of CNF utilization in various markets is hindered by its low production capacity and high price. As of 2018, the worldwide production of nanocellulose products (including fibrils and crystals) was about 12,290 dry tonnes/year, with CNF representing only 10% of this capacity (36). The low CNF production capacity reflects its current market prices, reaching up to $1,000/kg depending on the product specifications (e.g., fiber size, type of feedstock and pretreatment utilized, surface modification, etc.) (9,44). Thus, to promote the use of nanofibrils in applications such as plastics, we must continue developing lower-cost manufacturing processes (41).

Commonly, CNF is produced from bleached wood kraft fibers, a premium feedstock containing virtually pure cellulose costing US$800-1,600/tonne (varying with wood type, pulping and bleaching process, and location) (45,46) that undergo mechanical fibrillation to isolate the nanofibrils. Due to the high energy demand of mechanical fibrillation, different pretreatment techniques can be utilized to facilitate the fibrillation step and reduce energy requirements. TEMPO (2,2,6,6-Tetramethylpiperidin-1-oxyl) oxidation is one of the most widely accepted pretreatment technologies for the production of CNF. It promotes the oxidation of cellulose fibers,

increasing their surface charge density, which results in electrostatic repulsion between the fibers and high nanofibrillation yields (47). The main drawbacks of using TEMPO oxidation are the high chemical costs and TEMPO's toxicity (48) (TEMPO oxidation requires expensive separation processes, such as dialysis, to remove trace amounts of residual TEMPO from fibers). For these reasons, TEMPO oxidation is not suitable for industrial-scale operations. To achieve economic success on a large-scale, CNF production requires a more cost-effective conversion technology (49).

The production of lignocellulosic nanofibrils (LCNF) is a promising solution to this issue. It utilizes cheaper, lignin-containing feedstocks instead of the fully bleached pulp, along with mild treatments, resulting in high-yield products containing cellulose, hemicellulose, and lignin components (28). Studies have shown that hemicellulose and lignin can provide unique properties to the final materials. Hemicellulose is known to promote easier fibrillation and colloidal stability, while lignin provides hydrophobicity and improved barrier properties (29–32). Various feedstocks have been used to produce LCNF, including unbleached wood pulp, wood chips, sugarcane bagasse, switchgrass, wheat straw, among others (19). Wheat straw (WS), the by-product of wheat production comprising the stalk leftover after harvesting the wheat grains, is an excellent feedstock choice due to its high availability. The United States is the fourth largest wheat-producing country in the world (50), with an annual production of about 52 million tonnes during the 2019/20 period (51). Furthermore, because it is an agricultural residue, WS prices are considerably lower than that of other types of feedstocks, costing between US$60-100/tonne depending on quality and location (52). Thus, WS represents an inexpensive and abundantly available non-wood fiber source for the production of high-value lignocellulosic nanomaterials.

Several processes to produce LCNF have been reported in the literature, and excellent reviews of these processes can be found elsewhere (19,28). Among those, a relevant method includes LCNF production from Norway spruce fibers via SO_2-ethanol-water pulping, which is based on the AVAP® process employed by American Process Inc. (31). Still, the costs associated with this process can be high as it utilizes expensive woody biomass feedstock and more severe process conditions (elevated temperature and pressure). Ideally, a process should be simple, cheap, and environmentally friendly for easy scale-up, which can be achieved using mild reaction conditions (atmospheric pressure, low temperatures) and non-toxic chemicals. In this scenario, peracetic acid (PAA) pretreatment is a promising alternative, as this chemical is biodegradable and reacts with lignocellulosic biomass at temperatures lower than 100 °C. PAA is known for its strong oxidation potential that selectively removes lignin while simultaneously protecting carbohydrates from solubilizing, promoting higher yields. In addition, PAA may oxidize the reducing ends of carbohydrates, creating a negative surface charge that can help nanofibrillation and promote stable colloidal suspensions (53–55).

PAA pretreatment offers many advantages compared to the conventional TEMPO oxidation method for CNF production. PAA is less toxic and more environmentally friendly than TEMPO and provides better control over removing lignin and hemicellulose from the pulp material. TEMPO oxidation is an extensive reaction carried out using strong delignifying agents (NaClO), which results in a final material with very low lignin content and high hemicellulose losses. Thus, the PAA approach enables higher process yields than TEMPO oxidation by keeping more of the different native components from the original material. In addition, PAA and TEMPO have different oxidation mechanisms – PAA only oxidizes the reducing ends of carbohydrates, while TEMPO oxidizes the C6 hydroxyl groups of cellulose that are present in a much higher number.

Hence, the final surface charge of the fibrils produced via PAA and TEMPO will differ significantly. To this date, research employing PAA treatments for the production of CNF or LCNF remain relatively scarce. Studies on PAA-synthesized CNFs typically aim at the complete removal of lignin, and other subsequent treatments are sometimes performed for the complete removal of hemicellulose as well, resulting in pure cellulose CNFs with lower mass yields (56–58). To the best of our knowledge, no studies have conducted mild PAA pretreatment yet, aiming to keep as much hemicellulose and residual lignin in the final LCNFs for improved yields. The structure and composition of the nanofibrils produced via PAA treatment vary greatly from those prepared via conventional TEMPO oxidation, providing unique opportunities to examine how these differences influence their physico-chemical properties and their applications in polymer composites.

As mentioned above, CNFs can be used as additives in plastic composites to reduce the amount of petroleum-based compounds and improve the composites' properties. In particular, biodegradable and hydrophilic polymers, such as poly(vinyl alcohol) (PVA), are known to have inferior mechanical properties than their synthetic counterparts, such as polyethylene (PE), therefore requiring the incorporation of other various additives to enhance its properties (59). Previous studies have reported that CNFs can improve the mechanical performance of PVA nanocomposites when added at very low amounts (i.e., <5 wt.%) due to CNFs high aspect ratio, large surface area, and good interfacial interactions with PVA matrix. Most of these studies assessing CNF reinforcement of PVA either use commercially available CNFs (60,61), or utilize bleached pulp to produce the CNFs (62–64), while only one study thus far has investigated the use of LCNFs prepared from lignocellulosic biomass in such composites (65).

In this work, we aim to demonstrate that by utilizing low-cost agricultural residue feedstock (wheat straw) along with mild alkaline peroxide pulping followed by environmentally friendly PAA pretreatment instead of harsh TEMPO oxidation pretreatment, nanomaterials with good plastic reinforcing properties can be obtained. The proposed process comprising PAA pretreatment results in nanomaterials with different structure and composition than that obtained via TEMPO oxidation, thus the impact of such differences in their application in polymer composites is also investigated. Therefore, this work comprehensively investigates all steps involved in lignocellulosic nanomaterials production, from original residue feedstock to final product application. First, by using biomass raw material and mild process conditions, the hemicellulose and lignin components were preserved along with cellulose, resulting in lignocellulosic nanomaterials (nanofibrils and microfibrils) with high yields. The changes in the chemical composition of the WS fibers after each chemical reaction were also assessed. Then, the lignocellulosic nanomaterials produced via PAA pretreatment were thoroughly characterized (light transmittance, surface charge density, crystallinity, FTIR, fiber morphology, thermal stability) and compared to nanofibrils obtained via TEMPO oxidation. Finally, all fibrils produced were added to PVA plastic nanocomposites as reinforcing agents, and the final properties of the composites were correlated with the chemical and morphological characteristics of the fibrils.

2.3 Materials and Methods

2.3.1 Materials

Wheat straw (WS) bales were sourced from Snohomish County, WA. Sample preparation consisted of cutting the whole wheat straw into half-inch pieces using a hand pruner. The feedstock was air-dried (moisture content 6.7%) and stored in closed containers at ambient temperature until use.

Polyvinyl alcohol (99+% hydrolyzed, molecular weight 89,000-98,000) and 32% (w/w) peracetic acid were purchased from Sigma Aldrich. Other reagents include: 50% (w/w) sodium hydroxide (VWR Chemicals BDH), 50% (w/w) hydrogen peroxide (Cascade Columbia Distribution), diethylenetriamine pentaacetic acid (DTPA) 98+% (Acros Organics, Fisher Scientific), 2,2,6,6-Tetramethylpiperidine 1-oxyl (TEMPO) (Tokyo Chemical Industry), sodium bromide (VWR), sodium hypochlorite (VWR).

2.3.2 Alkaline peroxide pulping and refining

The mild delignification of wheat straw was done by alkaline peroxide pulping and the reaction conditions employed were selected after a comprehensive screening analysis (shown in Appendix A, Table A.1). First, untreated biomass was mixed with alkaline peroxide solution (15% NaOH, 7.5% H_2O_2, and 0.15% DTPA in water) and the reaction was held at 90°C for 150 min, followed by quenching in an ice bath. Next, the sample was vacuum filtered to separate the pulp from the spent liquor. The pulp was extensively washed with deionized (DI) water until the conductivity of the wash water was lower than 5 µS and the pH reached neutral. Finally, the washed pulp was refined using a laboratory PFI mill for 30,000 revolutions, resulting in WS refined pulp.

2.3.3 Peracetic acid pretreatment

WS refined pulp was treated with peracetic acid (PAA) based on a previously reported procedure (56) with modifications.. In their study, Yang et al. performed PAA treatment in four consecutive rounds, while in the present study the chemical pretreatment was only performed once. First, the refined pulp was mixed with PAA solution at pH 4.8 in a plastic bottle, and the reaction was carried out at 85 °C for 45 min. Vacuum filtration was used to separate the pretreated pulp from the spent chemicals and a two-step pulp wash was also performed according to methods described by Yang

et al. PAA pretreated pulp was mechanically fibrillated at 0.4% consistency for 30 min using a blender. The suspension obtained after fibrillation was centrifuged, resulting in two product fractions, LCNF and LCMF. LCMF was further subjected to homogenization at 0.1% consistency using a high-pressure microfluidizer coupled with an 80 μm diameter Z-type interaction chamber at a pressure of 10,000 psi (≈70 MPa) for 20 passes.

2.3.4 Lignocellulosic fibrils (nano and micro) production

PAA pretreated pulp was mechanically fibrillated using a blender and centrifuged, resulting in two product fractions that fall under the standard definition of "nanocellulose" or "cellulose nanomaterial" (i.e., fibrils composed predominantly of cellulose with any dimension in the nanoscale from 1 to 100 nm) (66,67). The supernatant fraction contained individual elementary fibrils up to 5 nm wide - denominated as lignocellulosic nanofibrils (LCNF) (4), while the precipitate contained fibrils 10-100 nm - denominated as lignocellulosic microfibrils (LCMF) (5,6). LCMF was further subjected to homogenization using a high-pressure microfluidizer and subsequently centrifuged to separate the homogenized H-LCNF (supernatant) and H-LCMF (precipitate). LCNF and H-LCNF suspensions were concentrated by vacuum-rotary drum evaporation at 90°C. All samples were stored in glass bottles at room temperature until use.

For comparison purposes, TEMPO-oxidized lignocellulosic nanofibrils (TEMPO-LCNF) were prepared from WS refined pulp based on a previously reported procedure (68) with minor modifications including a higher NaClO charge of 10 mmol/g pulp, and a total reaction time at pH 10-10.5 of 2 h followed by another 2 h at a pH 7. The pulp solution was centrifuged, and the precipitated pulp was dialyzed in DI water for several days. The resulting sample is the TEMPO-pretreated pulp. TEMPO-pretreated pulp was fibrillated at 0.4% consistency for 30 min using a blender. The suspension obtained was further sonicated using a horn sonicator for 2 min. The

sonicated solution was centrifuged to separate the TEMPO-LCNF (supernatant) from any rejects (precipitate). TEMPO-LCNF sample was stored in a glass bottle at room temperature until use.

In addition, a pretreatment control (PC) was also prepared by fibrillating the WS refined pulp (without pretreatment) with a blender, followed by centrifuging.

2.3.5 Characterization techniques

Mass yield after pulping and pretreatment

After pulping and pretreatment (PAA or TEMPO), the total mass yield was determined gravimetrically by comparing the oven-dry (OD) weight of fibers obtained after each process with that of the starting original WS.

Chemical composition

To evaluate the effects of each chemical treatment step performed in this study, the chemical composition of original WS, WS refined pulp, PAA pretreated pulp, and TEMPO pretreated pulp were assessed. The carbohydrates and lignin content (including both acid-soluble and acid-insoluble lignin) were quantified according to methods previously described by our research group (69–72). Ash content was measured gravimetrically (73), and total extractives content was determined by water and ethanol Soxhlet extraction with a 12 h reflux time (74).

Product separation yield

The product separation yield was determined by centrifugation. All samples underwent a centrifugation step to separate the final products. For TEMPO pretreatment, only one fraction of product was obtained (TEMPO-LCNF), whereas, for the process proposed in this study, two fractions of products (precipitate/supernatant) were obtained after centrifugation (LCMF/LCNF

and H-LCMF/H-LCNF). The product separation yields, expressed as percentages, were calculated by the OD weight ratio of each product fraction to the pre-centrifugation suspension.

Optical transmittance of suspensions

Optical absorption spectroscopy of 0.2 wt.% suspensions was conducted using UV/VIS/NIR Spectrophotometer (Lambda 750, PerkinElmer) in the visible region (from 400 to 800 nm) at a scan resolution of 1 nm. DI water was used as a blank. The light transmittance was evaluated using the percent transmittance at 660 nm (65).

Fiber morphology

Optical microscope images of LCMF and H-LCMF were collected using a Carl Zeiss Axiolab E re light microscope coupled with a Carl Zeiss Axiocam ERc 5s digital camera (Germany). Prior to imaging, 10 µL aliquots of LCMF and H-LCMF suspensions were drop-casted on clean glass microscope slides. Both samples had the same concentration before the analysis. ImageJ software was used to analyze the fiber width.

Scanning Electron Microscopy (SEM) images of LCMF and H-LCMF were collected using an Apreo S (Thermofisher Scientific) coupled with a standard ETD in-chamber SE detector and a T2 in-column SE detector. Operating conditions were at high vacuum with an acceleration voltage of 2 kV and beam current of 6.3 pA. SEM sample prep consisted of bath sonicating a 0.01 wt.% LCMF suspension for 3 min and drop-casting 10 µL onto a clean SiO_2 wafer (Ted Pella Inc.). The sample was sputter-coated with 4 nm thick platinum layer using a Leica EM ACE600 coater (Leica Microsystems) prior to imaging. The morphology was determined by measuring the width of at least 20 individual fibers using ImageJ software.

Atomic Force Microscopy (AFM) images of LCNF, H-LCNF, and TEMPO-LCNF were collected using a Cypher ES AFM (Oxford Instruments) in tapping mode with bluedrive

photothermal excitation and a scan rate of 2 Hz. First, samples were diluted with DI water to a 0.00055 wt.% concentration and bath sonicated for 5 min to promote dispersion. 50 µL of LCNF was drop-casted onto a freshly cleaved mica disc (Ted Pella Inc.) that was previously coated with 50 µL of L-lysine, rinsed with DI water, and air-dried. Differently, 10 µL of TEMPO-LCNF was drop-casted onto a freshly cleaved mica disc without any coating. Both samples were left to air dry for 1 h prior to imaging. Fiber morphology was determined by measuring the width and length of at least 20 individual fibrils. Gwyddion software was used to analyze the fiber width estimated by the fiber height, and ImageJ software was used to analyze the fiber length.

Conductometric titration and charge density

Charge density was determined by conductometric titration based on the method described by Besbes et al. (75) with minor modifications. 0.5 mL of 0.1 M HCl was added to 50 mL of 0.1 wt.% sample suspension and mixed for 10 min to protonate the carboxyl groups. Then, a titration was performed with 100 µL increments of 0.02 M NaOH, and the conductivity values were measured and recorded using a conductivity meter. The charge density (µmol COOH/g) was determined according to Equation 2.1, where V1 and V2 are the volumes of NaOH required to neutralize the excess HCl and carboxylic acid, respectively.

$$\text{Charge density} = \frac{(\text{V2} - \text{V1}) \times \ [\text{NaOH}]}{\text{sample oven dry weight}} \qquad \text{Eq. 2.1}$$

X-ray Diffraction (XRD)

Crystallinity was determined by X-ray Diffraction (XRD) using a Bruker D8 Discover coupled with a Pilatus 100K large-area 2D detector and a Cu Kα radiation generated at 50 kV and 1 mA. Diffractograms of neat films were taken over a 2Θ angular range of 10°-50° with 0.02° steps. The crystallinity index (CI) was calculated based on the Segal method, as described in Equation 2.2:

$$CI\ (\%) = \frac{I_t - I_a}{I_t} \qquad \text{Eq. 2.2}$$

Where I_t is the intensity of the crystalline peak (2 0 0) at 2Θ = 22.7° and I_a is the intensity of the amorphous peak (1 1 0) at 2Θ = 18° (76).

Fourier-transform infrared spectroscopy (FTIR)

Infrared spectra were analyzed using FT-IR Prestige-21 spectrometer (Shimadzu) coupled with a DLATGS detector attached to MIRacle ATR (PIKE Technologies). The spectrum was collected at ambient conditions in the range of 550-4000 cm^{-1} with a resolution of 4 cm^{-1} and from an accumulation of 40 scans.

Thermogravimetric analysis (TGA)

Thermal stability of different samples were assessed using thermogravimetric analyzer (TGA 550, TA Instruments). The samples were analyzed by heating from room temperature to 600 °C at a heating rate of 10 °C/min under nitrogen atmosphere (60 mL/min).

2.3.6 PVA composite films

PVA composite films preparation

Polyvinyl alcohol (PVA) composite films were prepared via casting method as previously reported (61) with minor modifications. PVA composite films were reinforced with 5 wt.% of lignocellulosic fibrils (LCMF, H-LCMF, LCNF, H-LCNF, and TEMPO-LCNF) unless otherwise specified, and a neat PVA sample was prepared as a control. Because the H-LCNF sample showed different reinforcing trends than all other samples (as shown in subchapter 2.4.6), PVA composites with different H-LCNF contents (2.5, 5.0, and 7.5 wt. %) were further prepared. As-prepared

nanocomposite films were conditioned for 48 h at 25°C and 50% relative humidity prior to further testing.

PVA composite films characterization

Optical transmittance spectra of PVA composite films were determined by UV/VIS/NIR Spectrophotometer with scans ranging from 400 to 800 nm. The light transmittance of different samples was evaluated using the percent transmittance at 660 nm (65).

Mechanical properties of composite films were determined using a tensile tester (standard method ASTM D638-10) with a gauge length of 50 mm (65). First, films were cut into 70 mm x 15 mm test specimens and their thickness was measured at five different points with a Digimatic Micrometer (Mitutoyo, Japan). The basis weight of each sample was determined according to the TAPPI method T410 (77), and the sample's density was calculated by dividing their basis weight by thickness. The test specimens' thickness and density are shown in Appendix A, Table A.3. The specific tensile strength and Young's modulus were calculated as the original values obtained from the stress-strain curves divided by each test specimen's density. A minimum of 5 test specimens per sample was tested.

The fracture surface of PVA composite films were examined using SEM with an acceleration voltage of 2 kV and beam current of 13 pA. The samples were fixed to a metal holder using carbon tape and sputter-coated with 4 nm thick platinum layer prior to imaging.

2.4 Results and Discussion

As seen in Figure 2.1, TEMPO-LCNF had a much higher separation yield than the other samples, resulting in only one product fraction. In contrast, two product fractions were obtained for the PAA process after each separation step. After PAA pretreatment and mechanical fibrillation, the yield

of LCMF was much higher than LCNF (96% and 4%, respectively). Then, by introducing the homogenization step, the yield of H-LCNF increased significantly to 36%, revealing that higher defibrillation energy is required to release the nanofibrils. Even though homogenization can be costly, this process change may be economically beneficial as nanofibrils are a higher value product compared to microfibrils.

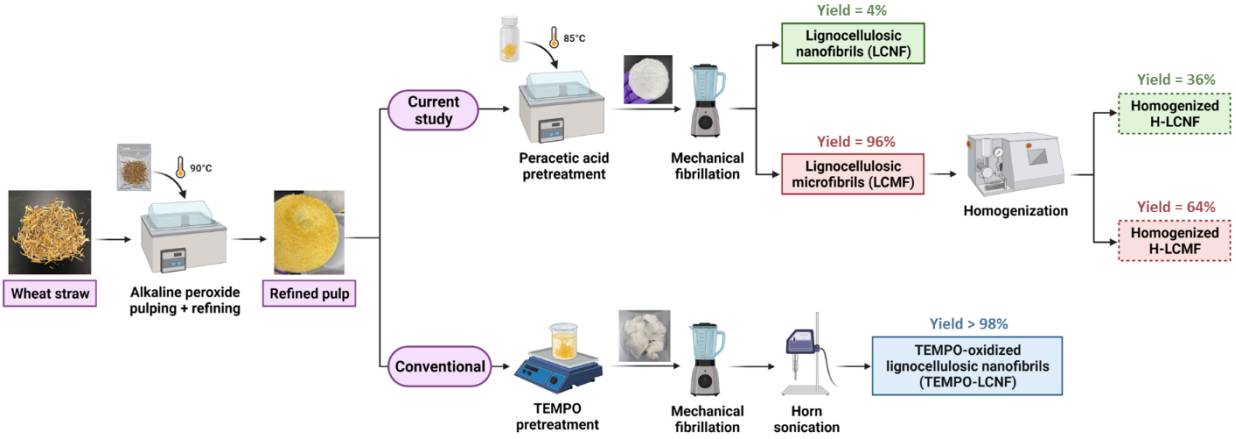

Figure 2.1. Illustration of the process developed to convert wheat straw to lignocellulosic nano and microfibrils via peracetic acid pretreatment. Conventional TEMPO oxidation pretreatment was performed as a comparison.

2.4.1 Effect of chemical treatments on fiber chemical composition

Changes in chemical composition and mass balance throughout the process, including total mass yield as well as sugar (cellulose and hemicellulose) and lignin recovery related to original WS, are presented in Table 2.1. The selected alkaline peroxide pulping conditions (for other screened conditions, see Appendix A, Table A.1) removed 81% of lignin from the original WS, resulting in pulp with only 8.2% lignin, thus validating the effectiveness of the delignification step. A similar pulping process was explored in prior studies, where a wheat straw delignification of up to 60% was obtained through alkaline peroxide pulping (78). The higher lignin removal obtained in the current study can be attributed to different reaction conditions (temperature, time, and chemical

charges). Unlike lignin, virtually all the cellulose (100%) and the majority of hemicellulose (80%) remained in the refined pulp, indicating a low sugar loss during the reaction. Hemicellulose was more susceptible to solubilization during pulping than cellulose because of its lower molecular weight, higher branching, and direct linkages with lignin (i.e., lignin-carbohydrate complexes). The delignification and partial solubilization of hemicelluloses linked to lignin result from the formation of radicals (hydroxyl and superoxide anion) during the reaction, causing the oxidation of lignin molecules to form alkali-soluble moieties (79,80).

In general, conventional delignification methods such as Kraft, soda, and sulfite pulping require high temperatures (above 100 °C) and high pressure, significantly increasing the production costs (81). Likewise, the high temperatures (135-155 °C) employed in SEW pulping (31) also require steam generation and pressurized systems, consequently increasing the capital costs of the process at a large scale. Besides the cost factor, the harsh conditions utilized by these pulping methods usually result in a final material containing only trace amounts of hemicellulose and lignin, thus lowering the yields. For instance, a study by Sánchez et al. reported that different pulping methods (soda, organosolv, and kraft) resulted in WS pulp yields between 40-50% (82). As for SEW pulping, the required high temperatures and acidic nature commonly lead to high hemicellulose solubilization, yielding fibers comprising mostly cellulose and some lignin depending on the reaction conditions (31). Therefore, treatments at alkaline pH and lower temperatures are desired to keep the hemicellulose in the product and increase yields. The mild alkaline peroxide pulping process utilized in the present study resulted in a substantial WS pulp yield of 66% by keeping most of the hemicellulose and part of the lignin in the fibers. The higher mass yield is good for the process' viability, as more of the original biomass feedstock is kept in the final product, and less is wasted.

After the delignification step, two different pretreatments (PAA and TEMPO oxidation) were separately performed and compared (Figure 2.1). The primary goal of PAA pretreatment was to oxidize the reducing ends of carbohydrates before the mechanical fibrillation step. PAA is known for its strong oxidation potential that selectively removes lignin while simultaneously protecting carbohydrates from solubilization (53,54). The PAA pretreatment resulted in higher mass yield (related to original WS biomass) than TEMPO pretreatment (53% and 48%, respectively) because of its higher cellulose, hemicellulose, and lignin recovery (Table 2.1). These results are attributed to the mild PAA delignification in contrast to the more aggressive TEMPO oxidation. The NaClO employed during TEMPO oxidation is a strong delignifying agent, resulting in TEMPO pretreated pulp with only 1% lignin content. In addition, PAA is a biodegradable, non-toxic chemical that does not require extensive dialysis time. Dialysis is commonly done after TEMPO oxidation; it takes several days and large amounts of water, thus reducing the feasibility of the process for large-scale operations. Therefore, PAA pretreatment is advantageous to be implemented at an industrial scale compared to TEMPO oxidation due to its high yield and simplicity – it employs a safe and biodegradable chemical that can be removed with simple rinsing process units.

Table 2.1. Chemical composition of original WS, WS refined pulp, PAA pretreated pulp, and TEMPO pretreated pulp, and mass balance results related to original WS.

	Chemical composition (%) [a]					**Mass balance [b]**			
	Cellulose	**Hemic.**	**Lignin**	**Ash**	**Extractives**	**Mass yield %**	**Cellulose recovery %**	**Hemic. recovery %**	**Lignin recovery %**
Original WS	35.6 ± 0.1	22.0 ± 0.0	28.1 ± 0.4	11.4 ± 0.1	13.4 ± 0.0	-	-	-	-
WS refined pulp	57.7 ± 0.7	26.6 ± 0.3	8.2 ± 0.1	1.9 ± 0.1	2.7 ± 0.3	65.8	99.9	79.6	19.2
PAA pretreated pulp	67.1 ± 0.5	25.5 ± 1.0	7.0 ± 0.4	0.3 ± 0.0	0.0 ± 0.0	52.9	99.7	61.3	13.2
TEMPO pretreated pulp	69.4 ± 0.9	19.6 ± 1.3	1.2 ± 0.0	0.0 ± 0.0	0.0 ± 0.0	48.0	93.5	42.8	2.1

[a] Chemical composition as a percentage of the OD weight of each sample. Average of triplicate measurements. For detailed carbohydrate composition, see Appendix A, Table A.2.

[b] Mass balance was calculated by assuming no mass loss during mechanical treatment steps and correlating the chemical composition and mass yield at each stage to the starting original WS.

2.4.2 Lignocellulosic fibrils suspensions and optical transmittance

After the mechanical treatments, all lignocellulosic fibrils (nano and micro) formed homogeneous gel-like suspensions with good colloidal stability (Figure 2.2 inset), while the pretreatment control (PC) was very unstable and quickly sedimented (Appendix A, Figure A.1). Suspension stability can be attributed to several factors, including small fibril widths, higher surface area, and electrostatic stabilization due to charge repulsion (83). These results demonstrate that the pretreatment step (either PAA or TEMPO) was essential to obtain fibrils with the appropriate morphology and surface chemistry to form stable aqueous dispersions. Furthermore, the fact that PAA pretreated fibrils (LCMF, LCNF, H-LCMF, and H-LCNF) presented good colloidal stability, even though their charge density was considerably lower than that of TEMPO-LCNF (Figure 2.3), can be attributed to their high hemicellulose content (Table 2.1). Hemicelluloses are known to improve fibrillation and contribute to colloidal stability by both coulombic (glucuronic acid groups in hemicellulose that provide negative charge) and steric repulsions (bulky side chains of hemicellulose that prevent cellulose fibers from aggregating) (28). Therefore, the mild process conditions employed in the present process were essential to keep as much hemicellulose as possible in the final product and enable colloidal stability of the lignocellulosic fibrils' suspensions even at low charge densities.

Figure 2.2 also shows the optical transmittance spectra of the different lignocellulosic fibrils' suspensions. It is known that light transmittance percentage can be correlated to the size of the fibrils dispersed, where larger fibrils scatter more light, resulting in lower transmission values (84). Thus, LCMF and H-LCMF exhibited a milk-white appearance and, consequently, had the lowest

light transmittances at 660 nm (24% and 11%, respectively) due to the presence of larger light-scattering fibrils. In contrast, the much higher transmittance of LCNF and H-LCNF (90% and 88%) indicates a smaller fibril size. TEMPO-LCNF presented similar behavior as LCNF and H-LCNF in suspension, with light transmittance of 88%, indicating that these fibrils are in the same size range.

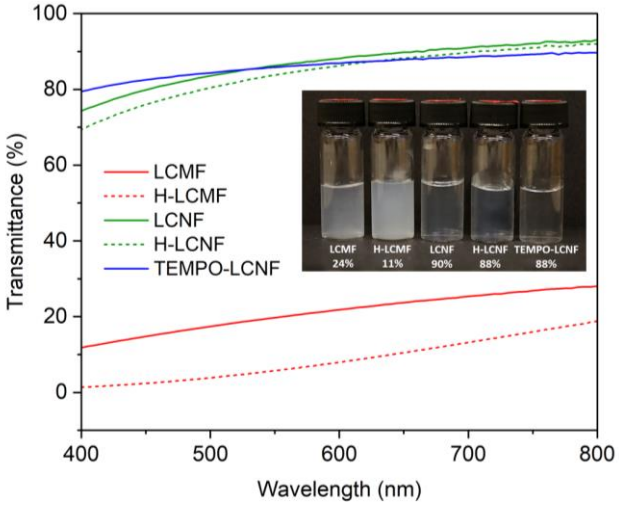

Figure 2.2. Optical transmittance spectra of different lignocellulosic fibrils suspensions. Inset shows a photograph of the suspensions and their respective percent transmittance at 660 nm.

2.4.3 Lignocellulosic fibrils surface chemistry

FTIR spectra showing specific chemical bonds of the lignocellulosic fibrils, as well as their charge density (CD) values obtained by conductometric titration, are shown in Figure 2.3. While the PAA oxidation mechanism targets only the reducing end-groups in polysaccharides, TEMPO oxidation targets the C6 hydroxyl groups in the cellulose fibers (66), and C6 hydroxyl groups are present in considerably larger numbers relative to reducing end-groups. For this reason, TEMPO-LCNF showed the highest CD (1088 μmol g^{-1}) among all samples, while PAA pretreated samples showed overall lower CD ranging from 105-266 μmol g^{-1}. LCNF/H-LCNF presented higher CD than LCMF/H-LCMF due to their smaller fiber size and higher surface area. The CD values

obtained for PAA pretreated fibers are consistent with those in the literature, where spruce holo-fibers treated with PAA showed CD varying from 200 to 270 μmol g^{-1} (56,85). Furthermore, CD values can be correlated with specific bonds in the FTIR spectra shown in Figure 2.3. The primary peak at 1601 cm^{-1} and the small shoulder at 1730 cm^{-1} are attributed to the C=O stretching of carboxyl groups (56,84,86,87). These peaks are more dominant in TEMPO-LCNF, therefore being proportional to its higher CD value. The absorption band at 1642 cm^{-1} is attributed to the C=O stretching of uronic acid carboxyl groups present in hemicellulose (82,88). This peak is more visible in PAA pretreated samples, consistent with the higher hemicellulose content of the PAA pretreated pulp relative to TEMPO pretreated pulp (Table 2.1).

While previous studies have also performed TEMPO oxidation of agricultural residues, the resulting CD may vary drastically with the type of feedstock, lignin content (i.e., dependent on the delignification process), and NaClO charge employed during TEMPO oxidation. It has been reported that both higher NaClO charges and lower lignin content positively correlate with the degree of oxidation during TEMPO pretreatment (89–91). For instance, pure cellulose isolated from rice straw presented a CD of approximately 1680 μmol g^{-1} after TEMPO oxidation with 10 mmol NaClO (89), while lignin-containing wheat straw pulp presented a much lower charge of 362 μmol g^{-1} after TEMPO oxidation with 5 mmol NaClO (84). When comparing the present study results with the latter reference (both used WS as feedstock and mild pulping as delignification method), it can be concluded that our TEMPO-LCNF showed a greater CD of 1088 μmol g^{-1} because of the higher NaClO charge of 10 mmol utilized in this study.

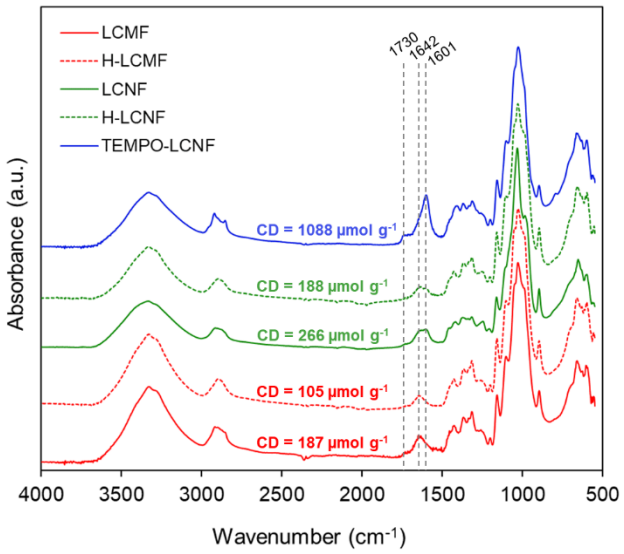

Figure 2.3. FTIR spectra showing specific chemical bonds of lignocellulosic fibrils and their respective charge density (CD) values. CD values were calculated based on conductometric titration curves (Appendix A, Figure A.2).

2.4.4 Lignocellulosic fibrils structure and morphology

Table 2.2 summarizes the different lignocellulosic fibrils' structural and morphological characteristics (crystallinity index, fiber width and length, and fiber aspect ratio). The crystalline structure of fibrils was assessed based on XRD results. The effect of both pretreatments on the crystallinity of WS fibers was evaluated by comparing the Crystallinity Index (CI) of PAA pretreated and TEMPO pretreated fibrils (Table 2.2) with that of PC (Appendix A, Figure A.3). PC showed a higher CI of 78.5%, while PAA pretreated fibrils (LCMF, LCNF, H-LCMF, and H-LCNF) had CI ranging from 65-71% and TEMPO-LCNF had a CI of 67%. The reduction in CI after TEMPO pretreatment can be explained by a change in the cellulose crystalline structure into a disordered structure due to the formation of sodium glucuronosyl units by oxidation (82,84,92). As for the PAA pretreatment, the decrease in CI can be explained by structural swelling of WS fibers and dissolution of crystalline cellulose during the reaction (93). The similarity between the

CI of LCMF, LCNF, and TEMPO-LCNF goes along with previously reported results in the literature, where TEMPO-LCNF from spruce had a CI of 64% and holo-CNF (i.e., fibers that went through peracetic acid pretreatment) had a CI of 65% (56).

Table 2.2. Structural and morphological characteristics (crystallinity index, fiber width and length, and fiber aspect ratio) of lignocellulosic fibrils.

	Crystallinity Index (%)	Fiber width (nm)	Fiber length (μm)	Fiber aspect ratio
LCMF	67.0	16.4 ± 5.1	-	-
H-LCMF	70.8	16.1 ± 5.3	-	-
LCNF	65.1	1.9 ± 0.6	0.77 ± 0.29	405
H-LCNF	65.5	2.7 ± 1.0	1.09 ± 0.76	404
TEMPO-LCNF	66.8	1.8 ± 0.4	1.01 ± 0.32	561

Figure 2.4 illustrates microscopy images (including optical microscopy, SEM, and AFM) and size distribution curves of all lignocellulosic fibrils compared in this study. Low magnification optical microscopy images of LCMF and H-LCMF revealed that the homogenization step drastically reduced the number of large unfibrillated fibers, resulting in a more homogeneous sample. The morphology of LCMF and H-LCMF were further assessed using SEM, confirming a uniform network of long and entangled microfibrils. Individual LCMF and H-LCMF microfibrils had similar average widths of 16.4 and 16.1 nm, respectively (Figure 2.4, Table 2.2), comparable to other microfibrils widths reported in the literature (4,61,94,95). Furthermore, LCMF and H-LCMF presented widths in the nanometer range and extensive lengths, resulting in a much higher aspect ratio than LCNF, H-LCNF, and TEMPO-LCNF (Figure 2.4).

LCNF showed similar morphology to conventional TEMPO-LCNF while undergoing a milder pretreatment. The fibril size of about 2 nm wide and 1 μm long is characteristic of individual elementary fibrils (4). After homogenization of the LCMF fraction, the H-LCNF obtained had

comparable morphology to both LCNF and TEMPO-LCNF (Figure 2.4, Table 2.2), but with a much higher separation yield than LCNF. TEMPO-LCNF exhibited the highest aspect ratio with a narrow width and length size distribution, while LCNF and H-LCNF had lower aspect ratios (405 and 404, respectively) and wider size distributions. H-LCNF presented a broader, right-skewed distribution than its non-homogenized counterpart, suggesting that microfluidizer-induced mechanical defibrillation yields both short and thin, as well as long and wide fibrils. Similar results have been reported by Yang et al. (56), where holo-CNF prepared by microfluidizer presented a wider fibril size distribution than those prepared using a blender. The more heterogeneous nature of H-LCNF may be attributed to a) the mild PAA pretreatment employed, resulting in low degree of oxidation, and b) mechanical exfoliation of the fiber's surface during the homogenization step, releasing fibrils of varied sizes.

The lignocellulosic fibril sizes obtained in the present study, especially LCNF and H-LCNF, are within the low range compared to previous studies on LCNF production (19), demonstrating the process' capabilities. Generally, the type of feedstock, process conditions, and mechanical fibrillation techniques utilized can largely impact the size of resulting fibrils (96). For instance, the process adopted by Rojo et al. used Norway spruce that underwent SO_2-ethanol-water pulping, mechanical treatment, and microfluidization, generating LCNF with widths ranging from 16 to 44 nm depending on the fibers' lignin content (31). Espinosa et al. produced LCNF from WS with widths varying from 6 - 14 nm via soda pulping and different pretreatment methods (TEMPO oxidation, enzymatic hydrolysis, and purely mechanical) followed by high-pressure homogenization (84). Bian et al. produced LCNF from WS and pulp waste with widths ranging from 12 - 47 nm using concentrated p-toluenesulfonic acid hydrolysis, disk grinding, alkaline peroxide bleaching, and dialysis (97). Finally, the TEMPO-LCNF produced from WS in this study

showed the same morphology as those prepared from hardwood bleached pulp (47). It should also be noted that the large variance in nanofibril widths reported in the literature can be associated with the broad use of the terms "nanofibril" and "nanocellulose," which may encompass any fibrils that are less than 100 nm wide (66).

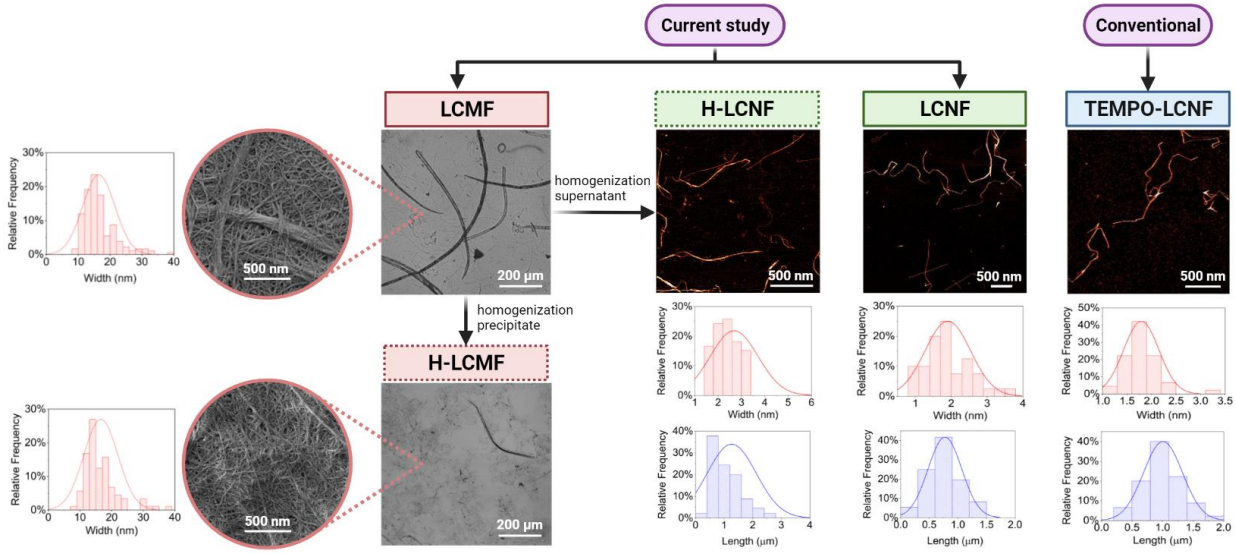

Figure 2.4. Microscope images and size distribution of different lignocellulosic fibrils. LCMF and H-LCMF show both optical microscope and SEM images; LCNF, H-LCNF, and TEMPO-LCNF show AFM images.

2.4.5 Thermal stability

The thermal stability and degradation behavior of the different lignocellulosic fibrils were tested by thermogravimetric analysis (TGA). The temperature at which maximum degradation rate occurs (T_{max}) and the residual mass percentage at 600 °C are presented in Figure 2.5. For all samples, a small weight loss (i.e., < 10%) was observed at temperatures up to 200 °C caused by evaporation of residual water in the fibers, while the most significant weight loss was observed between 200 – 400 °C (Figure 2.5).

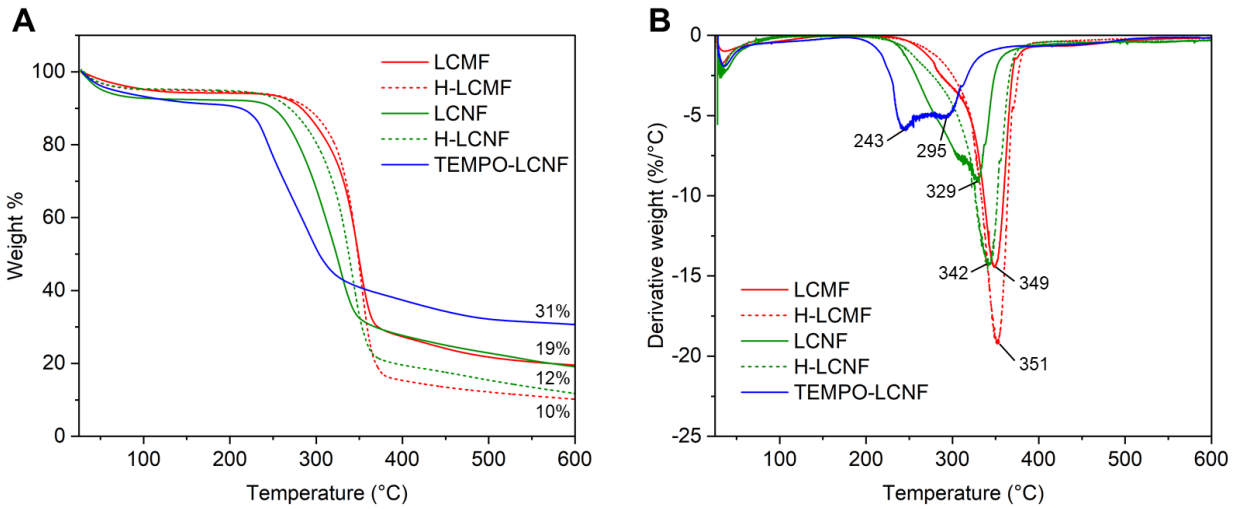

Figure 2.5. Thermal stability comparison of different lignocellulosic fibrils prepared. (A) TGA curves with the residual mass percentage at 600 °C; (B) derivative thermogravimetric (DTG) curves with T_{max} values.

TEMPO-LCNF clearly presented a different thermal degradation mechanism than PAA pretreated samples. TEMPO-LCNF had two prominent degradation peaks (Figure 2.5B) at lower temperatures (243 °C and 295 °C) and presented the highest residual mass (31%) (Figure 2.5A). The primary reason for this behavior is the presence of more carboxylic acid groups (i.e., higher charge density) in TEMPO-LCNF compared to the other samples (4,56,83,84), as seen in previous results in Figure 2.3. Those groups are less thermally stable compared to intra-chain bonds of cellulose, thus reducing the overall resistance to thermal degradation of the fiber. The first degradation peak (243 °C) can be correlated with the primary degradation of TEMPO-LCNF catalyzed by the acid groups formed during the oxidation. The second degradation peak (295 °C) can be associated with the slow charring process of solid residuals (98). The decomposition of TEMPO-LCNF at a wide range of lower temperatures promoted the formation of char residues (98), as seen by its higher residual mass percentage.

In contrast, all other lignocellulosic fibrils produced via PAA pretreatment presented only one prominent degradation peak and higher thermal stability than TEMPO-LCNF (Figure 2.5B), which can be correlated to the presence of fewer oxygen groups, as mentioned earlier, and to the higher lignin content of PAA pretreated samples. The latter observation is consistent with previous research in the literature, where a higher lignin content was found to improve the thermal stability of cellulose nanofibrils (99). Both microfibrils (LCMF and H-LCMF) were the most thermally stable (T_{max} at about 350 °C), which can be attributed to their larger fiber dimensions, the presence of possible bundles, and their higher crystallinity, which would provide higher resistance to chain scission. Furthermore, despite having similar morphologies, both nanofibrils produced via PAA pretreatment (LCNF and H-LCNF) showed higher thermal stability than TEMPO-LCNF, with T_{max} approximately 90 °C higher, due to lower charge density and higher lignin content.

2.4.6 PVA composite films characterization

The addition of 5 wt.% lignocellulosic fibrils as a reinforcing agent in PVA had minimal effects on the light transmittance compared to neat PVA, as illustrated in Figure 2.6A. The reinforcing effect of the different lignocellulosic fibrils on the mechanical properties of PVA composite films was assessed by tensile testing (the test specimens' thickness and density are shown in Appendix A, Table A.3). Figure 2.6B shows the specific tensile strength, specific Young's modulus, and elongation at break of different PVA composite films and their percentage increase or decrease related to neat PVA. Considerable improvements both in specific tensile strength and specific Young's modulus were achieved for all reinforced composites, indicating that the lignocellulosic fibrils (regardless of its type) exhibited good interfacial interactions with the PVA matrix, resulting in composites with increased strength and stiffness due to good dispersion and strong interactions between the fibrils and PVA (60,65).

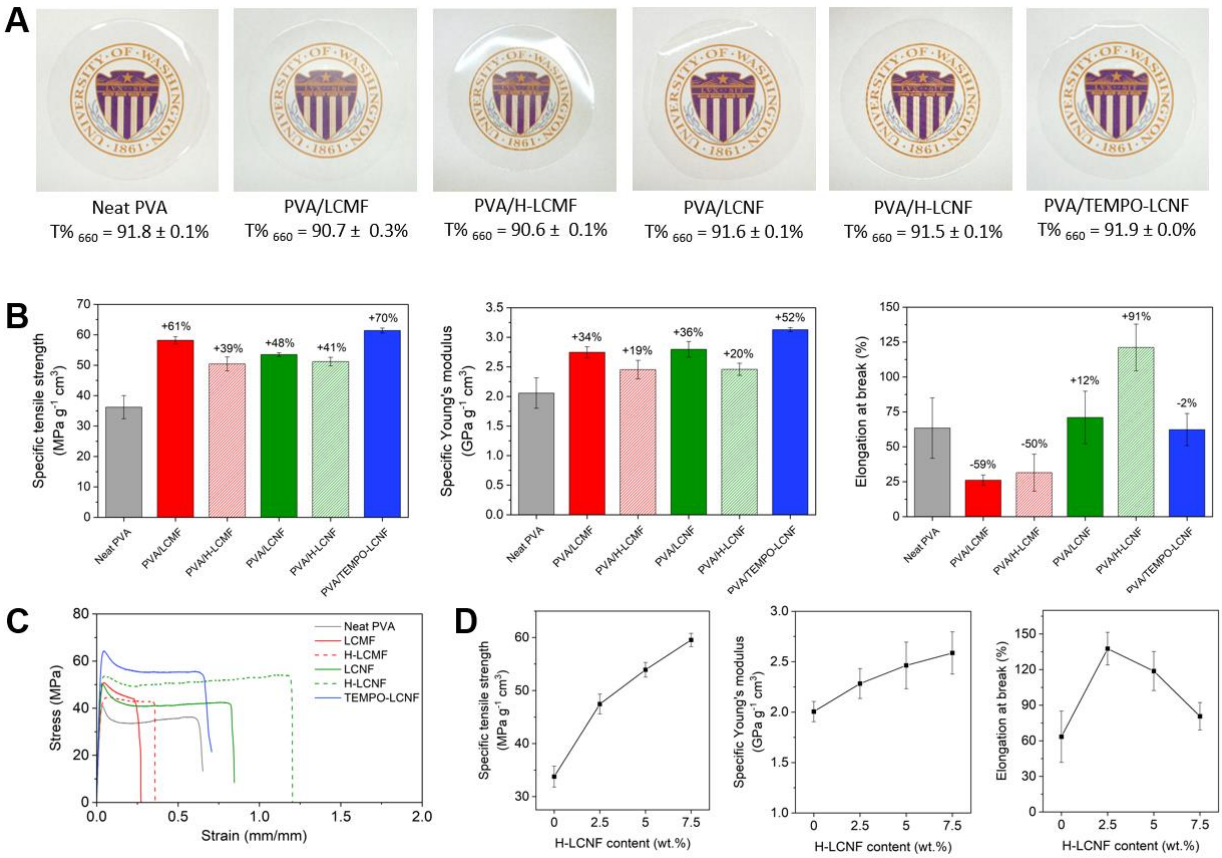

Figure 2.6. (A) Photographs of PVA composite films and optical transmittance values at 660 nm, (B) Mechanical properties (specific tensile strength, specific Young's modulus, and elongation at break) of PVA composite films, (C) Stress-strain curves of PVA composite films, and (D) Mechanical properties of PVA/H-LCNF composites as a function of H-LCNF content.

PVA/LCMF showed a 61% increase in specific tensile strength compared to neat PVA, while PVA/LCNF showed a 48% increase. This difference is possibly associated with LCMF's stronger fiber network and greater fiber size ratio than LCNF. The longer LCMF fibers allow increased matrix/fibril interaction and thus more effective load transfer between the polymer backbone and cellulose fiber. The superior specific tensile strength of PVA/TEMPO-LCNF compared to all other samples can be explained by its higher charge density, where the extensive surface functionalization provided better dispersion and most effective bonding between the fibers and PVA (62). PVA/LCMF and PVA/LCNF resulted in similar improvements in specific Young's

modulus (34% and 36%, respectively), while PVA/TEMPO-LCNF resulted in the most improvement (52%), indicating that the composite's stiffness is mainly affected by charge density rather than the size of the fibrils. This outcome was expected since Young's modulus is primarily related to the bonding between the different components in the composite, therefore being more susceptible to the material's chemical characteristics than its physical morphology.

The majority of the reinforced composites exhibited either similar or lower fracture strain values than that of neat PVA, with the most significant reduction in elongation at break observed for composites containing LCMF (-59%), which was the sample with the highest strength and modulus increases across all PAA pretreated fibrils. The higher fibril size of LCMF, as mentioned above, allows more interactions between the polymer and cellulose chains, which strengthens and stiffens the composite but reduces the amount of available chain sliding upon loading, leading to less elongation to break. This trend was expected considering that the addition of rigid cellulosic fillers to polymer matrices is known to reduce the extent of plastic deformations, decreasing elongation at break and toughness properties (60,65). Surprisingly, the PVA/H-LCNF specimens did not follow this behavior and showed a simultaneous strengthening and toughening of the polymer matrix compared to neat PVA, with augmentations in tensile strength and elongation at break of 41% and 91%, respectively (Figure 2.6C). PVA/H-LCNF presented the greatest fracture toughness value of 61.4 MJ/m^3, a 175% augmentation related to neat PVA (22.3 MJ/m^3 fracture toughness) (Appendix A, Table A.3). This outcome might be attributed to the right-skewed size distribution and more heterogeneous nature of H-LCNF (Figure 2.4), possibly improving filler dispersion and network structure in the PVA matrix. Since H-LCNF fibers show a larger fiber length distribution, they could sustain more chain unentaglement and/or sliding when subjected to mechanical loads compared to samples with tighter length distributions.

To further investigate the reinforcing mechanism of PVA with the addition of different reinforcing agents, the fracture surfaces of PVA composites were examined by SEM. Figure 2.7 shows a comparison of the fracture surfaces of neat PVA (A-B) and the composites reinforced with H-LCMF (C-D) and H-LCNF (E-F). While it was not possible to identify the presence of individual fibrils in the matrix, it is clear that the presence of either one of the reinforcing agents caused a drastic change in the deformation mechanism of PVA. Both agents caused extensive polymer fibrillation during tensile deformation, while neat PVA showed a smooth fracture surface. The observed fibrillation is seen uniformly throughout each composite, indicating that the lignocellulosic fibrils (either nano or micro) were evenly distributed within the sample. Moreover, it can be seen that the polymer matrix formed much longer and smoother fibrils before failure when reinforced with H-LCNF, suggesting a substantial ductility compared to the more abruptly fractured PVA/H-LCMF composite. The PVA/H-LCMF composite also presented some gap features in the fracture surface, indicating more debonding in the polymer matrix. These observations are in agreement with the elongation to break results obtained for PVA/H-LCNF and PVA/H-LCMF previously shown in Figure 2.6B.

This binary reinforcing and toughening trend was further confirmed for PVA composites prepared at different H-LCNF contents (Figure 2.6D). A progressive increase in tensile strength was observed at higher H-LCNF with an augmentation of 76% at 7.5 wt.% H-LCNF compared to neat PVA. Similarly, the specific Young's modulus increased with the H-LCNF content, reaching a maximum of 2.6 GPa g^{-1} cm^3 at 7.5 wt.% H-LCNF, which is 29% higher than neat PVA (2.0 GPa g^{-1} cm^3). This strengthening effect is related to the load-bearing of inherently rigid cellulose nanofibrils in the polymer matrix, demonstrating good interfacial interactions between H-LCNF and PVA (65). Finally, the elongation at break reached its maximum at 2.5 wt.% H-LCNF with a

fracture strain of 138% (117% augmentation compared to neat PVA) and gradually decreased at higher H-LCNF contents while remaining greater than that of neat PVA. The reduction in elongation observed beyond 2.5 wt.% H-LCNF might be ascribed to possible filler aggregation at higher loadings (63,65).

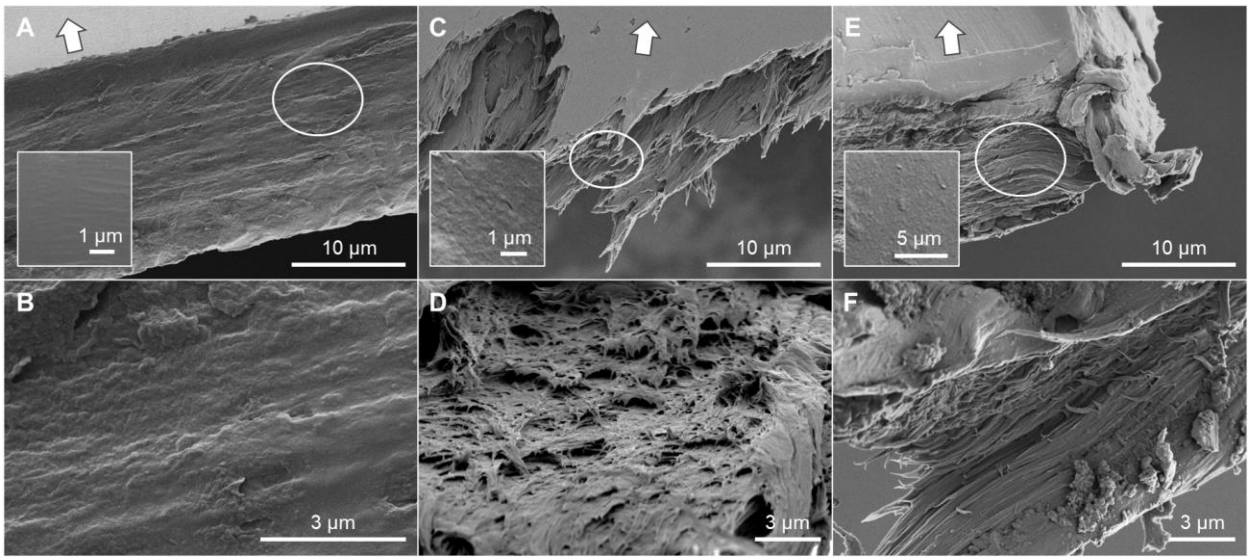

Figure 2.7. Representative SEM images of fractured surfaces at low and high magnifications of (A-B) neat PVA, (C-D) PVA/H-LCMF composite, and (E-F) PVA/H-LCNF composite. The arrows indicate the tensile load direction, while the circled areas highlight the approximated regions where the higher magnification images were taken. Inset images in Fig. 2.7A, B, and C show the top surface of each composite film.

Reports of simultaneous strengthening and toughening of CNF-reinforced PVA composites prepared by solvent casting are relatively scarce in the literature. Several studies reported Young's modulus and tensile strength improvements at comparable CNF contents related to neat PVA (60,65). The CNF reinforcement in these studies, however, came at the cost of significant reductions in elongation, as substantial as -50% in some instances, making the composite extremely brittle and not suitable for practical applications. The binary reinforcing and toughening effect observed was also seen, to a lesser extent, by Kassab et al., where PVA reinforced by 5 wt.%

TEMPO-oxidized CNF resulted in respective increases of 36%, 60%, and 58% in elastic modulus, tensile strength, and elongation compared to neat PVA (62). The present study showed a much greater improvement in elongation (91%) for PVA reinforced with 5 wt.% H-LCNF.

2.5 CONCLUSION

This work has demonstrated that lignocellulosic nanomaterials with outstanding plastic reinforcing properties can be produced from inexpensive agricultural waste feedstock via alkaline peroxide pulping followed by mild and more environmentally friendly PAA pretreatment. The unique aspect of the nanomaterials (nanofibrils and microfibrils) produced from agricultural residue and mild process conditions is that hemicellulose and lignin components were preserved, which was crucial for improving yields. Even though mild PAA pretreatment produced nanomaterials with lower surface charge density than TEMPO oxidation, it did not negatively affect the materials' properties. All samples showed good colloidal stability in aqueous media mainly due to coulombic and steric repulsions by hemicellulose on the fibril's surface. The lower charge density and higher lignin content of PAA pretreated materials resulted in higher thermal stability. In addition, regardless of the charge density, all fibrils exhibited good dispersion in the PVA matrix, leading to improvements in mechanical properties (tensile strength and Young's modulus) of the composites - with an exceptional case of simultaneous toughening and strengthening. The present work has demonstrated a new method to produce lignocellulosic nanomaterials using an agricultural waste feedstock, advocating for more robust commercial processes that can handle other low-purity, heterogeneous raw materials. This commercially viable process could produce nanomaterials at a large scale with commodity product economics, enabling their use in high-volume applications such as bioplastics.

Chapter 3. Techno-economic analysis of lignocellulosic nano-microfibrils (LCNMF) production from wheat straw

3.1 SUMMARY

Cellulose nano-microfibrils are sustainable biomass-derived materials with multiple potential applications that have not become a commercial product due to high production costs. This work presents a techno-economic analysis of low-cost lignocellulosic nano-microfibril (LCNMF) production from agricultural residues via an environmentally friendly process. The standalone process presented is comprehensive, including the areas: 1) Feedstock handling, 2) Pulping and refining, 3) Peracetic acid pretreatment, 4) Mechanical fibrillation, and 5) Wastewater treatment. A facility using 100-tonne wheat straw feedstock per day was modeled with process simulation software with a production capacity of 18,400 tonnes of LCNMF per year. The economic analysis found a minimum product selling price (MPSP) of US$4.60/kg at a 15% discount rate. The low MPSP was a result of the inexpensive wheat straw feedstock, which represented only 6% of variable operating costs, and the conversion process simplicity (low temperature, atmospheric pressure) resulting in low capital costs. Increasing the facility size dramatically reduced the capital cost due to economies of scale, resulting in MPSP reduction by 38%. In addition, co-location with a biorefinery proved advantageous since the LCNMF facility can use the wastewater treatment plant of the biorefinery, significantly reducing the production costs. This work demonstrates the outstanding economic potential of a standalone process to produce cost-competitive nanocellulose products of small widths (2-17 nm), promoting the commercialization of such products for many applications.

Pascoli DU, Seufitelli GVS, Dichiara AB, Bura R, Gustafson R.

Manuscript in preparation for publication

3.2 INTRODUCTION

Cellulose is the most abundant natural polymer on the planet, and due to its hierarchical structure, it can be broken down into smaller-size fibrils (96). These smaller fibrils are commonly referred to as nanofibrils (1-10 nm width, characteristic of elementary fibrils) and microfibrils (10-100 nm) (5,100). For simplicity, we use the term 'nano-microfibrils' to describe the broader class of fibrils less than 100 nm wide (i.e., comprising both nano and microfibrils). Cellulose nano-microfibrils (CNMF) have excellent mechanical properties, being extremely strong and lightweight. In addition, CNMF is biocompatible, has low thermal expansion and low density, and is biodegradable (1). With the world transitioning from a petroleum-based society to a more renewable era, there has been much interest in using CNMF as a sustainable material in various applications ranging from low-volume (e.g., biomedical, pharmaceuticals, electronics) to high-volume (e.g., paper products, packaging, bioplastics, automotive body, construction) (41). Despite the vast potential, most of these applications are still in laboratory and R&D stages, except for paper product applications, due to the current high prices of CNMF and low production capacities.

As of 2018, the total global production capacity of nanocellulose products (including fibers and crystals) was less than 40,000 tonne/year, with a striking 75% being microfibrils produced by pulp and paper mills that are used on-site in their own products (i.e., mills captive) (9,33,36,41). The remaining 25% primarily consists of pilot and some commercial-scale facilities producing various nanocellulose products available for purchasing, revealing that dedicated facilities were responsible for only a small fraction of the already-low global nanocellulose production capacity. While the pulp and paper mill integrated concept eliminates the need to dry and ship the final product, which decreases costs significantly, it also restricts the application potential of CNMF to only paper and packaging products. In addition, this integrated concept has low feedstock

flexibility since the high-purity wood bleached pulp produced in the mill is used for CNMF manufacture. Therefore, to have CNMF being used in high-volume markets other than paper and packaging, we must decrease the production costs to enable standalone commercial facilities that do not rely on integration with pulp and paper mills.

Generally, two major aspects significantly impact the production costs of CNMF: the feedstock used, and the process employed. CNMF is primarily produced from wood bleached pulp containing virtually pure cellulose, which costs between $800-1,400/dry tonne (45,46). Previous reports revealed that the cost of bleached pulp feedstock can account for 14% up to 60% of the total operating costs in CNMF manufacturing; this percentage largely depends on the type of processing utilized (mechanical vs. chemical) (23,101). In addition, the bleached pulp manufacturing process is not environmentally-friendly, given that it uses harsh cooking and bleaching processes that employ harmful chemicals and large amounts of energy. Making nano-microfibrils directly from biomass feedstocks, especially low-cost options like agricultural residues, offers a more economically feasible and sustainable pathway (19,23). Previous studies have shown that low-purity fibrils, also known as lignocellulosic nano-microfibrils (LCNMF), containing residual hemicellulose and lignin not only have unique properties (e.g., easier fibrillation, colloidal stability, hydrophobicity, and improved barrier properties) but also are more cost-competitive than pure cellulose fibrils due to cheaper feedstock and less severe processing conditions (29–32,41).

There has been some debate on the most cost-effective and environmentally-friendly process to produce nano-microfibrils. On the one hand, purely mechanical treatments are more energy-intensive and require several passes to obtain microfibrils at reasonable size distribution, but do not require expensive chemicals or long reaction times. On the other hand, introducing

pretreatment steps (such as TEMPO oxidation or enzymatic hydrolysis) can reduce the energy consumption during the mechanical treatment and produce smaller nanofibrils with narrower size distributions. However, most pretreatments increase other operating costs associated with chemical expenses and increase technological risk, making the process more difficult to scale up (25). Furthermore, TEMPO oxidation has environmental implications due to the use of toxic chemicals. Therefore, there are opportunities in this field to develop novel, economically feasible, and green processing technologies to produce nano-microfibrils, especially using waste biomass feedstocks. In particular, there is a need for techno-economic analysis (TEA) studies exploring green processing technologies to make nano-microfibrils using alternative feedstocks rather than wood pulp.

Only a handful of studies evaluating the production costs of CNMF or LCNMF at a commercial scale have been reported in the literature. Assis et al. investigated the cost of producing CNMF from bleached softwood kraft pulp based on the University of Maine's pilot technology using multiple disk refiner treatments to obtain the desired fibril size (23). Bondancia et al. performed a TEA of co-producing cellulose nanofibrils and nanocrystals from bleached eucalyptus kraft pulp via citric acid hydrolysis and ultrasonication (101). Clauser et al. designed a process to produce CNMF from eucalyptus sawdust in a biorefinery setting (102). Their CNMF production route consisted of hydrothermal pretreatment, alkaline soda-anthraquinone pulping, and oxygen bleaching to obtain nearly pure cellulose, followed by enzymatic hydrolysis pretreatment, refining, and high-pressure homogenization (102). Serra-Parareda et al. published a study on the production of LCNMF from thermomechanical spruce pulp via purely mechanical treatment using a PFI mill and a high-pressure homogenizer (103). Their process approach is based on the integrated concept with a pulp and paper mill to produce reinforced packaging paper (103).

The present work presents a comprehensive assessment of the technical and economic feasibility of LCNMF production at a commercial scale using inexpensive agricultural waste feedstock and employing a novel and environmentally friendly processing method previously developed by our research group (104). To the best of our knowledge, this is the first TEA study of nano-microfibrils production directly from agricultural residues. In addition, this is the first study to model a complete standalone process, including feedstock handling and wastewater treatment. For the economic assessment, new experimental data (including process conditions, reaction conversions, and mass and energy balance) collected in the present work were combined with data from our previous work (104) to be used as inputs in Aspen Plus model. The TEA resulted in the production costs and minimum product selling price (MPSP) of LCNMF. The impact of economies of scale and co-location on the production costs and MPSP are also assessed. This work is an important step in transitioning nanocellulose production from R&D to commercialization by demonstrating the economics of a new process for production of cost-competitive and environmentally friendly nanocellulose products.

3.3 MATERIALS AND METHODS

3.3.1 Raw material

Wheat straw (WS) from Snohomish County, WA, was used as feedstock for all the experimental work. The chemical composition of WS was determined in previous work and comprises 35.6% cellulose, 22.0% hemicellulose, 28.1% lignin, 11.4% ash, and 13.4% extractives (104). WS refined pulp was prepared via alkaline peroxide pulping and PFI refining, based on methods previously developed by our research group (104).

3.3.2 Laboratory experimentation

The process for preparing lignocellulosic nano-microfibrils (LCNMF) from WS refined pulp was based on the laboratory procedure developed previously by our research group (104) with modifications. The process uses mild conditions (low temperature and atmospheric pressure) and low-cost, green chemicals combined with mechanical treatments to produce LCNMF more cost-effectively (104). The present work contains further experimentations using different equipment and conditions to assess the scalability of the process, which are detailed below.

Peracetic acid (PAA) pretreatment

Briefly, WS refined pulp was mixed with 2 wt.% peracetic acid (PAA) solution (pH 4.8) at 5% solid consistency, and the reaction was carried out at 85 °C for 45 min. The PAA pretreated pulp was vacuum filtered and the PAA pretreated pulp underwent a 2-step wash with a caustic solution followed by DI water. The total mass yield after PAA pretreatment was determined gravimetrically by comparing the OD weight of fibers obtained with that of the starting raw material (WS). In addition, the chemical composition of PAA pretreated pulp was quantified according to methods previously described by our research group (69–72).

Mechanical fibrillation and LCNMF production

Following PAA pretreatment, the resulting pulp was fibrillated through a series of mechanical treatments to produce LCNMF. In our previous work, mechanical fibrillation and homogenization of PAA pretreated pulp were performed using a blender and a microfluidizer, respectively (104). In the present work, different combinations of mechanical methods were assessed to prepare LCNMF, including PFI refining and ultrasonication. The method resulting in the highest nanofibrillation production was utilized in the subsequent process modeling and TEA.

LCNMF characterization

The morphology of both nano and microfibrils comprising the LCNMF was assessed independently by scanning electron microscopy (SEM) and atomic force microscopy (AFM) techniques after separating the fractions via centrifugation. For detailed information about these characterization techniques, refer to Chapter 2 of this dissertation (subsection 2.3.5).

3.3.3 Process modeling and simulation

Mass and energy balances were obtained by modeling a large-scale process using Aspen Plus and WinGEMS simulation software. The complete process for LCNMF production from WS is summarized in Figure 3.1 and comprises five areas: 1) Feedstock handling, 2) Pulping and refining, 3) Peracetic acid pretreatment, 4) Mechanical fibrillation, and 5) Wastewater treatment. A detailed description of each process area is included below.

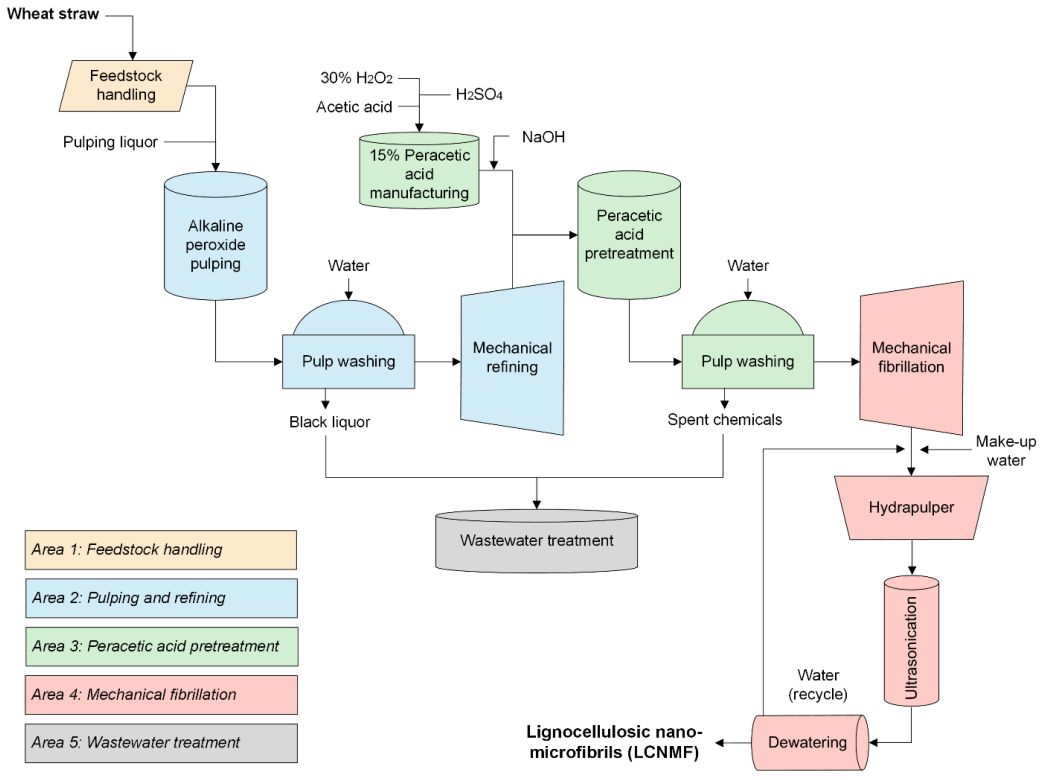

Figure 3.1. Process flow diagram of the modeled process for LCNMF production.

Area 1: Feedstock handling

The WS feedstock handling area was modeled following the NREL 2022 design for corn stover handling (105). In short, WS bales are delivered to the facility on trucks and directed to a series of handling steps that result in washed and milled WS that is free of dirt and tramp metals. The WS biomass is then conveyed to Area 2 for processing.

Area 2: Pulping and refining

100 OD tonne/day of WS feedstock is fed into a continuous reactor vessel, along with the pulping liquor containing NaOH, H_2O_2, and DTPA. All reaction condition parameters and conversion yields utilized in this model were based on our previous research study (104). The alkaline peroxide pulping reaction is held at 90°C, 1 atm, for 150 min at medium consistency. A total mass yield of 62 wt. % is obtained (based on original WS mass), with most lignin, ash, extractives, and some hemicellulose being solubilized during the reaction. The resulting pulp is directed to a series of three vacuum drum washers, a unit operation commonly utilized in the pulp and paper industry, which were modeled using WinGEMS software assuming a dilution factor of 1. Water is fed to the washers, and the dilute black liquor containing 98% of the dissolved solids exits on the opposite end, being sent to the wastewater treatment (WWT) plant. The washed pulp (with 2% dissolved solids) leaves the washer at 10% solid consistency and is directed to mechanical refining with a 50/60-in disk refiner (electricity demand calculated of 328 kW), producing WS refined pulp with a higher fiber surface area.

Area 3: Peracetic acid pretreatment

Peracetic acid (CH_3COOOH) solution is assumed to be produced on-site by reacting acetic acid (CH_3COOH) with 30% hydrogen peroxide (H_2O_2) at a 1:1.5 volume ratio in the presence of

sulfuric acid (H_2SO_4) as catalyst 1.5 wt.%. loading (Reaction 3.1), based on reaction parameters previously reported in the literature (106,107). The reaction takes place in a stainless steel tank at 50 °C for 4 h, and an extra storage tank is included. The resulting solution has a PAA concentration in equilibrium of approximately 15 wt.%.

$$CH_3COOH + H_2O_2 \overset{H_2SO_4}{\longleftrightarrow} CH_3COOOH + H_2O \qquad \text{(Reaction 3.1)}$$

The 15 wt.% PAA solution is mixed with NaOH at specific amounts to achieve a pH of 4.8 and is then combined with the refined WS pulp and pumped into a stirred tank where the PAA pretreatment takes place. The reaction is held at 85°C for 45 min at medium consistency and a total mass yield of 53 wt. % is obtained (based on original WS mass) after the pretreatment. The specific conversion yields utilized in the model were 3% cellulose to glucose, 13% xylan to xylose, 78% lignin to soluble lignin, 88% ash to soluble ash, and 100% extractives to soluble extractives - all calculated based on the chemical composition and the total mass yield. Because the fibers are still relatively big at this stage, the pretreated pulp can be washed with a conventional pulp washing system. The resulting pretreated pulp exits the reaction tank and is directed to a second pulp washer unit with the same configuration as in Area 2. The washed pretreated pulp leaves the washer at 10% solid consistency while the wastewater containing spent chemicals is directed to the WWT.

Area 4: Mechanical fibrillation

The combination of mechanical treatments utilized in the LCNMF production modeling was chosen based on the nanofibrillation yield results demonstrated in this work (as seen in the Results and Discussion section). First, washed pretreated pulp at 10% solid consistency is fibrillated using a disk refiner to increase fiber surface area. Then, the fibers are mixed with enough water to achieve a 1% solid consistency for the subsequent homogenization steps with a hydrapulper and a

continuous ultrasonicator. The hydrapulper is mainly responsible for promoting water absorption and fiber swelling to facilitate nanofibrillation, while the ultrasonicator improves the homogeneity of the sample and increases nanofibrillation yield. Finally, the LCNMF at 1% solid consistency passes through cross-flow ultrafiltration membranes for dewatering to achieve a final 5% solid consistency. The water removed in the ultrafiltration step is clean and is recycled back into the process. The final LCNMF product (at 5 wt.%) comprises a mixture of nano and microfibrils with an output of 53 tonne/day or 18,437 tonne/year (dry basis). The main parameters for Area 4 are summarized in Table 3.1.

Table 3.1. Parameters applied in the modeling and simulation of Area 4. Lab results were obtained in the present work.

Parameter	Value	Source
Mechanical fibrillation		
Solid consistency	10 wt. %	Lab result
Electricity demand	260 kW	
Hydrapulper		
Solid consistency	1 wt. %	Lab result
Electricity demand	1,060 kW	
Ultrasonication		
Solid consistency	1 wt. %	Lab result
Electricity demand	7,401 kW	
Dewatering		
Solid consistency	5 wt. %	Assumption
Production rate		
LCNMF production output	53 OD tonne/day	Lab result/Aspen

Area 5: Wastewater treatment

Finally, the wastewater treatment (WWT) plant was modeled based on NREL's 2011 process design (108). The combined wastewater streams originating from both pulp washers are first directed to anaerobic digestion, where microorganisms consume the organic matter to produce biogas (CH_4/CO_2). The biogas is fed to a gas water heater unit to generate the hot water needed in

reaction steps at Areas 2 and 3. After the anaerobic digestion, the wastewater is directed to aerobic digestion, where a relatively clean water stream is produced and sent to a clarifier and reverse osmosis to produce the treated water. Inorganic waste generated in WWT was assumed to be disposed of as solid waste. The treated water can then be reused in processes in other areas.

3.3.4 Techno-economic analysis (TEA)

Production costs of standalone facility

The production costs, including capital and operating, were estimated using Microsoft Excel spreadsheets based on the mass balance results obtained via modeling and simulation.

Capital investment was estimated based on equipment prices available from NREL reports, quotations provided by equipment suppliers, and other references. The size of the equipment was adjusted using the facility size ratio and a scaling exponent obtained from the literature. When necessary, Chemical Engineering Plant Cost Index (CEPCI) was used to adjust the equipment prices to the base year of 2019 (109). The total direct costs (TDC) comprise the installed equipment, warehouse, site development, and piping. The total indirect costs include prorateable expenses, field expenses, engineering and supervision, project contingency, and other expenses related to start-up. Direct and indirect costs result in fixed capital investment (FCI), and a working capital of 10% of the FCI was assumed. The total capital investment (TCI) is calculated as the sum of FCI and working capital. The breakdown of TCI are included in Appendix B, Table A.4.

Variable operating costs, including feedstock, chemicals, and utilities, were estimated using mass flow rates obtained in the simulation. Whenever necessary, price values of chemicals were adjusted to the year 2019 using the Inorganic Chemical Index (ICI) (110). Electricity price was assumed based on facility location in Lewis County, WA. Water costs were assumed to be zero since a wastewater treatment plant is included in the model, which provides clean water for the

process. Fixed operating costs, including all labor-associated expenses, maintenance, operating supplies, and property insurance, were also considered. The sum of variable and fixed operating costs results in the total operating costs. The breakdown of total operating costs is included in Appendix B, Table A.5.

Discounted Cash Flow Analysis and Minimum Product Selling Price (MPSP)

MPSP of LCNMF was estimated using discounted cash flow analysis by setting the net present value (NPV) to zero at the assumed discount rate. MPSP were estimated at discount rates of 0%, 7%, and 15%. The discount rate of 15% was chosen as the base case for all other economic analyses. The main financial assumptions used in the cash flow analysis are presented in Table 3.2. The facility's construction would take one year, during which the production capacity is zero.

Table 3.2. Main parameters used in the discounted cash flow analysis.

Parameter	Value
Operating days	350 days/year, 24 h/day
Production capacity in year 0	0%
Production capacity in year 1	50%
Production capacity in years 2+	100%
Financial horizon	10 years
Number of employees/area/day	4
Discount rate (baseline)	15%
Income tax rate	21%
Equity financing	60%

A sensitivity analysis was performed to determine how much the MPSP of LCNMF is affected by the main variable operating costs (i.e., acetic acid, hydrogen peroxide, feedstock, and electricity) and total capital cost. For this analysis, the cost values for each parameter were varied by ± 25%, and the resulting MPSP was calculated. In addition, the production costs and MPSP of a larger facility were estimated to elucidate how the plant size affects the economics of the process.

The larger plant size of 2,000 OD tonne/day of feedstock input was selected based on a standard Kraft pulp mill producing 1,000 OD tons/day of pulp (111).

Standalone vs. co-located scenarios comparison

The standalone facility (100 OD tonne/day feedstock input) was compared to a second scenario where it would be co-located with a biorefinery producing biofuels and (112). The co-located scenario would provide the following modifications related to the standalone case: 1) no expenses associated with WWT (i.e., capital cost and electricity) since the biorefinery's WWT system has more than sufficient capacity to treat waste from the LCNMF facility; 2) the biorefinery would provide free hot water to the LCNMF facility, therefore eliminating the capital (gas water heater tank) and operating (natural gas) costs associated with water heating; and 3) no site development costs. The production costs and MPSP of the co-located scenario were calculated and compared to the standalone scenario.

3.4 Results and Discussion

3.4.1 Laboratory experimentation

Chemical composition and mass yield

The WS pulp after alkaline peroxide pulping had the same chemical composition as that previously reported by our group (57.7% cellulose, 26.6% hemicellulose, 8.2% lignin, 1.9% ash, and 2.7% extractives) with a 62% total mass yield related to original WS (104). The PAA pretreated pulp prepared in the present work contained 74.1% cellulose, 30.9% hemicellulose, 2.4% lignin, and virtually no ash and extractives, with a total mass yield of PAA pretreated pulp related to original WS of 53%. The chemical composition percentages and mass yield results obtained were utilized to calculate the mass balance for each compound throughout the process.

The mass balance results were employed as input conversion percentages in the modeling and simulation for the two reaction steps (i.e., alkaline peroxide pulping and peracetic acid pretreatment).

Mechanical fibrillation and LCNMF production

The effectiveness of the different mechanical treatments was compared based on nanofibrillation yield, which is obtained via the centrifugation method and corresponds to the percentage of nanofibrils present in the suspension containing both nano and microfibrils (25). The different mechanical treatments tested for the production of LCNMF and their corresponding nanofibrillation yields are shown in Table 3.3, alongside other methods previously reported by our group. In our previous work, a one-step blending resulted in a low nanofibrillation yield of 4%, but when combined with another homogenization method (i.e., blending + microfluidization), the nanofibrillation yield increased significantly to 36% (104). Even though using a microfluidizer was satisfactory on a laboratory scale, this equipment is known to present major clogging issues due to its narrow microfluidic channels, requiring process shutdown for cleaning (113–115) that leads to down-time at the facility. Thus, we assessed substituting the microfluidizer with an ultrasonicator because it can operate continuously, presents less risk of clogging, and provides reliable results in decreasing fiber size (116). By doing a blending + ultrasonication treatment, a 24% nanofibrillation yield was achieved. Even though blending + ultrasonication treatment yield is lower than that obtained with blending + microfluidization treatment, ultrasonication imposes less technical limitations relative to microfluidization, so we consider the tradeoff of lower yield with more reliable operation to be worthwhile.

Table 3.3. Comparison of nanofibrillation yields after different mechanical treatments.

Mechanical treatment method	Nanofibrillation yield (%)	Source
Blending	4 %	(104)
Blending + Microfluidization	36 %	(104)
Blending + Ultrasonication	24 %	Present work
Refining	5 %	Present work
Refining + Ultrasonication	19 %	Present work
Refining + Blending + Ultrasonication	32 %	Present work

A test using a PFI refiner mill was also done. First, single-step refining resulted in a low yield of 5%, similar to that previously reported for the single-step blending treatment (104). Then, the combination of refining + ultrasonication treatments resulted in a 19% nanofibrillation yield, 5% less than blending + ultrasonication. We believe this difference is due mainly to the solid consistency employed during the mechanical treatment, seeing that blending was performed at very low consistency (0.4%) while refining was performed at medium consistency (10%). As a result of low consistency and high shear treatment, blending promoted higher water accessibility, resulting in greater fiber swelling and softening due to the breakage of hydrogen bonds between fibers, facilitating nanofibrillation (28). Furthermore, previous studies by Serra-Parareda et al. used a combination of refining + high-pressure homogenization on spruce thermomechanical pulp (25). As a result, the authors reported nanofibrillation yields ranging from 3 to 23% depending on the homogenization conditions (i.e., number of passes and pressure) (25), which are in accordance with the results obtained in the present work.

Finally, a 3-step mechanical treatment (i.e., refining + blending + ultrasonication) was tested, which resulted in the highest nanofibrillation yield of 32%. In this 3-step method, the refining step mainly increases the fiber surface area; the blending step facilitates fiber swelling and nanofibrillation; and the ultrasonication works as a homogenization step and improves

nanofibrillation yield. Because this method produced the highest nanofibrillation yield, it was selected to be employed in this work's process modeling and simulation. Specifically, the blending step of this 3-step method was modeled using hydrapulper equipment, which is commonly used in the pulp and paper industry for disintegrating waste paper and promoting fiber separation through powerful agitation (117).

LCNMF characterization

Because the LCNMF produced via the 3-step mechanical treatment process contained both nano and microfibrils in the mixture, the morphology of both fractions was assessed using different microscopy techniques. Figure 3.2 shows the AFM image of nanofibrils and SEM image of microfibrils, along with their width and length size distribution curves. Nanofibrils, which constitute 32% of the LCNMF product weight, had an average width of 2.8 ± 1.1 nm and length of 0.8 ± 0.5 µm (Figure 3.2A). It may be noted that the nanofibrils' length size distribution presents a right-skewed distribution. Furthermore, the remainder of LCNMF was constituted by microfibrils with 13.5 ± 3.5 nm width that formed a web-like network of very long fibrils (Figure 3.2B).

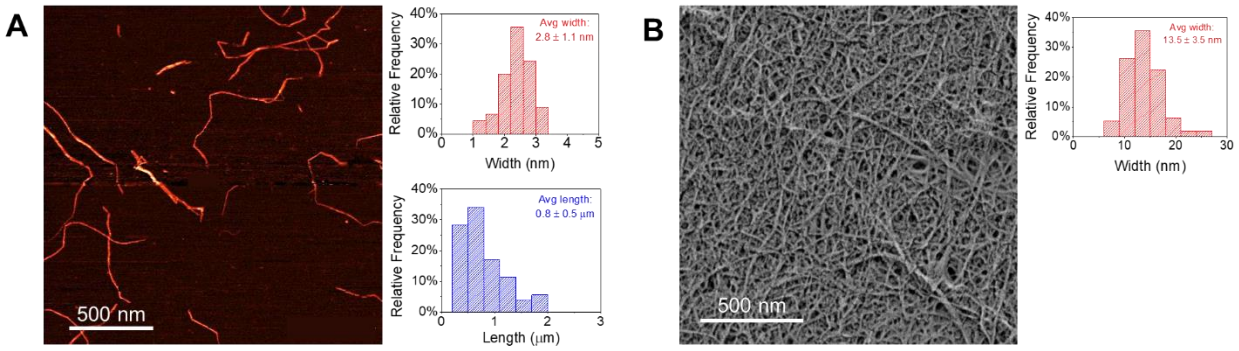

Figure 3.2. (A) AFM image of nanofibrils with width and length size distribution curves, (B) SEM image of microfibrils and width size distribution curve. Both fractions comprise the final LCNMF product.

The size of the LCNMF obtained from wheat straw using the process described in the present work is within the low size range compared to the largest producers of nano-microfibrils in the world (Figure 3.3). One can see that the leading producers primarily make microfibrils of larger sizes (and broader size ranges), except for Nippon Paper which produces nanofibrils with very small widths using the TEMPO oxidation technology (which is not ideal from an economic and environmental standpoint). Alternatively, this work presents a novel process to manufacture LCNMF with sizes primarily ranging between 2 - 17 nm, which are comparable to that obtained via TEMPO oxidation (as is the case of nanofibrils), and with bigger microfibrils that are still under 20 nm in width, indicating successful production of fibrils with narrow size distributions.

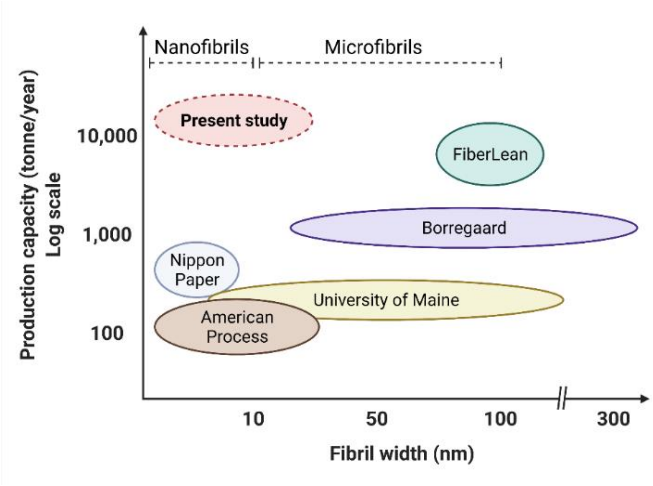

Figure 3.3. Schematic comparing the fibril size and production capacity of major CNMF manufacturers. The scheme is a visual representation of information obtained from various sources (36–40). The production capacity for the present study, represented in dashed lines, was obtained from process simulation results.

3.4.2 Techno-economic analysis

Production costs and MPSP

The breakdown of installed equipment costs per area is shown in Figure 3.4. Area 4 (mechanical fibrillation) and Area 5 (WWT) comprised 67% and 26% of the total installed equipment cost,

respectively, leaving just 7% of the remaining expenses for the three remaining areas combined. Areas 2 and 3 presented the lowest equipment cost due to the mild reaction conditions employed (temperatures below 100 °C), which require simple stirred reactors at atmospheric pressure – much cheaper than high-pressure reactors. Not surprisingly, the most expensive equipment in the entire process was the ultrasonicator in Area 4 (~ $40 million), followed by the WWT plant in Area 5 (~ $21 million), and the dewatering system in Area 4 (~ $13 million).

A previous study by Bondancia et al. included a similar ultrasonication step in their process, which corresponded to only 6% of their total equipment costs (101) - much lower than the percentage obtained in the present work (about 50%). The discrepancy between the two studies with respect to the cost of the unit operation of ultrasonication can be ascribed to the assumptions utilized in both studies. Bondancia et al. modeled the ultrasonication step to operate at 8% solid consistency. However, our laboratory experience found that the nanofibrils product is highly viscous at 8% solid consistency, making ultrasonication practically impossible to operate at this condition. Ultrasonication needs a certain amount of water to create the cavitation bubbles that promote homogenization of the fibers; hence a much lower solid consistency is required. For this reason, we opted to model the ultrasonication process to operate at a lower solid consistency of 1%, which resulted in a much larger and more costly unit operation relative to Bondancia's work.

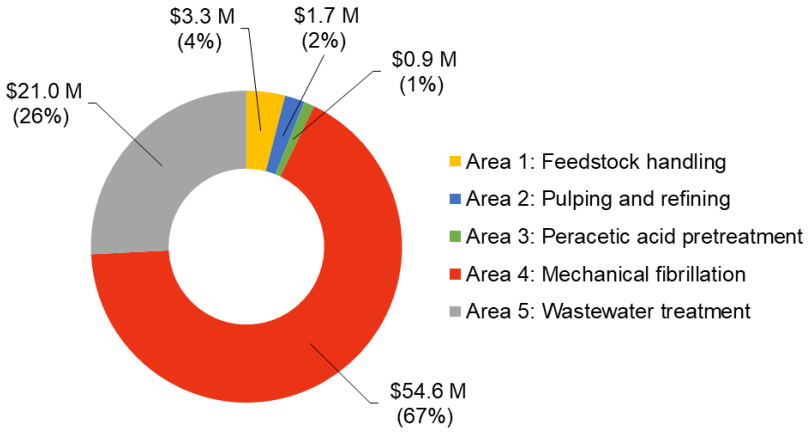

Figure 3.4. Breakdown of installed equipment costs (in US$ million) for LCNF production per area.

The variable operating costs associated with LCNMF production are shown in Figure 3.5, and the complete breakdown of all operating costs (variable and fixed) is included in Appendix B, Table A.5. Acetic acid and hydrogen peroxide, both utilized in peracetic acid production in Area 3, are the largest contributors to the variable operating costs of the process ($1,250/tonne LCNMF, 67% of total). These results are in agreement with a previous study using citric acid hydrolysis to produce cellulose nanofibrils and nanocrystals, where the cost of the citric acid represented 41% of the total operating cost (101). The electricity cost contributed to 12% of the total variable operating costs ($229/tonne LCNMF) due to the mechanical treatments in Area 4. Assis et al. have reported that electricity costs associated with disk refining represented ~15% of their manufacturing costs, ranging from $227-258/ton (or $249-283/tonne) (23). This comparison shows that the estimated electricity usage of the modeled factory agrees with previous reports, and even though ultrasonication is an energy-intensive unit operation, electricity is only a moderate fraction of the total operating cost. It should be noted that the price of electricity used in the present study (from Pacific Northwest location) is considered moderate compared to other regions of the country. Furthermore, the cost associated with the WS feedstock was relatively low, accounting

for only 6% of variable operating expenses. This demonstrates that using a low-cost agricultural residue as feedstock is economically advantageous, being one of the main advantages of the current process relative to those using bleached wood pulp feedstocks.

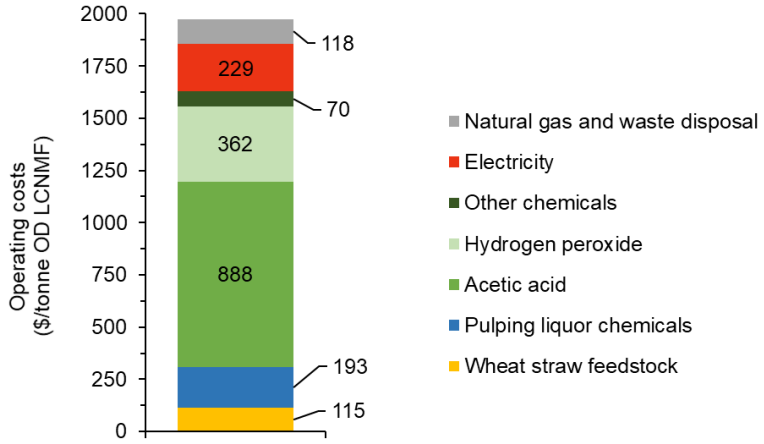

Figure 3.5. Breakdown of variable operating costs in US$ per tonne of LCNMF produced (dry basis).

The estimated total capital and operating costs of the modeled process were utilized to calculate the MPSP of LCNMF by discounted cash flow analysis (Table 3.4). The modeled facility had an LCNMF production capacity of 18,400 OD tonne/year with a 53% yield from the starting WS feedstock. The estimated total capital cost was US$154 million, and the operating cost was US$46 million per year. The MPSP of LCNMF ranged from US$3.73/kg (dry basis) at a 0% discount rate (i.e., break-even point) to US$4.60/kg at a favorable profit margin with a 15% discount rate. Although current market price information for CNMF or LCNMF is scarce, a few sources indicate that current prices can reach up to US$1,000/kg (dry basis) depending on the product specifications (e.g., fiber size, chemical composition, surface modification, etc.) (9,44,118), and we assume the low range of market price to be around US$100/kg. Thus, the present study shows that it is possible

to produce LCNMF at significantly lower prices (at least 20 times lower) than currently available purchasing options.

Even though the MPSP of US$4.60/kg is still not cheap enough to be sold as a commodity chemical level (usually around US$1/kg), it allows the LCNMF to be sold as an additive agent (e.g., coating, reinforcing, etc.) to be used in various existing products such as plastics, automotive body, packaging, paper, etc. For comparison purposes, polylactic acid (PLA) is another biomass-derived, biodegradable material that is currently being commercialized for many applications (e.g., packaging, paper coating, films, bags, etc.) (119). The process to manufacture PLA briefly consists of fermentation of sugars (mainly produced from corn, potatoes, and sugar beets) to produce the monomer lactic acid, followed by polymerization, which can also be costly (119,120). PLA pellets' current prices range between US$3-6/kg (121), being comparable to the LCNMF price of US$4.60/kg obtained in the present work.

Table 3.4. Summary of LCNMF production process parameters, capital and operating costs, and MPSP at different discount rates.

Main process parameters	
Feedstock input (OD tonne/day)	100
LCNMF yield from feedstock (OD wt. basis)	53%
Production capacity (OD tonne/year)	18,400
Total capital cost (US$ million)	**$154 M**
Direct costs	$92 M
Indirect costs	$55 M
Working capital	$7 M
Total operating cost (US$ million/year)	**$46 M**
Variable operating costs	$36 M
Fixed operating costs	$10 M
MPSP at 0% discount rate (US$/kg)	**$3.73**
MPSP at 7% discount rate (US$/kg)	**$4.10**
MPSP at 15% discount rate (US$/kg)	**$4.60**

The results obtained in this work can also be compared to previous TEA studies available in the literature, although this type of comparison is not straightforward. Several factors should be considered when comparing different TEA studies, including the assumptions utilized (e.g., production capacity, discount rate, process boundaries, etc.), the feedstock used (bleached or unbleached wood pulp, residues, etc.), the process technology (e.g., mechanical, chemical, enzymatic, etc.), and the final product specifications (e.g., fibril size, chemical composition, etc.). For example, Assis et al. reported that the MPSP of their microfibrils (widths between 20 – 100 nm) varied from $1.89 – $2.44/kg (dry equivalent), depending on the facility location, with a production capacity of 17,000 tonne/year (23). In their study, they considered only mechanical treatments (i.e., hydrapulper, buffer tank, and disk refiner); hence the capital costs were significantly lower (between US$18.5 – 37.7 million), which is reflected in their low MPSP. The present work, by contrast, considered a complete process starting with raw feedstock handling, and that has its own WWT plant, resulting in higher capital cost. Still, the MPSP of LCNMF (widths between 2 – 17 nm) was less than US$5/kg, demonstrating that competitive and high-quality nanocellulose products can be produced at a reasonable price via the present process. Another study by Bondancia et al. reported that the MPSP of their nanofibrils product (the exact fibril size was not described) ranged from $11.71 – 11.52/kg (dry equivalent) depending on hydrolysis time, with relatively lower production capacity between 874 – 1,193 tonne/year (101), being higher than the MPSP calculated in the present study.

A sensitivity analysis of the MPSP of LCNMF was performed by assuming a change of ±25% in variable operating costs and total capital cost. Figure 3.6 shows that MPSP is most sensitive to variations in capital costs (resulting in ±9% MPSP variation), followed by acetic acid (±5% MPSP variation) and hydrogen peroxide (±3% MPSP variation). Seeing that the two chemicals

represented the largest fraction of variable operating costs (Figure 3.5), their significant impact on MPSP was expected. Furthermore, variations in MPSP for feedstock and electricity were very low (about ±1%) due to their minor contribution to operating costs.

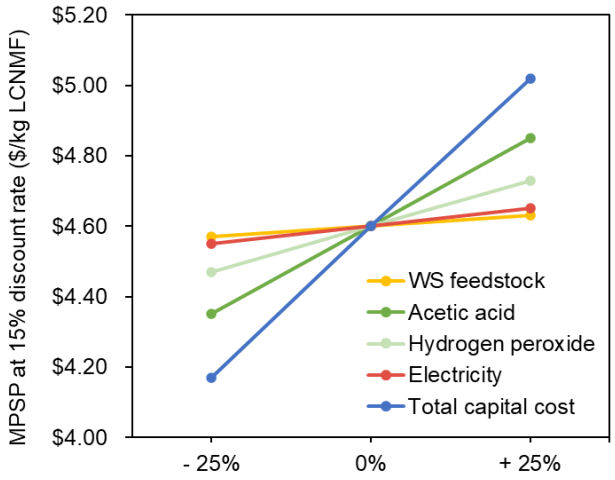

Figure 3.6. Sensitivity analysis of MPSP (at 15% discount rate) of LCNMF to ±25% variation of certain variable operating costs and total capital cost.

Impact of facility size

The impact of the facility size on the production costs (capital and operating) and MPSP was assessed by modeling a larger facility with a production rate 20 times greater than that of the facility considered in this study. The large facility led to a substantial reduction in costs, especially in capital costs, resulting in a lower MPSP (Table 3.5), which was expected based on previous research at the University of Washington (122). The capital cost per annual tonne of LCNMF produced was dramatically reduced by $5,812/kg (70% reduction) due to the economies of scale. On the other hand, the operating costs showed a lower reduction of 18%, which was expected since operating costs are approximately linear with the size of the facility. As a result, the MPSP (at a 15% discount rate) of the large facility was $2.84/kg, a 38% reduction compared to that of the

small one. Even though the capital cost of the large facility is relatively high (almost US$ 1 billion), the economies of scale helped reduce the MPSP closer to the target price for commodity products.

Table 3.5. Comparison of production costs and MPSP (at 15% discount rate) of LCNMF produced in small and large facilities.

	Small facility	**Large facility**
Feedstock input (OD tonne/day)	100	2,000
Production capacity (OD tonne LCNMF/year)	18,400	371,000
Capital cost (US$ million)	$154 M	$931 M
Capital cost (US$/annual tonne LCNMF)	$8,338	$2,510
Operating cost (US$ million/year)	$46 M	$764 M
Operating cost (US$/tonne LCNMF)	$2,502	$2,060
MPSP at 15% discount rate ($/kg)	**$4.60**	**$2.84**

Standalone vs. co-located scenarios

Most nano-microfibrils are currently produced through integrated processes with pulp and paper mills due to economic advantages such as in-house utilization in their paper products and elimination of shipping. However, this integrated concept limits the market potential of the fibrils, seeing that the sole purpose of this type of integration is to use the fibrils in the facility's existing products. The ultimate goal of the present work is to produce inexpensive nano-microfibrils that can be used in a wide range of applications. We therefore investigated the potential of co-locating with a biorefinery to reduce the capital and operating costs of the LCNMF production itself (Table 3.6). Another research project at the University of Washington developed a detailed biorefinery model to produce jet fuel, xylitol, and formic acid (112). The model involved integrating biochemical, thermochemical, and electrochemical processes to convert the glucose in the biomass feedstock into jet fuel via alcohol synthesis (i.e., ethanol), ethanol dehydration, ethylene oligomerization, and alkene hydrogenation. The CO_2 produced during fermentation is reacted with water in an electrochemical reactor to produce formic acid, and the xylose is converted into xylitol

via hydrogenation. Using this biorefinery model to investigate the potential of co-location with the LCNMF facility enabled the development of a rigorous integrated model.

In the co-located scenario, equipment costs of LCNMF production associated with Area 5 (including wastewater treatment plant and gas water heater) and site development expenses are eliminated, significantly reducing the capital cost by about $44 million. In addition, variable operating costs (electricity and natural gas) and labor costs associated with Area 5 are also eliminated, reducing operating costs by $4 million/year. These cost reductions resulted in a lower MPSP (at a 15% discount rate) of $3.87/kg of LCNMF (dry basis), which accounts for a 16% reduction in MPSP compared to the standalone scenario (Table 3.6). These results show that the final product can be more affordable by co-locating and eliminating the costs mainly associated with WWT. In addition, the biorefinery would also benefit from giving their hot water to the LCNMF process because they may not be able to dispose of hot water directly into receiving water streams without some cooling unit operation.

Table 3.6. Comparison of production costs and MPSP (at 15% discount rate) of LCNMF produced in standalone and co-located scenarios.

	Standalone	**Co-located**
Capital cost (US$ million)	$154 M	$110 M
Operating cost (US$ million/year)	$46 M	$42
MPSP at 15% discount rate ($/kg)	**$4.60**	**$3.87**

Similar co-location opportunities can be established with facilities other than biorefineries, such as corn-to-ethanol plants where the LCNMF facility can take advantage of the utilities already supporting the corn-to-ethanol process. There are many of those plants currently operating in the United States and they generate vast amounts of corn stover residue. The process shown in this study was proven successful with wheat straw feedstock, and in the future, it is possible to expand

to other types of agricultural residues, including corn stover. Therefore, by co-locating with corn-to-ethanol plants, the LCNMF facility may also utilize the ethanol plant's corn stover waste as feedstock to produce nano-microfibrils. This is not only beneficial for the ethanol plant since they will have a high-value purpose for their waste, but it also decreases the feedstock cost for the LCNMF facility.

3.5 CONCLUSION

This work demonstrated the technical and economic feasibility of a large-scale process to produce LCNMF directly from low-cost agricultural waste feedstock. The 100-tonne feedstock/day standalone facility can produce 18,400 tonnes of LCNMF per year with a MPSP of US$4.60/kg (at 15% discount rate). The LCNMF produced has widths ranging from 2-17 nm, being in the lower size range compared to current nano-microfibrils producers. The key parameters that enabled the economic feasibility of the process were the use of inexpensive feedstock (representing only 6% of variable operating costs) and the conversion process simplicity (low temperature, atmospheric pressure), which resulted in lower capital costs. The main variable operating cost drivers were the chemicals used to produce peracetic acid (67% of total), while the capital costs of Area 4 (mechanical fibrillation) and 5 (WWT) combined comprised 93% of the total. By increasing the facility size, the capital cost per annual tonne of LCNMF was dramatically reduced by 70%, and the resulting MPSP was lowered by 38% due to the economies of scale. In addition, co-location with a biorefinery was proven advantageous since the LCNMF facility can use the WWT plant of the bigger facility, causing a reduction in capital cost by about $44 million compared to the standalone scenario. Overall, the comprehensive process assessed in this work can produce LCNMF of small sizes at a competitive price (less than $5/kg). We conclude,

therefore, that our novel standalone process to produce cost-competitive nanocellulose products is economically feasible, promoting the commercialization of such products for many applications.

Chapter 4. Comparative study of lignocellulosic nanomaterials production from different heterogeneous waste feedstocks

4.1 SUMMARY

Nanocellulose products may be produced from various heterogeneous waste feedstocks such as agricultural residues, invasive plant species, and other low-cost lignocellulosic biomass, providing economic and sustainability advantages related to the conventional bleached wood pulp feedstock. However, for this to become a reality on a large scale, robust conversion processes that accommodate such heterogeneous feedstocks must be developed. In this study, three different heterogeneous waste feedstocks were utilized (corn stover, reed canary grass, and industrial hemp) to assess the robustness of a conversion process previously described by our group to make lignocellulosic nanomaterials. Lignocellulosic nanofibrils (LCNF) and microfibrils (LCMF) were successfully produced from all biomass feedstocks tested, but the original biomass's chemical and physical characteristics influenced the final nanomaterials' properties. The chemical composition and nature of the initial feedstock showed a direct effect on the total mass yields during the process as well as on the surface charge characteristics of the final nanomaterials. In addition, the physical characteristics of the feedstock affected the degree of delignification during the reactions, producing materials with different residual lignin contents. This work has demonstrated the successful production of nanomaterials from various highly-available, low-cost waste feedstocks, advocating for the large-scale production of nanocellulose products in the United States.

Pascoli DU, Dichiara AB, Gustafson R, Bura R.

Manuscript in preparation for publication

4.2 INTRODUCTION

Nanocellulose products have been primarily produced from bleached wood pulp, a high-purity, homogeneous feedstock comprising virtually pure cellulose (20). Yet, there has been an interest in utilizing low-purity, heterogeneous waste feedstocks containing other components besides cellulose (e.g., hemicellulose, lignin, pectin, ash, and/or extractives), such as agricultural residues, forest residues, and pulp and paper waste in nanocellulose production due to their economic and sustainability benefits (20,123). Utilizing low-purity feedstocks combined with mild processing conditions can generate a specific type of nanocellulose product containing cellulose, hemicellulose, and residual lignin (19,28) – therein referred to as lignocellulosic nanomaterials. Lignocellulosic nanomaterials have unique properties associated with their hemicellulose and lignin components, including colloidal stability, easier fibrillation, hydrophobicity, improved barrier properties, among others, which may be beneficial depending on the application (29–32).

Although utilizing low-purity, heterogeneous feedstocks is a promising solution to economic and environmental issues surrounding current nanocellulose production, the conversion processes to produce the nanocellulose must be robust enough to accommodate the impurities from these feedstocks. The ideal process should also be effective with different types of feedstocks to avoid a high dependency on a specific kind of raw material, which could limit the process' viability on a large scale (49). Ultimately, a robust process capable of running with various waste feedstocks can enable large-scale processing facilities to be built in different locations across the country since it could utilize any biomass available in the region.

In a previous study, our research group established a conversion process to produce lignocellulosic nanomaterials using wheat straw (WS) feedstock, a highly available food crop residue. The process consisted of mild alkaline peroxide pulping (for delignification) and peracetic

acid pretreatment (for carbohydrate oxidation) followed by mechanical treatments (for fibrillation), generating lignocellulosic nanomaterials with excellent properties (104). However, even though this conversion process represents a promising route to producing inexpensive nanomaterials from waste feedstocks, it is necessary to determine if it would also be effective with other types of feedstocks. Thus, the present work selected three different waste feedstocks, including another food crop residue (corn stover), an invasive grass species (reed canary grass), and an industrial lignocellulosic residue (industrial hemp), to evaluate the robustness of the conversion process.

Corn stover (CS) is an agricultural crop residue comprising the leftover stalks and leaves from corn production. CS is the largest source of agricultural residue in the United States, representing about 70% of total annual crop residue production, with availability estimated to reach up to 264 million dry tons by 2030 at a simulated price of $50/dry ton (124). Besides being mainly used in low-value applications such as animal bedding and cattle feed production (125), CS has also been the focus of several studies for biofuels and biochemicals production during the past years, including many reports from the National Renewable Energy Laboratory (NREL) (105,108,126), due to its high availability and low price.

Reed canary grass (*Phalaris arundinacea* L. - RCG) is a lignocellulosic perennial crop that can grow on marginal lands that are not suitable for food crops (127). RCG is considered an invasive species in United States wetlands, causing a reduction in native plant diversity and requiring management strategies to control its spread (128,129). Currently, RCG is primarily used in low-value agriculture applications such as hay production, straw or bedding for livestock, and soil conservation. Still, RCG has been studied for use in other applications, including the pulp and

paper industry as a replacement for hardwood fibers and other energy conversion processes (127,130).

Industrial hemp (*Cannabis sativa* L. - IH) is a fast-growing, non-wood plant fiber crop with low water and nutrient requirements that grows in various conditions (131,132). IH seeds are currently used for oil extraction, while the remaining stalks (which represent about 70% of the plant's dry weight) have been used in low-value applications or just gone to waste (131). Morphologically, IH stalks contain two types of fibers: bast (very long, about 10 to 20 times longer than fibers from hardwoods, softwoods, and agricultural residues) and core fibers (shorter, similar physical characteristics to hardwood fibers (130,133). Bast fibers are commonly used in ropes, paper, textiles, and composites, while core fibers are used in paper, construction materials, biofuels, and others (132).

These three biomass feedstocks have great potential for high-value applications, either due to their high availability, invasive nature, low-value market, or low water and nutrient requirements. Thus, in this work, we utilized CS, RCG, and IH to produce high-value lignocellulosic nanomaterials (nano and microfibrils) via the mild conversion process previously described by our research group (104). This work's goal is to assess the robustness of the conversion process by utilizing various heterogeneous waste feedstocks with different chemical and physical characteristics, and to understand how the inherent nature of the feedstocks may affect the process outcomes. The chemical composition of all biomass feedstocks before and after each chemical treatment was assessed and the recoveries of specific components (i.e., holocellulose and lignin) were calculated. Then, the lignocellulosic nanofibrils (LCNF) and microfibrils (LCMF) produced from each feedstock were compared in terms of light transmittance values, surface chemistry, crystallinity, and morphology. Ultimately, by proving that this process is robust and feedstock-

flexible, the potential to produce nanocellulose products can be enormous due to the high availability of heterogeneous waste feedstocks in the US.

4.3 MATERIALS AND METHODS

4.3.1 Raw materials

Three biomass feedstocks were utilized in this study. Corn stover (CS) ground to 6 mm particle size was sourced from Forest Concepts in Auburn, WA. Reed canary grass (RCG) bales were sourced from farms in Lewis County, WA, and cut into half-inch pieces using a hand pruner. Industrial hemp (IH) stalks were sourced from the Squaxin Island tribe, WA, and ground to 2 mm particle size. All biomass feedstocks were air-dried and stored in plastic buckets until use.

4.3.2 Alkaline peroxide pulping

The biomass feedstocks underwent alkaline peroxide pulping and refining following the procedure previously reported in our previous study (104).

4.3.3 Peracetic acid pretreatment

The refined pulps were submitted to peracetic acid (PAA) pretreatment based on the procedure reported in Chapter 3 of this dissertation (subsection 3.3.2).

4.3.4 Lignocellulosic fibrils (nano and micro) production

The PAA treated pulps were fibrillated using a blender, followed by homogenization with a horn ultrasonicator. The samples were then centrifuged to separate two product fractions: supernatant consisting of lignocellulosic nanofibrils (LCNF) and precipitate consisting of lignocellulosic microfibrils (LCMF). The LCNF suspensions were concentrated by vacuum-rotary drum evaporation at 90°C. All samples were stored in glass bottles at room temperature until use.

4.3.5 Characterization techniques

Chemical composition

The chemical composition of untreated biomass feedstocks, alkaline peroxide pulps, and PAA treated pulps were assessed following the same procedures reported in Chapter 2 (subsection 2.3.5).

Mass yield and component recovery after pulping and pretreatment

The total mass yield after pulping and PAA pretreatment was determined gravimetrically by comparing the oven-dry (OD) mass of pulp obtained after each process with that of the untreated biomass (Equation 4.1).

$$\text{Mass yield (\%)} = \frac{\text{Pulp mass after each reaction (g)}}{\text{Mass of untreated biomass (g)}} \times 100 \qquad \text{Eq. 4.1}$$

The recoveries of holocellulose (i.e., cellulose and hemicellulose) and lignin components after pulping and PAA pretreatment were calculated by correlating the mass yield and chemical composition at each stage to that of the untreated biomass (Equation 4.2).

$$\text{Component recovery (\%)} = \frac{\text{Amount of component in pulp (\%)} \times \text{Mass yield (\%)}}{\text{Amount of component in untreated biomass (\%)}} \qquad \text{Eq. 4.2}$$

Product separation yield

The product separation yield was determined by centrifugation. Two fractions of products were obtained after centrifugation: supernatant LCNF and precipitate LCMF. The product separation yields, expressed as percentages, were calculated by the OD weight ratio of each product fraction to the pre-centrifugation suspension (Equation 4.3).

$$\text{Separation yield (\%)} = \frac{\text{post-centrifugation LCNF or LCMF dry mass (g)}}{\text{pre-centrifugation LCNF + LCMF dry mass (g)}} \times 100 \qquad \text{Eq. 4.3}$$

Lignocellulosic fibrils characterization

Light transmittance of LCNF and LCMF suspensions was conducted using UV/VIS/NIR Spectrophotometer with scans ranging from 400 to 800 nm. Charge density was determined by conductometric titration. Crystallinity index was determined by X-ray diffraction (XRD). Fourier transform infrared spectroscopy (FTIR) was used to evaluate bonds within samples. Fiber morphology was characterized by scanning electron microscopy (SEM) and atomic force microscopy (AFM) techniques. For detailed information about these characterization techniques, refer to Chapter 2 of this dissertation (subsection 2.3.5).

4.4 Results and Discussion

Figure 4.1 summarizes the process steps to produce lignocellulosic nanomaterials from CS, RCG, and IH. First, each biomass feedstock underwent alkaline peroxide pulping and refining, producing refined pulps. Then, the pulps underwent PAA pretreatment, producing PAA treated pulps. In the specific case of IH, an additional PAA condition (referred to as PAA 10x) was carried out, producing PAA 10x treated pulp. Finally, all PAA treated pulps underwent mechanical fibrillation, homogenization, and separation, generating two product fractions: lignocellulosic nanofibrils (LCNF) and microfibrils (LCMF). The chemical composition of each untreated biomass and their pulps after each reaction step (i.e., pulping and PAA pretreatment) was assessed, and the obtained lignocellulosic nanomaterials (LCNFs and LCMFs) were characterized (light transmittance, surface chemistry, crystallinity, morphology, and thermal stability) and compared.

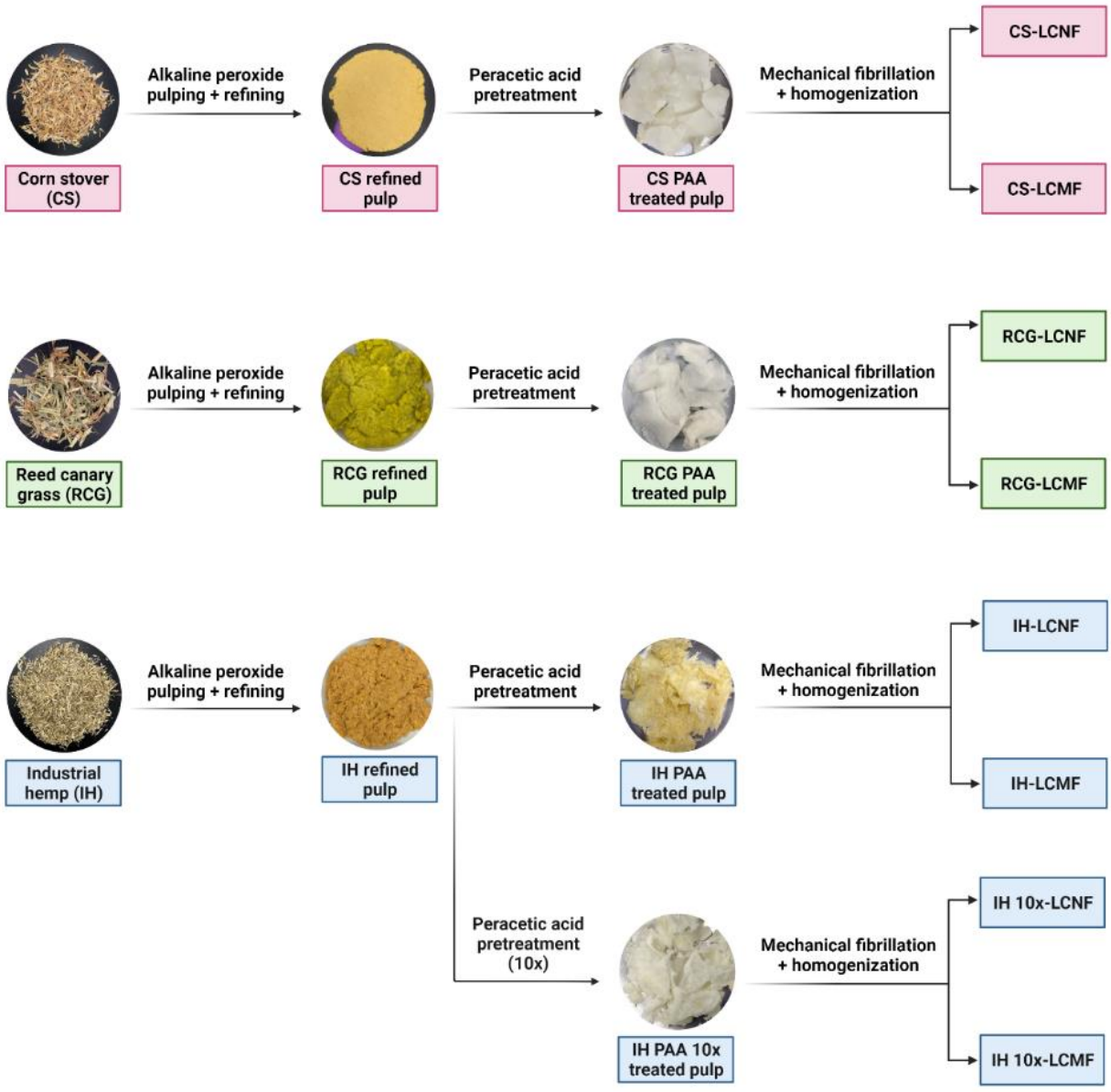

Figure 4.1. Summary of process steps to produce lignocellulosic nanomaterials (LCNF and LCMF) from different biomass feedstocks.

4.4.1 Effect of chemical treatments on biomass chemical composition

Figure 4.2 shows the effect of pulping and PAA pretreatment reactions on the chemical composition of each biomass feedstock by displaying the recovery percentages of holocellulose (corresponding to both cellulose and hemicellulose fractions) and lignin, the main components of

biomass. The total mass yield and complete chemical composition of each material are shown in Appendix C, Table A.6.

The goal of mild alkaline peroxide pulping was to remove lignin to a certain extent to enable the fibrillation while keeping most holocellulose intact for higher yields. Figure 4.2 shows that more than 76% of holocellulose was preserved in all feedstocks after pulping, demonstrating a relatively low carbohydrate loss during the reaction. Furthermore, RCG had the lowest total mass yield (49%) due to the original feedstock's high extractives and ash content (Appendix C, Table A.6), which were also removed during the pulping reaction. If desired, the RCG mass yield could be improved by using only the stem portion of the feedstock since the leaves are the parts that contain the most ash and extractives (130).

A high delignification during pulping was observed for both CS and RCG, with similar lignin removal percentages ranging from 78-81% (i.e., 19-22% lignin recovery), while IH had the lowest lignin removal of only 36% (Figure 4.2). The low lignin removal observed for IH is in accordance with a previous study by Wawro et al. The authors reported little effect on the lignin content of IH fibers after mild NaOH treatment (90 °C for 5 h) (134). The difference in delignification extent of IH compared to the other feedstocks can be explained by its inherited physical characteristics. Because IH stalks have a similar structure as woody biomass, alkaline pulping treatments performed on IH biomass are usually carried out at much higher temperatures (usually between 120-180 °C) (133,135), similar to the commonly used in hardwood pulping. Thus, the milder pulping condition employed in the present study (90 °C, atmospheric pressure) probably just solubilized the highly reactive lignin in IH, such as phenolic α-O-4 linkages that are easier to break during pulping at lower temperatures (136), while CS and RCG showed a more extensive delignification under the same conditions. These outcomes are in accordance with previous studies

from the literature, where Joachimiak et al. compared pulping yields and degree of delignification of a woody biomass (Birch sawdust) with that of a grass (Miscanthus stems) (137). The authors found that, under the same pulping conditions, the grass displayed much higher and faster delignification than the wood, which was attributed to chemical and morphological differences between the two feedstocks.

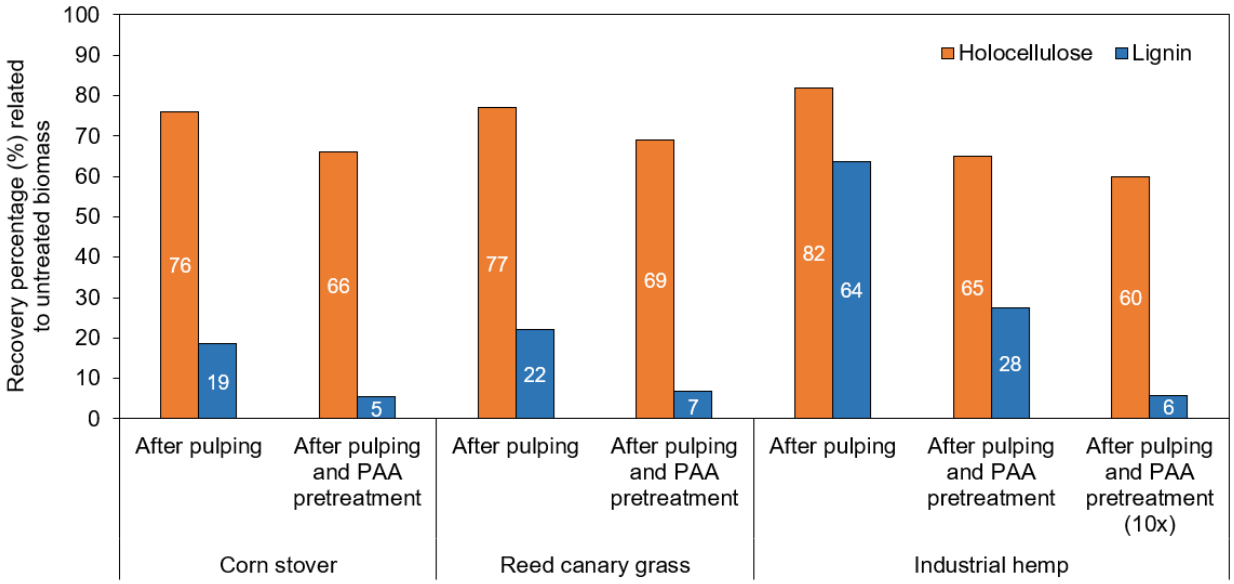

Figure 4.2. Recovery percentages of holocellulose and lignin components after pulping and PAA pretreatment related to untreated biomass.

After PAA pretreatment, all feedstocks displayed a trend of further delignification accompanied by minor carbohydrate loss (Figure 4.2), similar to previous studies employing PAA treatments on different feedstocks (54,138,139); therefore demonstrating the high selectivity of PAA towards lignin. Compared to the untreated biomass, both CS and RCG had low overall lignin recoveries (5-7%), while IH still had 28% of the original lignin in its composition. These results again demonstrate that IH lignin is more difficult to remove than that of CS and RCG under the same mild reaction conditions. Due to its higher residual lignin content, IH PAA treated pulp presented

a yellow-toned color, as shown in Figure 4.1. Furthermore, by increasing the amount of chemicals during PAA pretreatment of IH by 10x, a more substantial delignification was achieved (94% lignin removal), reaching similar recoveries to those obtained for CS and RCG under normal PAA pretreatment conditions. This improvement in delignification goes along with previous reports in the literature, where increased PAA concentration during a bleaching reaction at pH 5 improved the whiteness index (which can be directly correlated with lignin content) of IH pulp (140). Interestingly, the increase in PAA chemical load by 10x seemed to have mainly affected the lignin (as seen by a 22% difference in recovery compared to PAA at original reaction conditions) and not as much the holocellulose (only 5% difference). This outcome indicates that the lignin component is more sensitive to changes in PAA load than the carbohydrates (141), which may be attributed once again to high PAA selectivity towards lignin.

4.4.2 Nanomaterials characterization

Fibrils suspension and optical transmittance

Figure 4.3A shows photographs of the LCMF and LCNF suspensions obtained after mechanical fibrillation and homogenization of PAA treated pulps, along with their percent light transmittance values at 600 nm. The complete light transmittance spectra of each suspension are shown in Figure 4.3B. It can be seen in Figure 4.3A that the mild process utilized in this study successfully produced gel-like suspensions of LCNF and LCMF from all feedstocks tested. All LCNF fractions exhibited high light transmittance values (83-88% at 660 nm), an indication of nanofibrils of very small sizes, while all LCMF fractions showed a milk-white appearance and low transmittance values (3-8%) due to higher light scattering from bigger fibrils (84,142). In addition, all LCNFs and LCMFs demonstrated colloidal stability, which may be related to the presence of hemicellulose heteropolysaccharides (as seen by the presence of arabinan, galactan, xylan, and mannan in

Appendix C, Table A.7) that are known to promote colloidal stability by steric and coulombic forces (28). Furthermore, lignin is known to have a light absorption trait (142); thus, IH LCNF and IH LCMF presented lower transmittance values across the entire spectra (Figure 4.3B) due to their higher residual lignin content (12%) compared to the other samples (2-4%) (Appendix C, Table A.6). Interestingly, IH 10x-LCMF presented some fibrils aggregation (Figure 4.3A), while the other LCMFs showed a more homogeneous feature.

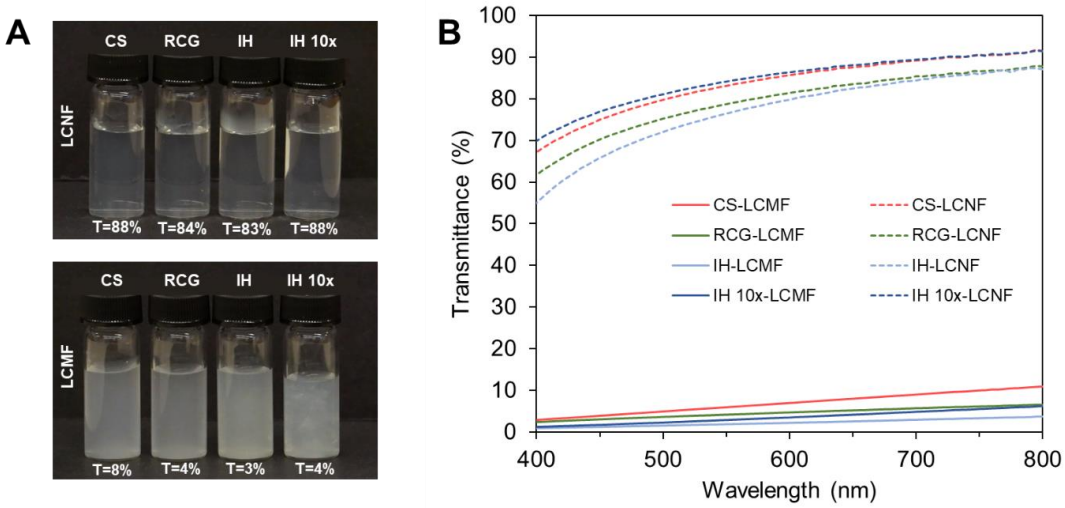

Figure 4.3. (A) Photograph of the suspensions and their respective percent transmittance at 660 nm. (B) Optical transmittance spectra of different lignocellulosic fibrils suspensions.

Surface chemistry

Figure 4.4 shows FTIR spectra with specific bonds of the LCNF (Figure 4.4A) and LCMF (Figure 4.4B) fractions obtained from each feedstock, along with the charge density (CD) values obtained by conductometric titration. It can be seen that both LCNFs produced from IH presented higher CD values (322-344 µmol g^{-1}) than those from CS and RCG (110-112 µmol g^{-1}) (Figure 4.4A). A similar trend was observed for LCMFs produced from IH, but to a lower extent (Figure 4.4B). The more prominent peak at 1604 cm^{-1} in FTIR spectra of both IH-LCNF and IH 10x-LCNF validated their higher CD values obtained via titration, as this particular band has been correlated

with carboxyl groups present in hemicellulose (143,144) that promote surface charge to the fibers. Furthermore, the peak at 1504 cm^{-1} corresponding to C=C stretching vibration of lignin aromatic rings (145) was more prominent in IH-LCNF and IH-LCMF samples, which agrees with the higher residual lignin content obtained for this sample.

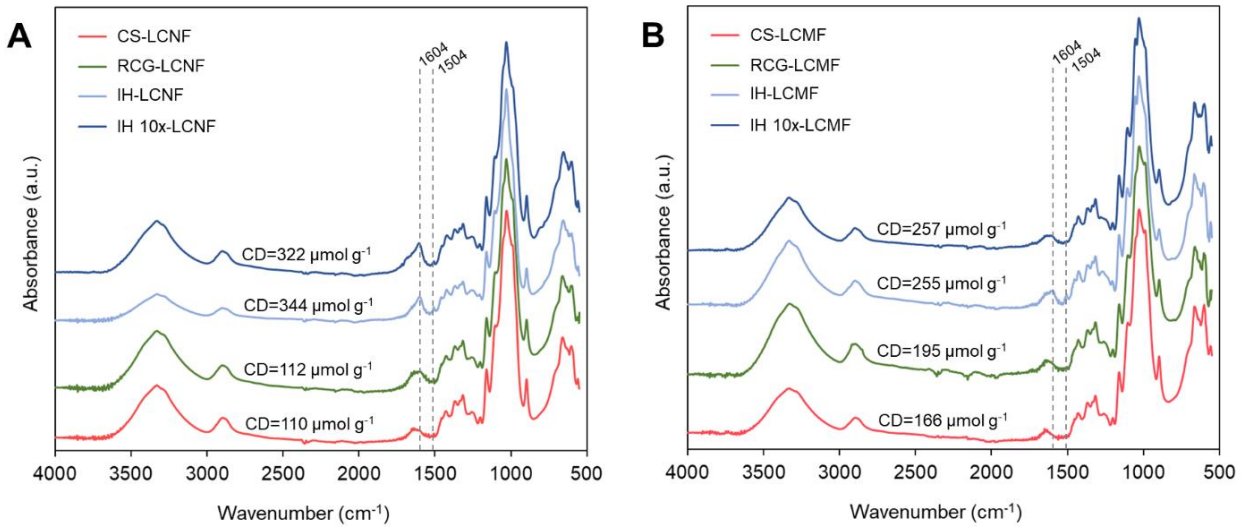

Figure 4.4. FTIR spectra showing specific chemical bonds of (A) LCNFs and (B) LCMFs of different biomass feedstocks. Charge density (CD) values obtained via conductometric titration are also shown (the titration curves are shown in Appendix C, Figure A.4).

To further investigate the higher CD of LCNFs and LCMFs produced from IH biomass, FTIR spectra of the pulps after alkaline peroxide pulping (i.e., before PAA treatment) were also assessed (Figure 4.5). Interestingly, IH pulp showed a much more prominent peak at 1604-16 cm^{-1} (which overlaps with water around 1630 cm^{-1}), which is associated with carboxyl groups of glucuronic acid in hemicellulose (143,144). In addition, the peaks at 780 cm^{-1} and around 1732 cm^{-1} appeared exclusively in IH pulp, therefore representing molecules that are inherent to this specific type of biomass. 780 cm^{-1} has been previously assigned to carboxyl groups of hemicellulose (146). The band around 1732 cm^{-1} has been attributed to C=O stretching vibration of either acetyl groups

present in xyloglucan (a specific type of hemicellulose present in IH biomass) (144,147,148) or carboxylic ester groups in pectin (149,150).

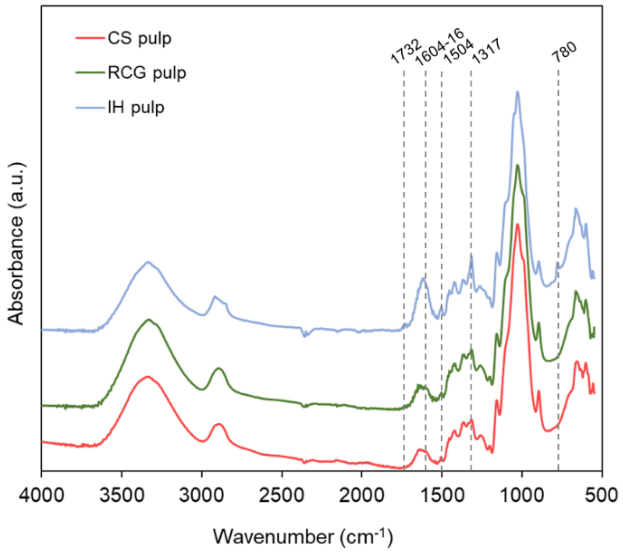

Figure 4.5. FTIR spectra showing specific chemical bonds of pulps of different biomass feedstocks.

The results above indicate that IH's higher carboxyl content compared to CS and RCG is mainly associated with hemicellulose acid groups and the presence of pectins. The literature has described that IH biomass has considerable galacturonic acid content, which can be attributed to the presence of pectin molecules such as rhamnogalacturonan-I (151,152). Correspondingly, the untreated IH biomass used in this study showed higher acetyl/uronic acids content (5.5%) compared to the other untreated feedstocks (3.1-3.8%) (Appendix C, Table A.6), confirming the presence of pectin substances in IH. Hence, it can be inferred that the higher CD obtained for LCNF and LCMF from IH biomass is attributed mainly to IH biomass's inherent hemicellulose and pectin compounds, with a posterior intensification during the oxidation reactions from PAA pretreatment. Finally, the peak at 1317 cm^{-1} has been assigned to C-O stretching of C5 substituted aromatic rings, such as syringyl and condensed guaiacyl units of lignin (143,144). This peak is present for all three pulps,

but it is more prominent in IH, probably as a result of IH pulp's higher lignin content (19%) compared to CS and RCG pulps (6 and 10%, respectively) (Appendix C, Table A.6).

Fiber structure and morphology

Table 4.1 summarizes the separation yields of lignocellulosic fibrils after centrifugation and their structural and morphological characteristics (crystallinity index, fibril width and length, and fibril aspect ratio). All feedstocks resulted in LCNF yields ranging from 25-34% (with corresponding LCMF yields of 66-75%), demonstrating that the process is robust and produces similar amounts of LCNF fraction. Among the three biomass feedstocks tested, IH and IH 10x samples showed the lowest LCNF yields (27 and 25%, respectively), with correspondingly the highest LCMF yields (73% and 75%), suggesting lower effectiveness of the mechanical treatments on IH biomass. Interestingly, the lignin content seemed to not play a crucial role in the extent of fibrillation of IH, as both IH and IH 10x resulted in similar LCNF/LCMF separation yields. This evidence suggests that varying lignin contents between 3-12% (Appendix C, Table A.6) did not affect the extent of release of nanofibrils from IH in the present process, which is a remarkable outcome.

Furthermore, the lower LCNF yields of samples prepared from IH compared to CS and RCG indicate a lower degree of "nanofibrils release" from the bigger fibrils in the original hierarchical structure of IH. This outcome may be related to the physical structure of IH biomass, which comprises two kinds of fibers known as bast and core fibers. Bast fibers are extremely long fibers with about 25 mm in cell length (as a comparison, softwood cells are about 3.5 mm in length), while core fibers have similar physical characteristics as hardwoods with 0.8 mm cell length (133). Therefore, the diverse fiber sizes in IH biomass could have caused incomplete fibrillation during the mechanical treatments, leading to lower LCNF yields.

The crystallinity index (CI) of the different lignocellulosic nanomaterials is also included in Table 4.1. Little difference was observed between the CI of LCNF and LCMF fractions produced from (from 64% to 75%).

Table 4.1. Separation yields of lignocellulosic fibrils after centrifugation and their structural and morphological characteristics (crystallinity index, fibril width and length, and fibril aspect ratio).

		Separation yield (%)	CI (%)	Fibril width (nm)	Fibril length (μm)	Fibril aspect ratio
LCNF	**CS**	30	71	2.1 ± 0.7	1.2 ± 0.7	585
	RCG	34	66	2.3 ± 1.4	1.4 ± 0.9	591
	IH	27	64	2.4 ± 0.9	1.4 ± 0.8	599
	IH 10x	25	66	2.8 ± 1.2	1.6 ± 1.2	565
LCMF	**CS**	70	72	16.9 ± 5.1	-	-
	RCG	66	69	14.3 ± 3.4	-	-
	IH	73	72	18.0 ± 12.3	-	-
	IH 10x	75	75	15.9 ± 9.3	-	-

The morphology of the LCNF fractions generated from different biomass feedstocks was characterized by AFM imaging (Figure 4.6), and the fibrils dimensions are included in Table 4.1. The AFM images revealed that all LCNFs had the morphology of elementary fibrils, with average widths ranging from 2.1-2.8 nm and lengths ranging from 1.2-1.6 μm. Such a similar range in width and lengths also resulted in comparable LCNF size ratios (565-599) (Table 4.1). These results demonstrate the effectiveness of the conversion process in producing LCNFs from a wide range of feedstocks with sizes corresponding to nanofibrils obtained via harsher TEMPO oxidation pretreatment using hardwood pulp feedstock (47). The size distribution curves for the width and length of each sample are also shown in Figure 4.6. RCG-LCNF presented a broad, right-skewed distribution for fibril width, indicating the presence of thinner and thicker nanofibrils, as reflected in its higher standard deviation. Also, all LCNFs showed a right-skewed distribution for nanofibril

length, especially the IH 10x-LCNF sample with the highest standard deviation. A surprising outcome related to the results shown in Table 4.1 and Figure 4.6 refers to both IH-LCNF and IH 10x-LCNF showing not only similar separation yields as previously mentioned but also similar nanofibril morphologies regardless of their different lignin contents.

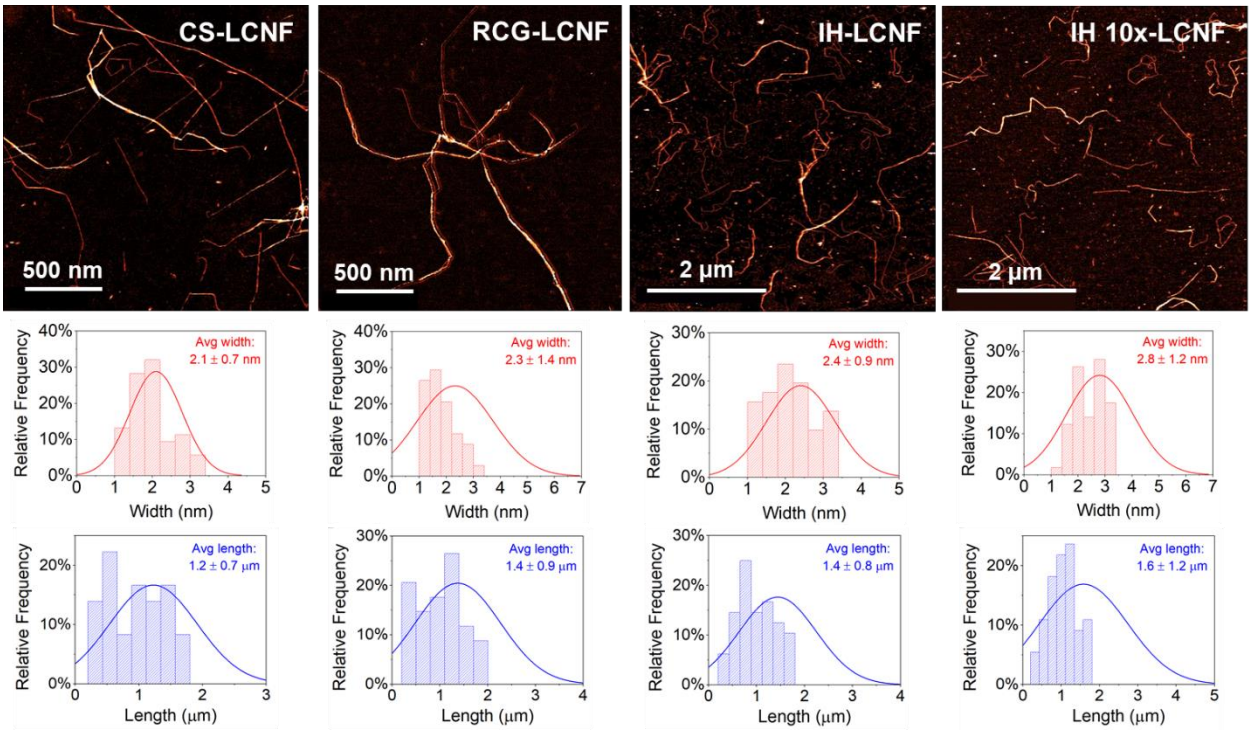

Figure 4.6. AFM images and size distribution curves of LCNF from different biomass feedstocks.

The morphology of the LCMF fractions was characterized by SEM imaging (Figure 4.7), and the fibrils widths are included in Table 4.1. Notably, CS and RCG feedstocks produced more uniform LCMFs than IH (Figure 4.7). IH-LCMF and IH 10x-LCMF presented several fibril bundles, supporting the above interpretation of incomplete fibrillation during IH processing, and therefore resulted in the highest average widths and the broadest standard deviations (Table 4.1). LCMFs produced from IH also presented broader, right-skewed width distribution curves than those produced from CS and RCG (Figure 4.7). Interestingly, IH 10x-LCMF had a lower standard

deviation than IH-LCMF, indicating that a lower lignin content could have helped reduce the occurrence of partially-fibrillated fibrils in the LCMF fraction. Overall, the average width of the LCMFs produced in this study varied between 14 and 18 nm, independent of the type of feedstock used. Our LCMFs have widths comparable to other studies (4,61,94,95), with the particular case of the LCMFs produced from IH biomass that contains a more heterogeneous size distribution comprising individual microfibrils and bundles.

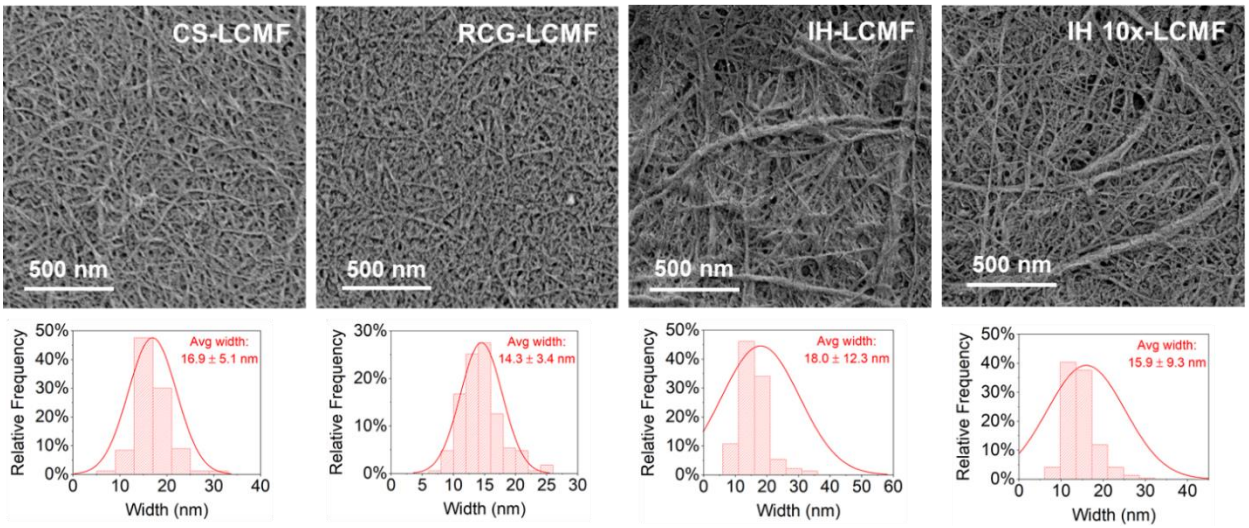

Figure 4.7. AFM images and size distribution curves of LCNF from different biomass feedstocks.

4.5 CONCLUSION

This study has demonstrated that lignocellulosic nanomaterials (LCNF and LCMF) were successfully produced from three heterogeneous waste feedstocks (CS, RCG, and IH) via the same conversion process at mild conditions. Yet, the different chemical and physical characteristics of the original biomass feedstock influenced various properties of the final nanomaterials. For instance, a feedstock with higher extractives and ash content (i.e., RCG in this study) resulted in lower total mass yield after pulping and PAA pretreatment due to the removal of such components

during the reactions. Then, a feedstock with physical characteristics similar to woody materials (i.e., IH in this study) demonstrated a much lower delignification yield during the mild reactions, resulting in nanomaterials with higher residual lignin content. Correspondingly, IH's physical structure and recalcitrance during the conversion process produced lower LCNF yields than the other feedstocks and an LCMF fraction with wider size distribution due to remaining partially fibrillated bundles. In addition, depending on the chemical characteristics of the original biomass, such as the presence of high contents of glucuronic acids in hemicellulose and/or pectin substances, the surface charge density of the final nanomaterials was significantly higher. Finally, different chemical compositions and the nature of the residual lignin can affect the thermal stability of the final nanomaterials.

Hence, the conversion process was surprisingly robust, producing lignocellulosic nanomaterials from very different types of heterogeneous feedstocks, including a food crop residue, an invasive grass species, and an industrial lignocellulosic residue. Using highly available waste feedstocks such as these can provide substantial economic and sustainability benefits to nanocellulose production, representing a significant effort in supporting their production on a large scale in various regions across the United States.

Chapter 5. Conclusion and Future Work

5.1 Conclusion

Nanocellulose is an excellent alternative to petroleum-based materials and chemicals in various applications due to its abundance, sustainability, and unique properties. Yet, major barriers such as high production costs hinder nanocellulose from achieving its full application potential. This research project aimed to develop a cost-effective and robust conversion process to produce lignocellulosic nanomaterials from low-cost waste feedstocks. The process developed consisted of mild alkaline peroxide pulping, peracetic acid pretreatment, and mechanical treatments that successfully generated two types of lignocellulosic nanomaterials (LCNF and LCMF).

Surprisingly, the process was effective with four different low-cost feedstocks, i.e., wheat straw, corn stover, reed canary grass, and industrial hemp. This remarkable finding demonstrates the process's robustness and potential to be established in various locations across the country due to its low feedstock dependency. However, the different chemical and physical characteristics of the feedstocks impacted the yields and properties of the final nanomaterials. In addition, the techno-economic analysis revealed that the process was economically feasible, mainly due to the use of a low-cost feedstock and mild reaction conditions that eliminated the need for expensive pressurized equipment and a steam generation system. The MPSP of lignocellulosic nanomaterials was further reduced by either increasing the facility size to achieve economies of scale or co-locating with another facility (e.g., biorefinery or corn-to-ethanol plant) to promote beneficial exchanges of process streams and equipment. Finally, the lignocellulosic nanomaterials obtained from wheat straw biomass presented excellent plastic reinforcement properties. A substantial improvement in mechanical properties was achieved, with a remarkable case of simultaneous strengthening and toughening of the composite, demonstrating their potential for application in composites and

packaging, which are the biggest market drivers for nanocellulose products nowadays. In sum, the present research successfully validated the conversion process effectiveness, economic feasibility, and robustness, as well as the application potential for the nanomaterials produced.

This work has shown significant efforts toward one of the biggest challenges of the 21st century, which is the transition from a petroleum-based economy to a more renewable and sustainable era. By developing more cost-effective technologies to produce nanocellulose, we can increase its production capacity worldwide and enable the use of this biomaterial in various applications as a sustainable alternative to petroleum-based materials. The present work targeted one of the greatest challenges to nanocellulose commercialization: high production costs. This complex problem cannot be solved by one specific research area; instead, it requires efforts across different fields to develop a viable solution. Hence, this research project presented a unique interdisciplinary approach that combined efforts in process engineering, computational modeling, and materials science toward the common goal of producing nanocellulose more cheaply and sustainably. Ultimately, this study aimed to make a scientific contribution towards the production of sustainable and cost-effective nanocellulose products that can become a reality in the future. For a new technology to be tangible, it must be effective and produce high-quality products; it must be robust; and most importantly, it must be cheap – and the present research has demonstrated that this can be possible.

5.2 FUTURE WORK

The research carried out in this project has established the early efforts from our research group to solve the nanocellulose high production costs issue, thus setting the stage for further research initiatives. One area worth investigating further is the fine-tuning of the process conditions to control the extent of cellulose, hemicellulose, and lignin removal during the reactions. By

obtaining nanomaterials with tailored chemical compositions, it will be possible to understand better how each component and its overall content affects the final properties of the nanomaterials. Another area worth exploring is expanding the feedstock portfolio to hardwoods (e.g., poplar), seeing that industrial hemp has many similarities to hardwoods, and it showed promising results in this work.

With the establishment that the lignocellulosic nanomaterials are economically feasible at their aqueous suspension state, further investigation should be carried out on the drying and redispersion of the nanomaterials. Drying nanocellulose products is a critical step when considering selling and shipping these nanomaterials to other industries. Thus, different drying methods should be tested, and the effect on the nanomaterial's properties should be investigated. Finally, from the final application point of view, the lignocellulosic nanomaterials should be added to other types of matrices, such as polylactic acid (PLA). PLA is a biomass-derived, biodegradable material with a hydrophobic nature, which can be challenging since most cellulosic materials are hydrophilic in nature. However, the presence of residual lignin in lignocellulosic nanomaterials can be a great asset due to its hydrophobic properties. Hence, this research area can provide a better understanding of how the lignin content of the nanomaterials can influence their dispersion on the PLA matrix.

BIBLIOGRAPHY

1. Dhali K, Ghasemlou M, Daver F, Cass P, Adhikari B. A review of nanocellulose as a new material towards environmental sustainability. Sci Total Environ. 2021;775:145871. DOI: 10.1016/j.scitotenv.2021.145871
2. Michelin M, Gomes DG, Romaní A, Polizeli M de LTM, Teixeira JA. Nanocellulose production: Exploring the enzymatic route and residues of pulp and paper industry. Molecules. 2020;25(15):1–36. DOI: 10.3390/molecules25153411
3. Mokhena TC, John MJ. Cellulose nanomaterials: new generation materials for solving global issues. Cellulose. 2020 Feb 1;27(3):1149–94. DOI: 10.1007/s10570-019-02889-w
4. Meng Q, Fu S, Lucia LA. The role of heteropolysaccharides in developing oxidized cellulose nanofibrils. Carbohydr Polym. 2016;144:187–95. DOI: 10.1016/j.carbpol.2016.02.058
5. Adel AM, El-Gendy AA, Diab MA, Abou-Zeid RE, El-Zawawy WK, Dufresne A. Microfibrillated cellulose from agricultural residues. Part I: Papermaking application. Ind Crops Prod. 2016;93:161–74. DOI: 10.1016/j.indcrop.2016.04.043
6. Spence KL, Venditti RA, Rojas OJ, Habibi Y, Pawlak JJ. A comparative study of energy consumption and physical properties of microfibrillated cellulose produced by different processing methods. Cellulose. 2011;18(4):1097–111. DOI: 10.1007/s10570-011-9533-z
7. Dufresne A. Cellulose nanomaterials as green nanoreinforcements for polymer nanocomposites. Philos Trans R Soc A. 2018 Feb 13;376. DOI: 10.1098/rsta.2017.0040
8. Delgado-Aguilar M, González I, Tarrés Q, Alcalà M, Pèlach MÀ, Mutjé P. Approaching a low-cost production of cellulose nanofibers for papermaking applications. BioResources. 2015;10(3):5330–44. DOI: 10.15376/biores.10.3.5330-5344
9. Balea A, Fuente E, Monte MC, Merayo N, Campano C, Negro C, et al. Industrial Application of Nanocelluloses in Papermaking: A Review of Challenges, Solutions, and Market Perspectives. Molecules. 2020;25:526–56. DOI: 10.3390/molecules25030526
10. Amoroso L, De France KJ, Milz CI, Siqueira G, Zimmermann T, Nyström G. Sustainable Cellulose Nanofiber Films from Carrot Pomace as Sprayable Coatings for Food Packaging Applications. ACS Sustain Chem Eng. 2022 Jan 10;10(1):342–52. DOI: 10.1021/acssuschemeng.1c06345

11. Sánchez-Gutiérrez M, Bascón-Villegas I, Espinosa E, Carrasco E, Pérez-Rodríguez F, Rodríguez A. Cellulose Nanofibers from Olive Tree Pruning as Food Packaging Additive of a Biodegradable Film. Foods. 2021;10:1–15. DOI: 10.3390/foods10071584
12. Hubbe MA, Ferrer A, Tyagi P, Yin Y, Salas C, Pal L, et al. Nanocellulose in Thin Films, Coatings, and Plies for Packaging Applications: A Review. BioResources. 2017;12(1):2143–233.
13. Choudhury RR, Sahoo SK, Gohil JM. Potential of bioinspired cellulose nanomaterials and nanocomposite membranes thereof for water treatment and fuel cell applications. Cellulose. 2020;27(12):6719–46. DOI: 10.1007/s10570-020-03253-z
14. Mahfoudhi N, Boufi S. Nanocellulose as a novel nanostructured adsorbent for environmental remediation: a review. Cellulose. 2017;24(3):1171–97. DOI: 10.1007/s10570-017-1194-0
15. Balea A, Fuente E, Blanco A, Negro C. Nanocelluloses: Natural-based materials for fiber-reinforced cement composites. A critical review. Polymers (Basel). 2019;11(3). DOI: 10.3390/polym11030518
16. Hoeng F, Denneulin A, Bras J. Use of nanocellulose in printed electronics: A review. Nanoscale. 2016;8(27):13131–54. DOI: 10.1039/c6nr03054h
17. Faruk O, Sain M, Farnood R, Pan Y, Xiao H. Development of Lignin and Nanocellulose Enhanced Bio PU Foams for Automotive Parts. J Polym Environ. 2014;22(3):279–88. DOI: 10.1007/s10924-013-0631-x
18. Salimi S, Sotudeh-Gharebagh R, Zarghami R, Chan SY, Yuen KH. Production of Nanocellulose and Its Applications in Drug Delivery: A Critical Review. ACS Sustain Chem Eng. 2019;7(19):15800–27. DOI: 10.1021/acssuschemeng.9b02744
19. Liu K, Du H, Zheng T, Liu W, Zhang M, Liu H, et al. Lignin-containing cellulose nanomaterials: Preparation and applications. Green Chem. 2021;23(24):9723–46. DOI: 10.1039/d1gc02841c
20. Yu S, Sun J, Shi Y, Wang Q, Wu J, Liu J. Nanocellulose from various biomass wastes: Its preparation and potential usages towards the high value-added products. Environ Sci Ecotechnology. 2021;5:100077. DOI: 10.1016/j.ese.2020.100077
21. García A, Gandini A, Labidi J, Belgacem N, Bras J. Industrial and crop wastes: A new source for nanocellulose biorefinery. Ind Crops Prod. 2016;93:26–38. DOI:

10.1016/j.indcrop.2016.06.004

22. Abdul Khalil HPS, Davoudpour Y, Islam MN, Mustapha A, Sudesh K, Dungani R, et al. Production and modification of nanofibrillated cellulose using various mechanical processes: A review. Carbohydr Polym. 2014;99:649–65. DOI: 10.1016/j.carbpol.2013.08.069
23. de Assis CA, Iglesias MC, Bilodeau M, Johnson D, Phillips R, Peresin MS, et al. Cellulose micro- and nanofibrils (CMNF) manufacturing - financial and risk assessment. Biofuels, Bioprod Biorefining. 2018;12:251–64. DOI: 10.1002/bbb.1835
24. The University of Maine Process Development Center. Nanocellulose Products [Internet]. [cited 2022 May 12]. Available from: https://umaine.edu/pdc/nanocellulose/nanocellulose-products/
25. Serra-Parareda F, Aguado R, Tarrés Q, Mutjé P, Delgado-Aguilar M. Chemical-free production of lignocellulosic micro- and nanofibers from high-yield pulps: Synergies, performance, and feasibility. J Clean Prod. 2021;313:1–10. DOI: 10.1016/j.jclepro.2021.127914
26. Nechyporchuk O, Belgacem MN, Bras J. Production of cellulose nanofibrils: A review of recent advances. Ind Crops Prod. 2016;93:2–25. DOI: 10.1016/j.indcrop.2016.02.016
27. Ashori A, Babaee M, Jonoobi M, Hamzeh Y. Solvent-free acetylation of cellulose nanofibers for improving compatibility and dispersion. Carbohydr Polym. 2014;102(1):369–75. DOI: 10.1016/j.carbpol.2013.11.067
28. Solala I, Iglesias MC, Peresin MS. On the potential of lignin-containing cellulose nanofibrils (LCNFs): a review on properties and applications. Cellulose. 2020;27(4):1853–77. DOI: 10.1007/s10570-019-02899-8
29. Chaker A, Alila S, Mutjé P, Vilar MR, Boufi S. Key role of the hemicellulose content and the cell morphology on the nanofibrillation effectiveness of cellulose pulps. Cellulose. 2013;20(6):2863–75. DOI: 10.1007/s10570-013-0036-y
30. Iwamoto S, Abe K, Yano H. The effect of hemicelluloses on wood pulp nanofibrillation and nanofiber network characteristics. Biomacromolecules. 2008;9(3):1022–6. DOI: 10.1021/bm701157n
31. Rojo E, Peresin MS, Sampson WW, Hoeger IC, Vartiainen J, Laine J, et al. Comprehensive elucidation of the effect of residual lignin on the physical, barrier,

mechanical and surface properties of nanocellulose films. Green Chem. 2015;17(3):1853–66. DOI: 10.1039/c4gc02398f

32. Delgado-Aguilar M, González I, Tarrés Q, Pèlach MÀ, Alcalà M, Mutjé P. The key role of lignin in the production of low-cost lignocellulosic nanofibres for papermaking applications. Ind Crops Prod. 2016;86:295–300. DOI: 10.1016/j.indcrop.2016.04.010
33. Miller J. Nanocellulose: Market perspectives. Tappi J. 2019;18(5):313–6.
34. Reports and Data. Nanocellulose Market [Internet]. 2020. [cited 2022 May 13]. Available from: https://www.reportsanddata.com/report-detail/nanocellulose-market
35. Expert Market Research (EMR). Global Nanocellulose Market Outlook [Internet]. [cited 2022 May 13]. Available from: https://www.expertmarketresearch.com/reports/nanocellulose-market
36. TAPPI Nano Division. Cellulose Nanomaterials Production Summary. 2018;
37. FiberLean Technologies. MFC and its applications in papermaking [Internet]. 2017. Available from: https://www.fiberlean.com/mfc-and-its-applications-in-papermaking-2/
38. Larsson PA, Riazanova A V., Cinar Ciftci G, Rojas R, Øvrebø HH, Wågberg L, et al. Towards optimised size distribution in commercial microfibrillated cellulose: a fractionation approach. Cellulose. 2019;26(3):1565–75. DOI: 10.1007/s10570-018-2214-4
39. Nippon Paper Group. Cellulose nanofiber manufacturing technology and application development [Internet]. Available from: https://www.nipponpapergroup.com/english/research/organize/cnf.html
40. The University of Maine Process Development Center. Cellulose Nanofibril Safety Data Sheet, Version 1. 2017. p. 1–9.
41. Li T, Chen C, Brozena AH, Zhu JY, Xu L, Driemeier C, et al. Developing fibrillated cellulose as a sustainable technological material. Nature. 2021;590(7844):47–56. DOI: 10.1038/s41586-020-03167-7
42. Statista. Global plastics industry - statistics & facts [Internet]. 2021 [cited 2022 Apr 10]. Available from: https://www.statista.com/topics/5266/plastics-industry/#dossierKeyfigures
43. Bottiglieri J. TAPPI Nano 2019: Focus on New Markets [Internet]. 2019 [cited 2021 Nov 21]. Available from: https://paper360.tappi.org/2019/10/03/2346/
44. Nanografi. Cellulose Nanofiber [Internet]. [cited 2021 Nov 8]. Available from:

https://nanografi.com/popular-products/cellulose-nanofiber-cellulose-nanofibril-nanofibrillated-cellulose-cnfs/

45. Natural Resources Canada. Current lumber, pulp and panel prices [Internet]. 2022 [cited 2022 Apr 10]. Available from: https://www.nrcan.gc.ca/our-natural-resources/domestic-and-international-markets/current-lumber-pulp-panel-prices/13309
46. Marzouk J. Pulp and Paper Perspectives Q2 2018 [Internet]. [cited 2021 Nov 21]. Available from: https://www.hilcovaluationservices.com/news-media/perspectives/pulp-and-paper-perspectives-q2-2018
47. Saito T, Kimura S, Nishiyama Y, Isogai A. Cellulose nanofibers prepared by TEMPO-mediated oxidation of native cellulose. Biomacromolecules. 2007;8(8):2485–91. DOI: 10.1021/bm0703970
48. Sigma-Aldrich Corporation. TEMPO [Internet]. [cited 2021 Nov 8]. Available from: https://www.sigmaaldrich.com/US/en/product/aldrich/214000
49. Pascoli DU, Aui A, Frank J, Therasme O, Dixon K, Gustafson R, et al. The US bioeconomy at the intersection of technology, policy, and education. Biofuels, Bioprod Biorefining. 2021;1–18. DOI: 10.1002/bbb.2302
50. WorldAtlas. Top Wheat Producing Countries [Internet]. [cited 2022 Apr 9]. Available from: https://www.worldatlas.com/articles/top-wheat-producing-countries.html
51. USDA. Wheat Outlook. 2020.
52. USDA. National Hay, Feed & Seed Weekly Summary. 2018.
53. Sharma N, Bhardwaj NK, Singh RBP. Environmental issues of pulp bleaching and prospects of peracetic acid pulp bleaching: A review. J Clean Prod. 2020;256:120338. DOI: 10.1016/j.jclepro.2020.120338
54. Kumar R, Hu F, Hubbell CA, Ragauskas AJ, Wyman CE. Comparison of laboratory delignification methods, their selectivity, and impacts on physiochemical characteristics of cellulosic biomass. Bioresour Technol. 2013;372–81. DOI: 10.1016/j.biortech.2012.12.028
55. Jääskeläinen AS, Tapanila T, Poppius-Levlin K. Carbohydrate reactions in peroxyacetic acid bleaching. J Wood Chem Technol. 2000;20(1):43–59. DOI: 10.1080/02773810009349623
56. Yang X, Reid MS, Olsén P, Berglund LA. Eco-Friendly Cellulose Nanofibrils Designed

by Nature: Effects from Preserving Native State. ACS Nano. 2020;14(1):724–35. DOI: 10.1021/acsnano.9b07659

57. Barbash VA, Yashchenko O V., Gondovska AS, Deykun IM. Preparation and characterization of nanocellulose obtained by TEMPO-mediated oxidation of organosolv pulp from reed stalks. Appl Nanosci. 2022;12(4):835–48. DOI: 10.1007/s13204-021-01749-z
58. Nascimento P, Marim R, Carvalho G, Mali S. Nanocellulose produced from rice hulls and its effect on the properties of biodegradable starch films. Mater Res. 2016;19(1):167–74. DOI: 10.1590/1980-5373-MR-2015-0423
59. Ibrahim MM, El-Zawawy WK, Nassar MA. Synthesis and characterization of polyvinyl alcohol/nanospherical cellulose particle films. Carbohydr Polym. 2010;79(3):694–9. DOI: 10.1016/j.carbpol.2009.09.030
60. Lee H, You J, Jin HJ, Kwak HW. Chemical and physical reinforcement behavior of dialdehyde nanocellulose in PVA composite film: A comparison of nanofiber and nanocrystal. Carbohydr Polym. 2020;232:115771. DOI: 10.1016/j.carbpol.2019.115771
61. Lu J, Wang T, Drzal LT. Preparation and properties of microfibrillated cellulose polyvinyl alcohol composite materials. Compos Part A Appl Sci Manuf. 2008;39(5):738–46. DOI: 10.1016/j.compositesa.2008.02.003
62. Kassab Z, Mansouri S, Tamraoui Y, Sehaqui H, Hannache H, Qaiss AEK, et al. Identifying Juncus plant as viable source for the production of micro- and nano-cellulose fibers: Application for PVA composite materials development. Ind Crops Prod. 2020;144:112035. DOI: 10.1016/j.indcrop.2019.112035
63. Liu D, Sun X, Tian H, Maiti S, Ma Z. Effects of cellulose nanofibrils on the structure and properties on PVA nanocomposites. Cellulose. 2013;20(6):2981–9. DOI: 10.1007/s10570-013-0073-6
64. Niazi MBK, Jahan Z, Berg SS, Gregersen ØW. Mechanical, thermal and swelling properties of phosphorylated nanocellulose fibrils/PVA nanocomposite membranes. Carbohydr Polym. 2017;177(August):258–68. DOI: 10.1016/j.carbpol.2017.08.125
65. Espinosa E, Bascón-Villegas I, Rosal A, Pérez-Rodríguez F, Chinga-Carrasco G, Rodríguez A. PVA/(ligno)nanocellulose biocomposite films. Effect of residual lignin content on structural, mechanical, barrier and antioxidant properties. Int J Biol Macromol.

2019;141:197–206. DOI: 10.1016/j.ijbiomac.2019.08.262

66. Isogai A, Saito T, Fukuzumi H. TEMPO-oxidized cellulose nanofibers. Nanoscale. 2011;3(1):71–85. DOI: 10.1039/c0nr00583e
67. International Organization for Standardization. ISO/TS 20477: 2017: Nanotechnologies - Standard terms and their definition for cellulose nanomaterial. 2017.
68. Gu J, Hu C, Zhang W, Dichiara AB. Reagentless preparation of shape memory cellulose nanofibril aerogels decorated with Pd nanoparticles and their application in dye discoloration. Appl Catal B Environ. 2018;237:482–90. DOI: 10.1016/j.apcatb.2018.06.002
69. Pascoli DU, Suko A, Gustafson R, Gough HL, Bura R. Novel ethanol production using biomass preprocessing to increase ethanol yield and reduce overall costs. Biotechnol Biofuels. 2021;14(1):1–18. DOI: 10.1186/s13068-020-01839-0
70. Hörhammer H, Dou C, Suko A V, Gustafson R, Bura R. Removal of non-structural components from poplar whole-tree chips to enhance hydrolysis and fermentation performance. Biotechnol Biofuels. 2018;11. DOI: 10.1186/s13068-018-1219-4
71. Dou C, Marcondes WF, Djaja JE, Bura R, Gustafson R. Can we use short rotation coppice poplar for sugar based biorefinery feedstock? Bioconversion of 2-year-old poplar grown as short rotation coppice. Biotechnol Biofuels. 2017;10(1):15. DOI: 10.1186/s13068-017-0829-6
72. Dou C, Bura R, Ewanick S, Morales-Vera R. Blending short rotation coppice poplar with wheat straw as a biorefinery feedstock in the State of Washington. Ind Crops Prod. 2019;132:407–12. DOI: 10.1016/j.indcrop.2019.02.033
73. Sluiter A, Hames B, Ruiz RO, Scarlata C, Sluiter J, Templeton D, et al. Determination of ash in biomass: laboratory analytical procedure (LAP). 2008; DOI: TP-510-42622
74. Sluiter A, Ruiz R, Scarlata C, Sluiter J, Templeton D. Determination of extractives in biomass: laboratory analytical procedure (LAP). 2008; DOI: NREL/TP-510-42619
75. Besbes I, Alila S, Boufi S. Nanofibrillated cellulose from TEMPO-oxidized eucalyptus fibres: Effect of the carboxyl content. Carbohydr Polym. 2011;84(3):975–83. DOI: 10.1016/j.carbpol.2010.12.052
76. Nam S, French AD, Condon BD, Concha M. Segal crystallinity index revisited by the simulation of X-ray diffraction patterns of cotton cellulose Iβ and cellulose II. Carbohydr

Polym. 2016;135:1–9. DOI: 10.1016/j.carbpol.2015.08.035
77. TAPPI. Grammage of paper and paperboard (weight per unit area) T 410 om-08. 1998.
78. Yuan Z, Wen Y, Li G. Production of bioethanol and value added compounds from wheat straw through combined alkaline/alkaline-peroxide pretreatment. Bioresour Technol. 2018;259:228–36. DOI: 10.1016/j.biortech.2018.03.044
79. Fang JM, Sun RC, Salisbury D, Fowler P, Tomkinson J. Comparative study of hemicelluloses from wheat straw by alkali and hydrogen peroxide extractions. Polym Degrad Stab. 1999;66:423–32. DOI: 10.1016/S0144-8617(99)00136-8
80. Sun JX, Mao FC, Sun XF, Sun RC. Comparative study of hemicelluloses isolated with alkaline peroxide from lignocellulosic materials. J Wood Chem Technol. 2004;24(3):239–62. DOI: 10.1081/WCT-200038170
81. Bian H, Wu X, Luo J, Qiao Y, Fang G, Dai H. Valorization of alkaline peroxide mechanical pulp by metal chloride-assisted hydrotropic pretreatment for enzymatic saccharification and cellulose nanofibrillation. Polymers (Basel). 2019;11(2). DOI: 10.3390/polym11020331
82. Sánchez R, Espinosa E, Domínguez-Robles J, Loaiza JM, Rodríguez A. Isolation and characterization of lignocellulose nanofibers from different wheat straw pulps. Int J Biol Macromol. 2016;92:1025–33. DOI: 10.1016/j.ijbiomac.2016.08.019
83. Kaffashsaie E, Yousefi H, Nishino T, Matsumoto T, Mashkour M, Madhoushi M, et al. Direct conversion of raw wood to TEMPO-oxidized cellulose nanofibers. Carbohydr Polym. 2021;262:117938. DOI: 10.1016/j.carbpol.2021.117938
84. Espinosa E, Domínguez-Robles J, Sánchez R, Tarrés Q, Rodríguez A. The effect of pre-treatment on the production of lignocellulosic nanofibers and their application as a reinforcing agent in paper. Cellulose. 2017;24(6):2605–18. DOI: 10.1007/s10570-017-1281-2
85. Yang X, Berthold F, Berglund LA. Preserving Cellulose Structure: Delignified Wood Fibers for Paper Structures of High Strength and Transparency. Biomacromolecules. 2018;19(7):3020–9. DOI: 10.1021/acs.biomac.8b00585
86. Tang Z, Li W, Lin X, Xiao H, Miao Q, Huang L, et al. TEMPO-Oxidized cellulose with high degree of oxidation. Polymers (Basel). 2017;9(9):3–4. DOI: 10.3390/polym9090421
87. Okita Y, Saito T, Isogai A. TEMPO-mediated oxidation of softwood thermomechanical

pulp. Holzforschung. 2009;63(5):529–35. DOI: 10.1515/HF.2009.096

88. Zhang L, Chen K, Peng L. Comparative Research about Wheat Straw Lignin from the Black Liquor after Soda-Oxygen and Soda-AQ Pulping: Structural Changes and Pyrolysis Behavior. Energy and Fuels. 2017;31(10):10916–23. DOI: 10.1021/acs.energyfuels.7b01786
89. Jiang F, Han S, Hsieh Y Lo. Controlled defibrillation of rice straw cellulose and self-assembly of cellulose nanofibrils into highly crystalline fibrous materials. RSC Adv. 2013;3(30):12366–75. DOI: 10.1039/c3ra41646a
90. Ma P, Zhai H. Selective TEMPO-Mediated Oxidation of Thermomechanical Pulp. BioResources. 2013;8(2):4396–405. DOI: 10.15376/biores.8.3.4396-4405
91. Morcillo-Martín R, Espinosa E, Rabasco-Vílchez L, Sanchez LM, Haro J De, Rodríguez A. Cellulose Nanofiber-Based Aerogels from Wheat Straw : Influence of Surface Load and Lignin Content on Their Properties and Dye Removal Capacity. Biomolecules. 2022;12:232. DOI: 10.3390/biom12020232
92. Puangsin B, Yang Q, Saito T, Isogai A. Comparative characterization of TEMPO-oxidized cellulose nanofibril films prepared from non-wood resources. Int J Biol Macromol. 2013;59:208–13. DOI: 10.1016/j.ijbiomac.2013.04.016
93. Gharpuray MM. Structural modification of lignocellulosics by pretreatments to enhance enzymatic hydrolysis. Biotechnol Bioeng. 1983;25(1):157–72.
94. Siró I, Plackett D. Microfibrillated cellulose and new nanocomposite materials: A review. Cellulose. 2010;17(3):459–94. DOI: 10.1007/s10570-010-9405-y
95. Henriksson M, Henriksson G, Berglund LA, Lindström T. An environmentally friendly method for enzyme-assisted preparation of microfibrillated cellulose (MFC) nanofibers. Eur Polym J. 2007;43(8):3434–41. DOI: 10.1016/j.eurpolymj.2007.05.038
96. Dufresne A. Nanocellulose: A new ageless bionanomaterial. Mater Today. 2013;16(6):220–7. DOI: 10.1016/j.mattod.2013.06.004
97. Bian H, Gao Y, Luo J, Jiao L, Wu W, Fang G, et al. Lignocellulosic nanofibrils produced using wheat straw and their pulping solid residue: From agricultural waste to cellulose nanomaterials. Waste Manag. 2019;91:1–8. DOI: 10.1016/j.wasman.2019.04.052
98. Wang N, Ding E, Cheng R. Thermal degradation behaviors of spherical cellulose nanocrystals with sulfate groups. Polymer (Guildf). 2007;48(12):3486–93. DOI:

10.1016/j.polymer.2007.03.062

99. Nair SS, Yan N. Effect of high residual lignin on the thermal stability of nanofibrils and its enhanced mechanical performance in aqueous environments. Cellulose. 2015;22(5):3137–50. DOI: 10.1007/s10570-015-0737-5

100. Lavoine N, Desloges I, Dufresne A, Bras J. Microfibrillated cellulose – Its barrier properties and applications in cellulosic materials: A review. Carbohydr Polym. 2012;90(2):735–64. DOI: 10.1016/j.carbpol.2012.05.026

101. Bondancia TJ, De Aguiar J, Batista G, Cruz AJG, Marconcini JM, Mattoso LHC, et al. Production of Nanocellulose Using Citric Acid in a Biorefinery Concept: Effect of the Hydrolysis Reaction Time and Techno-Economic Analysis. Ind Eng Chem Res. 2020;59(25):11505–16. DOI: 10.1021/acs.iecr.0c01359

102. Clauser NM, Felissia FE, Area MC, Vallejos ME. Design of nano and micro fibrillated cellulose production processes from forest industrial wastes in a multiproduct biorefinery. Chem Eng Res Des. 2021;167:1–14. DOI: 10.1016/j.cherd.2020.12.003

103. Serra-Parareda F, Aguado R, Arfelis S, Xifré R, Fullana-i-Palmer P, Delgado-Aguilar M. Techno-economic and environmental evaluation of a market pulp reinforced with micro-/nanofibers as a strengthening agent in packaging paper. J Clean Prod. 2022;347(February):131265. DOI: 10.1016/j.jclepro.2022.131265

104. Pascoli DU, Dichiara AB, Roumeli E, Gustafson R, Bura R. Lignocellulosic nanomaterials production from wheat straw via peracetic acid pretreatment and their application in plastic composites. Carbohydr Polym. 2022;295. DOI: doi.org/10.1016/j.carbpol.2022.119857

105. Aden A, Ruth M, Ibsen K, Jechura J, Neeves K, Sheehan J, et al. Lignocellulosic Biomass to Ethanol Process Design and Economics Utilizing Co-Current Dilute Acid Prehydrolysis and Enzymatic Hydrolysis for Corn Stover. Natl Renew Energy Lab. 2002;(June).

106. Zhao X, Zhang T, Zhou Y, Liu D. Preparation of peracetic acid from hydrogen peroxide. Part I: Kinetics for peracetic acid synthesis and hydrolysis. J Mol Catal A Chem. 2007;271:246–52. DOI: 10.1016/j.molcata.2007.03.012

107. Duan L, Yu W, Li Z. Analysis of structural changes in jute fibers after peracetic acid treatment. J Eng Fiber Fabr. 2017;12(1):33–42. DOI: 10.1177/155892501701200104

108. Humbird D, Davis R, Tao L, Kinchin C, Hsu D, Aden A, et al. Process Design and

Economics for Biochemical Conversion of Lignocellulosic Biomass to Ethanol. Natl Renew Energy Lab. 2011;

109. Towering Skills. CEPCI Cost Indices [Internet]. Available from: https://www.toweringskills.com/financial-analysis/cost-indices/#chemical-engineering-plant-cost-index-cepci
110. U.S. Bureau of Labor Statistics. Producer Price Index by Commodity: Chemicals and Allied Products: Basic Inorganic Chemicals, retrieved from FRED, Federal Reserve Bank of St. Louis [Internet]. [cited 2022 Mar 13]. Available from: https://fred.stlouisfed.org/series/WPU0613#0
111. Aue Energy Consulting, Benjamin A. Thorp I, Center for Technology Transfer I, D&S Design and Engineering, Science Applications International Corporation. Pulp & Paper Industry. Energy Best Practice Guidebook. 2005.
112. Seufitelli GVS, El-Husseini H, Pascoli DU, Bura R, Gustafson R. Techno-economic analysis of an integrated biorefinery to convert poplar into jet fuel, xylitol, and formic acid. [Manuscript under review]. Biotechnol Biofuels Bioprod. 2022;
113. Carrillo CA, Laine J, Rojas OJ. Microemulsion systems for fiber deconstruction into cellulose nanofibrils. ACS Appl Mater Interfaces. 2014;6(24):22622–7. DOI: 10.1021/am5067332
114. Wei J, Zhou Y, Lv Y, Wang J, Jia C, Liu J, et al. Carboxymethyl cellulose nanofibrils with a treelike matrix: Preparation and behavior of pickering emulsions stabilization. ACS Sustain Chem Eng. 2019;7(15):12887–96. DOI: 10.1021/acssuschemeng.9b01822
115. Du H, Parit M, Wu M, Che X, Wang Y, Zhang M, et al. Sustainable valorization of paper mill sludge into cellulose nanofibrils and cellulose nanopaper. J Hazard Mater. 2020;400:123106. DOI: 10.1016/j.jhazmat.2020.123106
116. Hielscher Ultrasonics. Ultrasonic Production of Nano-Structured Cellulose [Internet]. [cited 2022 Mar 27]. Available from: https://www.hielscher.com/ultrasonic-production-of-nano-structured-cellulose.htm
117. CNBM International Pulp & Paper. Low-consistency Pulper [Internet]. [cited 2022 Mar 27]. Available from: http://www.paperpulpingmachine.com/paper-pulper-machine/low-consistency-pulper/
118. Cellulose Lab. Cellulose Lab Nanocellulose Product Price List 2020-2021 [Internet].

[cited 2022 Apr 2]. Available from: https://www.celluloselab.com/price/CelluloseLab Product Price List 2020.htm

119. Drumright RE, Gruber PR, Henton DE. Polylactic Acid Technology. Adv Mater. 2000;12(23):1841–6. DOI: 10.1002/1521-4095(200012)12:23<1841::aid-adma1841>3.3.co;2-5
120. Li G, Zhao M, Xu F, Yang B, Li X, Meng X, et al. Synthesis and Biological Application of Polylactic Acid. Molecules. 2020;25(21). DOI: 10.3390/molecules25215023
121. Alibaba [Internet]. [cited 2022 Apr 2]. Available from: https://www.alibaba.com
122. Crawford JT, Shan CW, Budsberg E, Morgan H, Bura R, Gustafson R. Hydrocarbon bio-jet fuel from bioconversion of poplar biomass: Techno-economic assessment. Biotechnol Biofuels. 2016;9(1):1–16. DOI: 10.1186/s13068-016-0545-7
123. Pennells J, Godwin ID, Amiralian N, Martin DJ. Trends in the production of cellulose nanofibers from non-wood sources. Cellulose. 2020;27(2):575–93. DOI: 10.1007/s10570-019-02828-9
124. U.S. Department of Energy. US Billion-Ton Update: Biomass Supply for a Bioenergy and Bioproducts Industry. 2011. DOI: 10.1089/ind.2011.7.375
125. Iowa Corn Promotion Board (ICPB). Sustainable corn stover harvest. 2013.
126. Davis R, Grundl N, Tao L, Biddy MJ, Tan ECD, Beckham GT, et al. Process Design and Economics for the Conversion of Lignocellulosic Biomass to Hydrocarbon Fuels and Coproducts: 2018 Biochemical Design Case Update: Biochemical Deconstruction and Conversion of Biomass to Fuels and Products via Integrated Biorefinery Path. Renew Energy. 2018;(November):147.
127. Jensen EF, Casler MD, Farrar K, Finnan JM, Lord R, Palmborg C, et al. Reed Canary Grass: From Production fo End Use. In: Perennial Grasses for Bioenergy and Bioproducts. Elsevier Inc.; 2018. p. 153–73. DOI: 10.1016/b978-0-12-812900-5.00005-9
128. Spyreas G, Wilm BW, Plocher AE, Ketzner DM, Matthews JW, Ellis JL, et al. Biological consequences of invasion by reed canary grass (Phalaris arundinacea). Biol Invasions. 2010;12(5):1253–67. DOI: 10.1007/s10530-009-9544-y
129. Maurer DA, Lindig-Cisneros R, Werner KJ, Kercher S, Miller R, Zedler JB. The replacement of wetland vegetation by reed canarygrass (Phalaris arundinacea). Ecol Restor. 2003;21(2):116–9. DOI: 10.3368/er.21.2.116

130. Finell M. The use of reed canary-grass (Phalaris arundinacea) as a short fibre raw material for the pulp and paper industry. Swedish University of Agricultural Sciences. 2003.
131. Marrot L, Candelier K, Valette J, Lanvin C, Horvat B, Legan L, et al. Valorization of Hemp Stalk Waste Through Thermochemical Conversion for Energy and Electrical Applications. Waste and Biomass Valorization. 2022;13(4):2267–85. DOI: 10.1007/s12649-021-01640-6
132. Crini G, Lichtfouse E, Chanet G, Morin-Crini N. Applications of hemp in textiles, paper industry, insulation and building materials, horticulture, animal nutrition, food and beverages, nutraceuticals, cosmetics and hygiene, medicine, agrochemistry, energy production and environment: a review. Environ Chem Lett. 2020;18(5):1451–76. DOI: 10.1007/s10311-020-01029-2
133. Correia F, Roy DN, Goel K. Chemistry and delignification kinetics of Canadian industrial hemp. J Wood Chem Technol. 2001;21(2):97–111.
134. Wawro A, Batog J, Gieparda W. Chemical and enzymatic treatment of hemp biomass for bioethanol production. Appl Sci. 2019;9(24):1–11. DOI: 10.3390/app9245348
135. Zhao J, Xu Y, Wang W, Griffin J, Roozeboom K, Wang D. Bioconversion of industrial hemp biomass for bioethanol production: A review. Fuel. 2020;281(June). DOI: 10.1016/j.fuel.2020.118725
136. Akpan EI. Chemistry and structure of lignin. In: Sustainable Lignin for Carbon Fibers: Principles, Techniques, and Applications. 2019. p. 1–50. DOI: doi.org/10.1007/978-3-030-18792-7_1 1
137. Joachimiak K, Wojech R, Wójciak A. Comparison of Miscanthus giganteus and birch wood NSSC pulping. Part 1: The effects of technological conditions on certain pulp properties. Wood Res. 2019;64(1):49–58.
138. Kundu C, Samudrala SP, Kibria MA, Bhattacharya S. One-step peracetic acid pretreatment of hardwood and softwood biomass for platform chemicals production. Vol. 11, Scientific Reports. 2021. DOI: 10.1038/s41598-021-90667-9
139. Wi SG, Cho EJ, Lee DS, Lee SJ, Lee YJ, Bae HJ. Lignocellulose conversion for biofuel: A new pretreatment greatly improves downstream biocatalytic hydrolysis of various lignocellulosic materials. Biotechnol Biofuels. 2015;8(1):1–11. DOI: 10.1186/s13068-015-0419-4

140. Gedik G, Avinc O. Bleaching of Hemp (Cannabis Sativa L.) Fibers with Peracetic Acid for Textiles Industry Purposes. Fibers Polym. 2018;19(1):82–93. DOI: 10.1007/s12221-018-7165-0
141. Lyu Q, Chen X, Zhang Y, Yu H, Han L, Xiao W. One-pot fractionation of corn stover with peracetic acid and maleic acid. Bioresour Technol. 2021;320(PA):124306. DOI: 10.1016/j.biortech.2020.124306
142. Oliaei E, Lindén PA, Wu Q, Berthold F, Berglund L, Lindström T. Microfibrillated lignocellulose (MFLC) and nanopaper films from unbleached kraft softwood pulp. Cellulose. 2020;27(4):2325–41. DOI: 10.1007/s10570-019-02934-8
143. Zhuang J, Li M, Pu Y, Ragauskas AJ, Yoo CG. Observation of potential contaminants in processed biomass using fourier transform infrared spectroscopy. Appl Sci. 2020;10(12):1–13. DOI: 10.3390/app10124345
144. Gandolfi S, Ottolina G, Riva S, Fantoni GP, Patel I. Complete chemical analysis of carmagnola hemp hurds and structural features of its components. BioResources. 2013;8(2):2641–56. DOI: 10.15376/biores.8.2.2641-2656
145. Li X, Wei Y, Xu J, Xu N, He Y. Quantitative visualization of lignocellulose components in transverse sections of moso bamboo based on ftir macro- and micro-spectroscopy coupled with chemometrics. Biotechnol Biofuels. 2018;11(1):1–16. DOI: 10.1186/s13068-018-1251-4
146. Lv P, Almeida G, Perré P. TGA-FTIR analysis of torrefaction of lignocellulosic components (cellulose, xylan, lignin) in isothermal conditions over a wide range of time durations. BioResources. 2015;10(3):4239–51.
147. Putnina A, Kukle S, Gravitis J. STEX Treated and Untreated Hemp Fiber Comparative Structural Analysis. Sci J Riga Tech Univ Mater Sci Text Cloth Technol. 2011;6(March):36–42.
148. Zhao J, Xu Y, Wang W, Griffin J, Wang D. Conversion of liquid hot water, acid and alkali pretreated industrial hemp biomasses to bioethanol. Bioresour Technol. 2020;309(April):123383. DOI: 10.1016/j.biortech.2020.123383
149. Dai D, Fan M. Characteristic and Performance of Elementary Hemp Fibre. Mater Sci Appl. 2010;1(6):336–42. DOI: 10.4236/msa.2010.16049
150. Szymanska-Chargot M, Zdunek A. Use of FT-IR Spectra and PCA to the Bulk

Characterization of Cell Wall Residues of Fruits and Vegetables Along a Fraction Process. Food Biophys. 2013;8(1):29–42. DOI: 10.1007/s11483-012-9279-7

151. Bag R, Beaugrand J, Dole P, Kurek B. Treatment of chenevotte, a co-product of industrial hemp fiber, by water or hydrochloric acid: Impact on polymer mobility in the lignified cell walls. J Wood Sci. 2012;58(6):493–504. DOI: 10.1007/s10086-012-1282-6
152. Petit J, Gulisano A, Dechesne A, Trindade LM. Phenotypic Variation of Cell Wall Composition and Stem Morphology in Hemp (Cannabis sativa L.): Optimization of Methods. Front Plant Sci. 2019;10(July). DOI: 10.3389/fpls.2019.00959
153. Davis R, Tao L, Scarlata C, Tan ECD, Ross J, Lukas J, et al. Process Design and Economics for the Conversion of Lignocellulosic Biomass to Hydrocarbons : Dilute-Acid and Enzymatic Deconstruction of Biomass to Sugars and Catalytic Conversion of Sugars to Hydrocarbons. Natl Renew Energy Lab. 2015;(March).
154. ChemAnalyst. Hydrogen Peroxide Price Trend and Forecast [Internet]. 2022 [cited 2022 Apr 27]. Available from: https://www.chemanalyst.com/Pricing-data/hydrogen-peroxide-1169
155. U.S. Energy Information Administration. Natural Gas [Internet]. Available from: https://www.eia.gov/naturalgas/
156. Peters MS, Timmerhaus KD, West RE. Analysis of Cost Estimation. In: Plant Design and Economics for Chemical Engineers. 5th ed. McGraw Hill; p. 227–78.

APPENDIX A. Supplementary information – Chapter 2

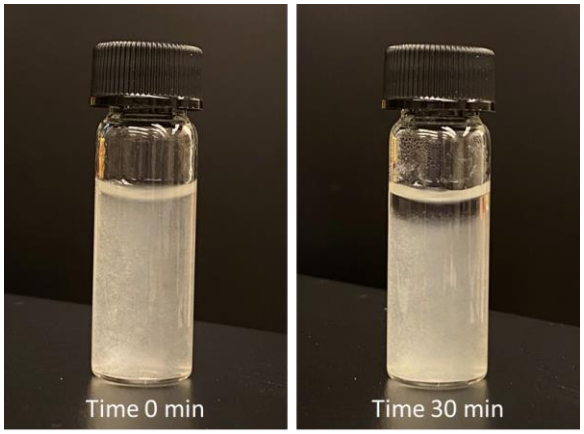

Figure A.1. Suspension stability test of Pretreatment control (PC) at time 0 and after 30 min

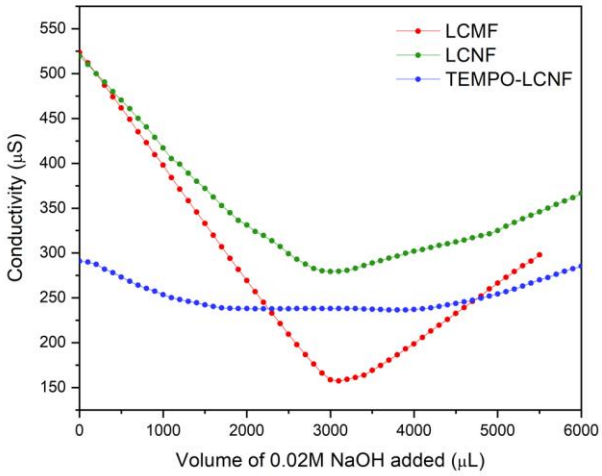

Figure A.2. Conductometric titration curves of different samples. The curve region showing a conductivity plateau is associated with the quantity of weak carboxylic acid groups present in the sample and therefore is related to the oxidation degree. Charge density was calculated based on the NaOH volume consumed in the plateau region.

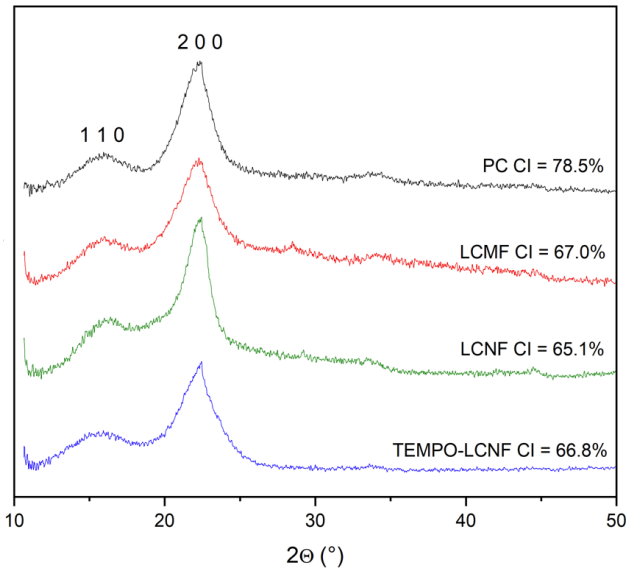

Figure A.3. X-ray diffraction spectra and corresponding CI of different samples. XRD analysis was performed to assess the effect of both pretreatments on the crystallinity of WS fibers.

Table A.1. Summary of all process conditions tested during the screening stage and the chemical composition of the resulting fibers. Screening of process conditions included feedstock composition (whole WS vs. node-free WS), feedstock moisture (dry vs. soaked), reaction pH (acidic vs. alkaline), reaction times (60, 75, and 150 min), solvents (water, glycerol, and 50/50 mixture of both), and presence vs. absence of hydrogen peroxide (H_2O_2) during the alkaline reactions. The selected reaction conditions are highlighted.

Experimental parameters							**Pulp chemical composition**			
Feedstock	**Time (min)**	**Temp (°C)**	**Solvent**	**NaOH charge**	**H_2O_2 charge**	**H_2SO_4 charge**	**Cellulose content %**	**Hemicellulose content %**	**Lignin content %**	**Ash content %**
Dry wheat straw (clean)	60	90	water	15%	7.5%	-	55.9	24.4	9.6	1.8
Soaked WS (clean)	60	90	water	15%	7.5%	-	56.6	24.4	8.4	1.7
Dry wheat straw (clean)	75	90	water	15%	7.5%	-	56.8	24.8	8.8	1.5
Soaked WS (clean)	75	90	water	15%	7.5%	-	56.6	24.5	8.7	1.6
Dry wheat straw (clean)	75	90	100% glycerol	15%	7.5%	-	44.4	25.0	21.4	6.7
Dry wheat straw (clean)	75	90	100% glycerol	15%	-	-	44.5	24.7	21.2	6.8
Dry wheat straw (clean)	225	90	100% glycerol	15%	-	-	46.9	25.4	18.0	5.6
Dry wheat straw (clean)	75	90	50% glycerol	15%	-	-	51.7	26.9	11.3	1.9
Dry wheat straw (clean)	225	90	50% glycerol	15%	-	-	52.5	26.7	10.7	1.8
Dry wheat straw (clean)	150	90	water	15%	7.5%	-	59.1	26.0	8.4	1.2
Dry wheat straw (clean)	75	90	water	15%	-	-	56.2	24.8	11.5	1.3
Dry wheat straw (clean)	75	90	100% glycerol	-	-	1%	40.7	23.7	27.1	6.8
Dry wheat straw (clean)	75	90	100% glycerol	-	-	5%	30.4	22.2	27.3	6.6
Dry wheat straw (clean)	75	90	50% glycerol	-	-	1%	39.3	23.0	29.7	6.9
Dry wheat straw (clean)	75	90	50% glycerol	-	-	5%	38.9	22.1	28.6	6.3
Dry wheat straw (clean)	75	90	water	-	-	1%	38.8	23.9	27.1	9.5
Dry wheat straw (clean)	75	90	water	-	-	5%	37.7	23.2	29.7	9.7
Dry WHOLE wheat straw	75	90	water	15%	7.5%	-	55.2	25.1	9.1	1.9
Dry WHOLE wheat straw	**150**	**90**	**water**	**15%**	**7.5%**	**-**	**55.8**	**25.7**	**7.9**	**1.9**
Dry wheat straw (clean)	150	90	water	15%	-	-	54.9	24.5	9.8	1.8

Table A.2. Relative carbohydrate composition of original WS, WS refined pulp, PAA pretreated pulp, and TEMPO pretreated pulp.

	Arabinan	Galactan	Glucan	Xylan	Mannan
Original WS	2.9	0.9	62.7	33.6	0.0
WS refined pulp	2.8	0.4	67.9	28.9	0.0
PAA pretreated pulp	2.0	0.0	71.6	26.4	0.0
TEMPO pretreated pulp	1.8	0.0	73.0	25.2	0.0

Table A.3. Tensile test specimen's thickness, density, and resulting mechanical properties of PVA composites reinforced with 5 wt.% lignocellulosic fibrils.

	Thickness (μm)	Density (g cm^{-3})	Specific tensile strength (MPa g^{-1} cm^3)	Specific Young's modulus (GPa g^{-1} cm^3)	Elongation at break (%)	Fracture toughness (MJ/m^3)
Neat PVA	39.0 ± 0.8	1.26 ± 0.04	36.2 ± 3.8	2.1 ± 0.3	63.4 ± 21.6	22.3
PVA/LCMF	79.1 ± 2.4	0.86 ± 0.03	58.2 ± 1.2	2.7 ± 0.1	26.1 ± 3.7	11.7
PVA/H-LCMF	74.6 ± 6.7	0.89 ± 0.03	50.4 ± 2.3	2.5 ± 0.2	31.5 ± 13.2	15.0
PVA/LCNF	52.6 ± 0.6	1.16 ± 0.04	53.5 ± 0.6	2.8 ± 0.1	71.0 ± 18.8	35.0
PVA/H-LCNF	57.8 ± 2.0	1.18 ± 0.05	51.2 ± 1.4	2.5 ± 0.1	121.1 ± 16.7	61.4
PVA/TEMPO-LCNF	58.2 ± 4.8	1.06 ± 0.03	61.4 ± 0.8	3.1 ± 0.0	62.3 ± 11.5	38.3

APPENDIX B. Supplementary information – Chapter 3

Table A.4. Breakdown of Total Capital Investment (TCI). ISBL refers to Inside-Battery-Limits equipment cost (i.e., excluding feedstock handling and wastewater treatment).

	Assumption	Source	Cost ($)
Total installed equipment costs			**$81,478,066**
Warehouse	4% of ISBL installed cost	(126)	$2,293,276
Site development	9% of ISBL installed cost	(126)	$5,159,870
Piping	5% of ISBL installed cost	(126)	$2,579,935
Total direct costs (TDC)			**$91,511,146**
Prorateable expenses	10% of TDC	(126)	$9,151,115
Field expenses	10% of TDC	(126)	$9,151,115
Home office and construction	20% of TDC	(126)	$18,302,229
Project contingency	10% of TDC	(126)	$9,151,115
Other costs (start-up, permits, etc.)	10% of TDC	(126)	$9,151,115
Total indirect costs			**$54,906,688**
Fixed capital investment (FCI)			**$146,417,834**
Working capital	5% of FCI	(126)	$7,320,892
Total capital investment (TCI)			**$153,738,726**

Table A.5. Breakdown of Total Operating Costs. ISBL refers to Inside-Battery-Limits equipment cost (i.e., excluding feedstock handling and wastewater treatment).

	Price	**Source**	**Cost ($/year)**
Feedstock (wheat straw)	$60.63/tonne	(52)	$2,121,949
NaOH	$352.42/tonne	(153)	$2,488,548
DTPA	$2,000/tonne	Alibaba	$105,000
H_2O_2	$680.00/tonne	(154)	$8,468,040
Acetic acid	$750.00/tonne	Alibaba	$16,380,000
H_2SO_4	$88.00/tonne	(126)	$77,834
Membrane replacement	$0.03 * equipment cost	(126)	$400,433
Natural gas	$239.00/tonne	(155)	$1,770,217
Grid electricity in PNW	$0.05/kWh	Personal communications	$4,220,930
Waste disposal	$31.81/tonne	(108)	$402,478
Total variable costs			**$36,435,429**
Operating labor salaries	Total of 4 employees/area		$2,500,000
Operating supervision	15% of operating labor	(156)	$375,000
Labor burden	90% of total salaries	(126)	$2,250,000
Maintenance	3% of ISBL installed cost	(126)	$1,719,957
Laboratory charges	15% of operating labor	(156)	$375,000
Operating supplies	1% of FCI	(156)	$1,464,178
Property insurance	1% of FCI	(126)	$1,024,925
Total fixed costs			**$9,709,060**
Total operating costs			**$46,144,488**

APPENDIX C. Supplementary information – Chapter 4

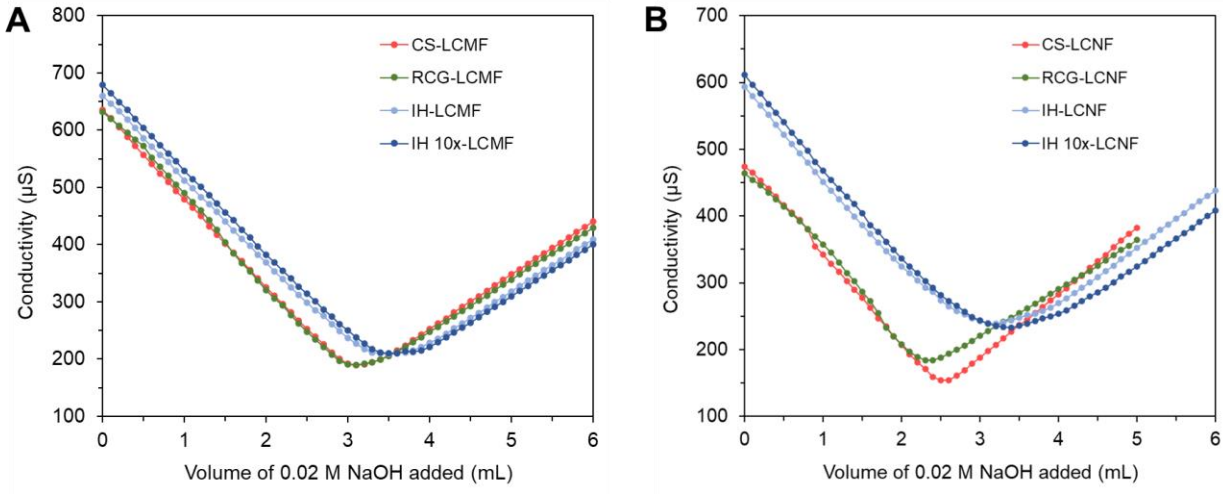

Figure A.4. Conductometric titration curves of (A) LCMF and (B) LCNF from different feedstocks.

Table A.6. Total mass yield and chemical composition of untreated biomass feedstocks, alkaline peroxide pulps, and PAA treated pulps of corn stover (CS), reed canary grass (RCG), and industrial hemp (IH).

			Chemical composition (% of oven-dry weight)				
		Total mass yield (%)	Holocellulose [a] %	Uronic/acetic acids %	Lignin %	Ash %	Extractives %
Untreated	CS	-	71.9 ± 2.1	3.8 ± 0.2	21.3 ± 0.2	3.4 ± 0.1	7.8 ± 0.1
	RCG	-	50.4 ± 0.4	3.1 ± 0.1	21.5 ± 0.2	8.2 ± 0.1	29.6 ± 0.1
	IH	-	55.5 ± 0.2	5.5 ± 0.2	19.3 ± 0.2	5.2 ± 0.0	16.5 ± 0.3
Pulp	CS	60.6	90.3 ± 0.3	0.0 ± 0.0	6.5 ± 0.2	1.3 ± 0.2	2.1 ± 0.5
	RCG	49.0	79.5 ± 0.3	0.0 ± 0.0	9.7 ± 0.2	2.3 ± 0.1	4.2 ± 0.1
	IH	64.4	70.7 ± 3.4	0.0 ± 0.0	19.1 ±0.1	3.5 ± 0.2	3.0 ± 0.3
PAA treated pulp	CS	50.2	95.0 ± 0.3	0.0 ± 0.0	2.3 ± 0.3	< 0.1	NM
	RCG	40.0	86.7 ± 2.5	0.0 ± 0.0	3.6 ± 0.1	0.2 ± 0.0	NM
	IH	44.2	81.3 ± 0.5	0.0 ± 0.0	12.0 ± 0.2	2.2 ± 0.1	NM
	IH 10x PAA	36.2	92.7 ± 1.0	0.0 ± 0.0	3.1 ± 0.1	1.5 ± 0.0	NM

NM = Not measured

[a] For detailed carbohydrate composition of holocellulose, see Table A.8

Table A.7. Relative carbohydrate composition in holocellulose of untreated biomass, alkaline peroxide pulps, and PAA treated pulps of the different biomass feedstocks.

		Arabinan	Galactan	Glucan	Xylan	Mannan
Untreated	**CS**	3.4	1.1	58.5	37.0	0.0
	RCG	5.7	2.5	60.7	31.0	0.0
	IH	2.3	3.5	70.8	21.2	2.2
Pulp	**CS**	2.3	0.4	64.7	32.6	0.0
	RCG	5.3	1.4	62.7	30.6	0.0
	IH	0.7	1.7	72.3	23.6	1.6
PAA treated	**CS**	2.3	0.3	66.1	31.4	0.0
	RCG	2.4	0.5	69.7	27.4	0.0
	IH	0.3	0.9	71.8	25.7	1.3
	IH 10x PAA	0.3	0.8	72.1	24.6	2.2

VITA

Danielle Uchimura Pascoli was born in São Paulo, Brazil, in 1992. After graduating from Poliedro high school in São José dos Campos, she started studying Biochemical Engineering at the Engineering School of Lorena, University of São Paulo (EEL-USP) in 2010. During college, Danielle also worked as an undergraduate research assistant at the Department of Biotechnology for one year. In August 2013, she was awarded the Brazilian Scientific Mobility Program scholarship to study abroad in the United States, where she continued her Engineering studies at Rose-Hulman Institute of Technology. During her exchange program, Danielle also participated in the Research Experiences for Undergraduates: Bioenergy Systems program at the University of Nebraska in the Summer of 2014. Danielle returned to Brazil in November 2014 and received her Bachelor of Science degree in Biochemical Engineering from EEL-USP in June 2017. After graduation, she started working with Prof. Renata Bura in the Biofuels and Bioproducts Laboratory at the University of Washington (UW). In June 2019, she received her Master of Science degree from the School of Environmental and Forest Sciences. Danielle continued working with Prof. Renata Bura towards her Ph.D. degree at the UW, during which she joined the Consortium for Advanced Bioeconomy Leadership Education program. In August 2022, Danielle received her Ph.D. degree in Bioresource Science and Engineering from the UW.